Distribution Agreement

In presenting this thesis or dissertation as a partial fulfillment of the requirements for an advanced degree from Emory University, I hereby grant to Emory University and its agents the non-exclusive license to archive, make accessible, and display my thesis or dissertation in whole or in part in all forms of media, now or hereafter known, including display on the world wide web. I understand that I may select some access restrictions as part of the online submission of this thesis or dissertation. I retain all ownership rights to the copyright of the thesis or dissertation. I also retain the right to use in future works (such as articles or books) all or part of this thesis or dissertation.

Signature:

Juliet Victoria Santiago

Juliet Victoria Santiago
Name

12/13/2023 | 4:53 AM EST
Date

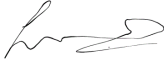|	
Title	Proteomic and transcriptomic signatures of microglia-derived extracellular vesicles and extension into in vivo systems.

Author	Juliet Victoria Santiago
Degree	Doctor of Philosophy
Program	Biological and Biomedical Sciences
	Neuroscience

Approved by the Committee
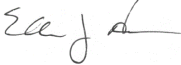
Srikant Rangaraju
Advisor

Tamara Caspary
Committee Member

Ellen Hess
Committee Member

Allan Levey
Committee Member

Nicholas Seyfried
Committee Member

Committee Member

Accepted by the Laney Graduate School:

_____

Kimberly Jacob Arriola, Ph.D, MPH
Dean, James T. Laney Graduate School

_____

Date

Proteomic and transcriptomic signatures of microglia-derived extracellular vesicles and extension into in vivo systems.

By

Juliet Victoria Santiago
B.Sc. University of Florida, 2018

Advisor: Srikant Rangaraju, MBBS MS

An abstract of
A dissertation submitted to the Faculty of the James T. Laney School of
Graduate Studies of Emory University in partial fulfillment of the requirements for
the degree of Doctor of Philosophy
Graduate Division of Biological and Biomedical Science
Neuroscience

2023

Abstract

Proteomic and transcriptomic signatures of microglia-derived extracellular vesicles and extension into in vivo systems.

By Juliet Victoria Santiago

Microglia are resident immune cells of the brain that play important roles in mediating inflammatory responses in several neurological diseases via direct and indirect mechanisms. In neurodegenerative diseases, microglia can convert from homeostatic to disease-associated-microglial (DAM) states which play dual roles in disease pathogenesis, resulting in disease-promoting as well as protective responses. Insights into microglial functions in neurodegenerative disease and neuroinflammation can be gained by comprehensive molecular characterization of microglia, at both the proteomic and transcriptomic level. Although microglia-mediated neuroinflammation has emerged as a key pathological mechanism in neurodegenerative diseases, there is a gap in knowledge of how different microglial states contribute to disease pathogenesis. One indirect mechanism may involve extracellular vesicle (EV) release, such that the molecular cargo transported by microglia-derived EVs can have functional effects by facilitating intercellular communication with recipient cells. The molecular composition of microglia-derived EVs, and how microglial activation states impact EV composition and EV-mediated effects in neuroinflammation, remain poorly understood. This thesis includes the foundational in vitro studies identifying unique molecular profiles of microglia-derived EVs that are determined by microglial activation state. By combining proteomic and transcriptomic methods, we obtained comprehensive molecular profiles of BV2 microglia-derived EVs under homeostatic and stimulated conditions. Our analyses revealed novel state-specific proteomic and transcriptomic signatures of microglia-derived EVs. Particularly, lipopolysaccharide (LPS) activation had the most profound impact on proteomic and transcriptomic compositions of microglia-derived EVs. Additionally, we found that EVs derived from LPS-activated microglia were able to induce pro-inflammatory transcriptomic changes in resting responder microglia, confirming the ability of microglia-derived EVs to relay functionally-relevant inflammatory signals. These comprehensive molecular datasets represent important resources for the neuroscience and omics communities, and provide novel insights into the role of microglia-derived EVs in neuroinflammation. These in vitro experiments were fundamental for developing a novel method to characterize the proteome of microglia and their EVs in vivo using TurboID-based proximity labeling. Our findings reveal that the microglial proteome cannot be labeled in vivo using TurboID-based proximity labeling with the *Rosa26-floxSTOP-TurboID;Tmem119-CreERT2* mice, despite successful labeling of the cell proteome and EV proteome in TurboID-BV2 microglia and astrocytic *Rosa26-floxSTOP-TurboID;Aldh1l1-CreERT2* mice. This thesis includes foundational experiments along with newly developed techniques to interrogate the possibility of characterizing cell-type specific EVs in vivo.

Proteomic and transcriptomic signatures of microglia-derived extracellular vesicles and extension into in vivo systems.

By
Juliet Victoria Santiago
B.Sc. University of Florida, 2018

Advisor: Srikant Rangaraju, MBBS MS

A dissertation submitted to the Faculty of the James T. Laney School of
Graduate Studies of Emory University in partial fulfillment of the requirements for
the degree of Doctor of Philosophy
Graduate Division of Biological and Biomedical Science
Neuroscience

2023

Acknowledgements

Table of Contents

<u>Abbreviations</u>

Alzheimer's disease (AD), Central Nervous System (CNS), EV (Extracellular vesicle), CNS (Central nervous system), LPS (Lipopolysaccharide), Toll like Receptors (TLRs), Pattern like Receptors (PRRs), amyloid-β (Aβ), neurofibrillary tangles (NFTs), late onset AD (LOAD), Genome wide association studies (GWAS), Disease associated microglia (DAM), IL-10 (Interleukin-10), TGF-β (Transforming growth factor beta), TEM (Transmission electron microscopy), NTA (Nano tracking analysis), LFQ-MS (Label-free quantification mass spectrometry), mRNA (messenger RNA), miRNA (micro RNA), TNF (Tumor necrosis factor), CCT (Chaperonin containing TCP1 (CCT/TRiC)), GSEA (Gene set enrichment analysis), GO (Gene ontology), DEP (Differentially enriched protein), DEG (Differentially expressed gene), DEX (Differential expression), PCA (Principal component analysis), FET (Fisher's Exact Test), IF (Immunofluorescence).

I.   Chapter 1. Introduction

i.   Microglia and neuroinflammation

The discovery of microglia

For over a century, scientists have been able to visualize and illustrate brain cells following the groundbreaking work of Camillo Golgi in 1873[1, 2]. Golgi's discovery of a staining technique that enabled the visualization of complex and intricate structures with immense detail, was pivotal in future efforts to study the central nervous system (CNS)[1, 2]. Later on, Spanish neuroscientist, Santiago Ramón y Cajal, mapped the entire structure of nerve cells using Golgi's staining technique[2]. This work formed the basis of the *Neuron Doctrine*, whereby individual nerve cells, or neurons, form the developmental, functional and structural units of the nervous system[2]. However, Cajal's research interests were not limited to just neurons; it was also in glia[3]. Glia research began in the mid 19th century when Rudolf Virchow coined the term "Neuroglia" to describe a connective interstitial substance in the brain and spinal cord that surround nerve cells[4]. Later, William Ford Robertson introduced the term 'mesoglia' to describe mesoderm-derived phagocytic cells that are distinct from neurons and neuroglia[5]. In the early 20th century, Cajal renamed these mesoglia the 'third elements of the nervous system' due to their separate origins from neurons and macroglia, and phagocytic nature[3, 4]. The concept of the "third element" was later refined by a student of Cajal, Pío del Río-Hortega, who described the third element as 'microglia' to further discriminate them based on their fine processes, distribution, and function, which was discovered using silver carbonate stain techniques[4-7]. Following these breakthrough and novel methodologies, microglia research has expanded considerably, broadening the original classification of the 'third element' to a much more dynamic and ever changing cell type in the CNS.

Microglia origin and development

As previously mentioned, one of the major distinguishing factors of microglial cells is their origin[6]. Microglia have a hemopoietic origin and display macrophage markers[8]. This was first described by Perry

et al. in 1990, where they used an immunohistochemical localization technique and a macrophage-specific antigen F4/80 and discovered that F4/80 positive cells that invade the brain during early developmental stages undergo several forms before finally transitioning into microglia[8]. However, it should be noted that initially microglia were thought to be derived from macrophage like cells that originated in the neuro-ectoderm. It was not until the work of Takashani and Naito that clearly demonstrated that microglia are derived from embryonic yolk sac progenitors during the first wave of hematopoiesis and then migrate to the brain during the early stages of CNS development[9]. More specifically in humans, microglia are thought to colonize the brain as early as the 3rd gestational week[10], with maturation and major colonization occurring between gestational weeks 12 and 35[5, 11]. In rodents, microglia colonize the brain between embryonic day 12 through 16[12, 13]. After microglia colonization of the brain parenchyma, the maturation and the survival of microglia are highly dependent on various molecules including colony stimulating factor 1 receptor (CSFR1) and transforming growth factor beta (TGFβ)[14, 15].

<u>Heterogeneity of microglia</u>

Microglia are widely distributed throughout the brain and spinal cord but are not uniformly distributed[16]. Similarly to neurons, microglia are found primarily in grey matter compared to white matter. Areas of the brain that are densely populated with microglia include the hippocampus, basal ganglia, and substantia nigra. On the other hand, less densely populated areas include the cerebellum and brain stem. The cerebral cortex demonstrates an average density of microglia. It is estimated that microglia comprise 10-12% of the cells in CNS[16].

Microglia can be classified by their morphology which varies depending on their location in the brain. Microglia that portray a rounded morphology with short, thick processes, are found in areas lacking a blood brain barrier. Microglia with longer processes are typically found in fibre tracts. More radially branched microglia are found throughout the neuropil and can be highly dynamic and complex[16]. The processes on microglia allow for consistent monitoring of their local environment, such that microglia can rapidly change their phenotype in response to any disturbance.

Microglia activation

Microglia are the resident immune cells of the CNS and can change their morphology and phenotype in response to changes in their environment[17]. Under resting conditions, microglia display a ramified appearance with long processes that extend from the cell body. In this state, resting microglia express several receptors including Cx3cr1, P2ry12, and Tmem119, which may interact with ligands that help maintain homeostasis[18]. This state is also characterized by low expression of antigen presenting surface molecules, such as major histocompatibility complex (MHC) proteins[19]. During development, resting microglia are critical for shaping the synaptic environment through selective elimination of inappropriate synapses[20]. The long processes that extend from the cell body of resting microglia allow them to constantly survey their environment in the brain. In doing this, microglia can respond quickly to signals and transform into an activated state. The morphology of activated microglia is characterized by an ameboid shape with short processes that allow the microglia to phagocytose pathogens, dead cells, and cellular debris[17, 21]. This phenotypic shift from homeostatic to activated microglia, is hallmarked by changes in signaling and gene expression that can result in the release of key molecules and factors that can be either beneficial or pathogenic (*for further explanation please see Chapter 1.3)*.

Innate immunity and molecules that mediate microglia inflammatory responses

A crucial function of microglia is the ability to generate an innate immune response. Innate immune responses are not specific to any particular pathogen but rather depend on phagocytic cells, such as microglia, to identify features of pathogens and disease/pathogen associated molecular patterns (damage-associated molecular patterns or pathogen-associated molecular patterns, respectively)[22]. Microglia are equipped with toll like receptors (TLRs) on their cell surface[22]. TLR signaling pathways lead to the activation of the transcription factor nuclear factor-kappaB (NF-ϰB), which controls the expression of pro-inflammatory cytokines[23]. Humans express 10 functional TLRs (TLR1-10) and mice express 12 (TLR1-9, TLR11-13). These TLRs play a significant role in innate immunity through the recognition of pathogen-associated stimulants. For example, TLRs on microglia, can detect lipopolysaccharide (LPS), interferon

gamma (IFN-γ), beta amyloid (Aβ), and other pro-inflammatory cytokines[22]. Upon initiation of an immune response, activated microglia can release pro-inflammatory cytokines including interleukins 1 and 6, nitric oxide synthase (NOS), Tumor Necrosis Factor alpha (TNFα), along with chemokines (CCL2, CCL5, and CXCL8)[24-26].

In addition to the release of cytokines and chemokines in response to injury or inflammation, microglia also upregulate complement receptors[19]. The complement cascade is a critical mechanism involved in innate immune response. In activated microglia, complement components (C1, C2, C3, C4) can target pathogens for phagocytosis and lysis following a series of cleavages and proteolytic steps in the complement cascade[19, 27].

<u>The relevance of lipopolysaccharide-induced inflammation</u>

The endotoxin lipopolysaccharide (LPS) is the major component of the outer membrane of gram-negative bacteria[28, 29]. Gram-negative bacteria are the cause of numerous infectious diseases that can affect both humans and animals[28]. As mentioned previously, the innate immune system is the first line of defense against pathogen or bacterial infiltration, which utilizes immune cells equipped with pattern like receptors (PRRs) that contain TLRs to detect these harmful factors. LPS is a potent pathogen-associated molecular pattern (PAMP) that activates PRRs, thus initiating a downstream signaling cascade that triggers an inflammatory response[29, 30]. More specifically, TLR4 (toll-like receptor 4) is the LPS-recognizing receptor that is expressed in several immune and non-immune cells[31, 32]. TLR4 is predominately associated with microglia in the CNS. Following LPS binding, TLR4 undergoes homodimerization and activates downstream signaling cascades, including the MyD88 and TRIF-dependent pathway[31-33]. Activation of the MyD88- or TRIF-dependent pathway leads to the activation of mitogen-activated protein kinases (MAPKs) and IkB kinases (IKKs) which in turn activate transcription factors that regulate the expression of pro-inflammatory mediators including IL-1β, IL-6, IL-8, TNF-α, NO, and type I interferons[29, 33].

LPS-induced effects can also be independent of TLR4 signaling[34]. LPS may be detected by transient receptor potential (TRP) channels, which are a superfamily of ion channels present in several cell types.

TRP channels that respond to LPS include transient receptor potential ankyrin 1 (TRPA1), transient receptor potential vanilloid 4 (TRPV4), transient receptor potential cation channel subfamily V member 1 (TRPV1), and transient receptor potential melastatin 3 and 8 (TRPM3 and TRPM8)[35]. The role of a majority of these TRP channels in LPS-induced inflammatory responses is poorly understood with conflicting opinions[35-37]. TRP channels have been found to be predominately involved in pain reactions, including neurogenic inflammation caused by LPS[38]. However, some studies investigating the TRPV4 channel, which is detected in brain cells along with TRPA1 and TRPV1, demonstrate that activation of TRPV4 can exacerbate inflammatory responses and trigger neuroinflammation[36, 39].

Another mode of pattern recognition in innate immunity is through caspases. LPS is detected intracellularly by specialized inflammatory caspases (caspase 4 and 5 in humans and caspase 11 in mice)[40]. Caspases detect cytosolic LPS and initiate cell membrane permeabilization and pyroptosis, which is an inflammatory mode of programmed cell death[41, 42]. Furthermore, LPS-activated caspases can promote the activation of NLR family pyrin domain-containing-3 (NLRP3) inflammasome and thus induce an inflammatory response[29].

LPS as a model of neuroinflammation in neurodegenerative disease; strengths and limitations

Recapitulating all neurodegenerative disease features in a model has not yet been achieved. More importantly, not every genetic model of neurodegeneration also successfully models neuroinflammation, which is a key pathological hallmark of neurodegenerative diseases, such as Alzheimer's disease, Parkinson's disease, and amyotrophic lateral sclerosis[43]. In neurodegenerative diseases, neuroinflammation can be complex, having both a beneficial and detrimental effect (*for further explanation please see Chapter 1.3*)[43]. In addition, neuroinflammation typically precedes the development of neurodegenerative pathologies[44]. Therefore, it is important to study the effect of neuroinflammation itself to understand how it can impact neurodegenerative disease. LPS is utilized as one of the most potent pro-inflammatory stimuli, therefore making it a widely used model of inflammation. The administration of LPS initiates an inflammatory response in the brain which is mainly mediated by TLR4 in microglia[45]. Several studies have shown that LPS-induced neuroinflammation can result in neurodegeneration and cognitive or behavioral

dysfunction[46, 47]. For example, Huffman et al. found that LPS-induced brain inflammation and cognitive dysfunction is reduced following percutaneous vagus nerve stimulation in mice[46]. Furthermore, systemic LPS administration in adult mice can activate microglia to continuously release proinflammatory factors and induce neurotoxicity[47]. In addition, LPS has also been shown to drive pathogenic hallmarks of AD including amyloidosis and tau hyperphosphorylation[48]. In human AD brains, LPS has been found to be elevated in the neocortex and hippocampus[49]. LPS has also been widely used in vitro with cell culture models. Data from numerous studies involving LPS treated cell cultures, demonstrate that LPS has the capacity to activate microglia, resulting in the production of pro-inflammatory cytokines and neurotoxicity[50-52].

Some of the limitations of the LPS model is that the microglial response can differ between transgenic and non-transgenic mice. For example, transgenic APP/PS1 mice exhibited diminished LPS-induced immune response with aging following LPS treatment, whereas the opposite was seen in age-matched LPS treated wild-type mice[53]. Furthermore, studies have shown that the serotype, route of administration, duration, and dose of the LPS endotoxin can produce varied results. For example, even though LPS induced inflammation typically leads to the perpetuation of neurodegenerative processes, low dose LPS pretreatment has been shown to have neuroprotective effects and alleviate inflammatory responses[54, 55]. Overall, LPS is a well-studied model to understand the impact of inflammation on neurodegenerative disease progression and pathology.

ii. Neuroinflammation in Alzheimer's disease

As previously mentioned, microglia are the resident immune cell of the CNS and can mediate neuroinflammatory responses. Inflammatory activation of microglia is a central mechanism in neurodegenerative diseases such as Alzheimer's disease (AD). Activated microglia have been shown to influence AD progression and pathology through morphological and molecular changes. This section discusses how microglia-mediated neuroinflammation contributes to AD pathophysiology.

Alzheimer's disease prevalence and genetic landscape

AD is a devastating neurodegenerative disorder that causes progressive deterioration of cognitive function and memory[56]. AD affects 44 million individuals worldwide, including more than 6 million Americans, and is ranked as the most common neurodegenerative disease and the sixth leading cause of death in the United States[57]. AD pathology is characterized by pathological protein aggregation of amyloid-β (Aβ), in the form of extracellular plaques, and tau, in the form of intracellular neurofibrillary tangles[56]. Some important risk factors for AD include age, genetics, and family history. After the age of 65, the risk of AD doubles every 5 years[58]. Even though age is the greatest known risk factor of AD, it is important to note that AD and other dementias are not a normal part of aging[58]. Genetic risk factors for AD include dominantly inherited mutations in *amyloid protein precursor (APP), presenilin-1 (PSEN1),* and *presenilin-2 (PSEN2),* with PSEN1 being the most commonly involved gene[59]. Mutations in these genes are rare and are a known cause of familial, early-onset Alzheimer's disease (EOAD)[60]. The second most commonly involved gene, *APP*, encodes the amyloid β precursor protein[60]. The amyloid β peptide is derived from the proteolytic cleavage of the amyloid β precursor protein by the β-secretase and the γ-secretase complex[60]. The aggregation of the amyloid β peptide in the brain is a key event in AD pathogenesis. *PSEN1* and *PSEN2* encode the presenilins which are homologous transmembrane proteins and are components of the γ-secretase complex[60, 61]. Patients with PSEN mutations display a significant increase in the total level of the more aggregation-prone form of the amyloid β peptide, Aβ42. Overall, EOAD mutations are associated with increased aggregation of the amyloid β peptide in the brain[61].

The most common form of AD is late-onset AD (LOAD), or commonly referred to as sporadic AD, which occurs in individuals 65 years of age and older[62]. Genetic risk factors contribute strongly to developing LOAD. The most important genetic risk factor is *APOE*[63]. Carriage of the *APOE* ε4 or ε3 alleles greatly increases the risk of developing dementia and AD[63]. Other susceptibility genes, such as *TREM2*, *SORL1*, and *ABCA7* also increase the risk of developing AD and if combined, may be useful in predicting the hazard scores for AD development[64]. LOAD has similar clinical and pathological features to EOAD but is characterized by decreased Aβ clearance rather than an over production of Aβ peptide[65]. In addition,

there are several modifiable risk factors in AD that include diabetes mellitus, hypertension, obesity, alcohol abuse, smoking, depression, and low physical activity[66].

Due to the growing prevalence of AD globally, there is an urgent need for disease modifying therapeutics to prevent cognitive decline and memory loss. Traditional therapeutic interventions involve drugs to control or reduce cognitive and behavioral symptoms associated with AD[67]. Cholinesterase inhibitors are commonly used to treat mild to moderate AD by preventing the breakdown of acetylcholine, a neurotransmitter believed to be important for cognitive function[67]. Another medication used are N-methyl-D-aspartate (NMDA) antagonists which can help decrease symptoms associated with later stages of AD[67]. Providers may also prescribe antidepressants or antipsychotics to treat behavioral symptoms associated with AD[68]. These medications only aid in managing symptoms and improving quality of life but do not modify disease course[69].

However, more recently the FDA has granted accelerated approval for the immunotherapy interventions Aducanumab and Lecanemab[70, 71]. These interventions utilize amyloid-targeting monoclonal antibodies to help reduce amyloid plaque burden[70]. In clinical studies performed in individuals with early stage AD, the amyloid-targeting monoclonal antibodies slowed the rate of cognitive decline and reduced the levels of Aβ in the brain[70]. However, life threatening side effects including increased incidence of amyloid-related imaging abnormalities (ARIA) with brain swelling or hemorrhaging have been linked with Aducanumab[72]. Therefore, expert panels have made several recommendations to mitigate potential risk and side effects, such as performing routine MRIs and to provide clear communication with patients to ensure patient-centered informed decision-making. Currently both these medications are only provided under specific situations while further clinical studies are being conducted[72].

Alzheimer's disease pathophysiology

Alois Alzheimer first described the key pathological lesions of AD in 1907[73]. Those pathological lesions are what we know today as amyloid plaques and neurofibrillary tangles. AD is a progressive neurodegenerative disease initially characterized by memory and cognitive impairment which later affects behavior, speech, movement, and balance[74]. AD is characterized by a long preclinical phase, where

individuals can be cognitively normal, but still present brain amyloid β deposition and tau pathology[75]. The model of AD pathophysiology assumes that each biomarker (Aβ, tau, neurodegeneration) follows a nonlinear course marked by sequential change, whereby amyloid β deposition precedes tau-mediated neuronal dysfunction and degeneration[75, 76]. The time between the preclinical phase and the onset of cognitive decline can be between 15-20 years[77]. In a longitudinal study conducted by Bateman et al. they found that Aβ deposition, as measured by positron-emission tomography (PET), was detected 15 years before expected symptom onset[77]. Increased concentrations of tau protein in the CSF and an increase in brain atrophy were detected 15 years before expected symptom onset[77]. There are interindividual differences that may determine when an individual transitions into the clinical phase of AD. These include environmental factors, genetics, brain and cognitive reserve, and coexisting pathologies[75]. Diagnosis of AD in the preclinical phase is dependent on cerebrospinal fluid and PET imaging state biomarkers that are grouped by amyloid-β, abnormal tau protein, or neurodegeneration[56]. Stage biomarkers can determine the severity of the AD which includes tau-PET and neurodegeneration biomarkers[56].

Pathological diagnosis of AD can be ascertained at the macroscopic and microscopic level. At the macroscopic level, AD pathology is characterized as cortical brain atrophy accompanied by enlargement of the frontal and temporal horns of the lateral ventricles[78]. Another observation is the loss of neuromelanin pigmentation in the locus coeruleus[78]. At the microscopic level, features of AD include the presence of extracellular Aβ and intracellular neurofibrillary tangles (NFTs), which are required for diagnosis[78]. As previously mentioned, Aβ plaques are formed by the extracellular accumulation of Aβ40 and Aβ42 peptides that result from the abnormal processing of APP by the β- and γ-secretases, and an imbalance in production and clearance of Aβ[78-80]. Intraneuronal NFTs result from abnormal phosphorylation (hyperphosphorylation) of tau[81]. The normal function of tau is to stabilize microtubules; however, abnormal phosphorylation of tau or the microtubule-associated protein tau (Mapt) degrades microtubules and facilitates tau aggregation into paired helical filaments, which are both thought to cause neuronal toxicity[81].

The formation and spread of extracellular deposits of amyloid protein and intraneuronal NFTs have been characterized by the Braak staging method, which was defined by German anatomist Heiko Braak in

1991[82, 83]. Braak staging focuses on the location of Aβ plaques and NFTs. In stage A, Aβ plaques develop in the basal frontal and temporal lobes[82]. From there, they spread into the association cortex and the hippocampus (stage B). In stage C, Aβ plaques infiltrate all cortical areas. Along with staging Aβ plaque formation, Braak also staged intraneuronal NFTs development[82]. In earlier stages (stages I-II), intraneuronal lesions develop initially in the transentorhinal region of the brain. Then in stages III and IV, NFTs are now present in the limbic regions, which includes the hippocampus. The appearance of clinical symptoms initiates in stages III and IV. In stages V and VI, NFTs are extensive in the neocortical regions of the brain and AD is fully developed[82].

Inflammation in aging contributes to vulnerability in prodromal Alzheimer's disease

The term "imflamm-aging" was coined by Francheschi in the early 2000s[84]. This phenomenon is described as chronic upregulation of pro-inflammatory responses that is accompanied by aging and provoked by continuous antigenic load and stressors[84]. This pro-inflammatory response is marked by increased levels of pro-inflammatory cytokines and other inflammatory molecules[85, 86]. Inflamm-aging is characterized by an age-associated reduction of T-cells resulting in a decline in adaptive immunity[87]. Another feature of inflamm-aging is an increased number of antigen experienced cells[88]. The upregulation of pro-inflammatory cytokines and reduction of the adaptive immune response are believed to exacerbate AD pathology[89]. For example, studies have shown that IFN-γ and pro-inflammatory cytokines released by microglia trigger the production and toxicity of Aβ peptide, suggesting that inflamm-aging may contribute to prodromal AD[90, 91]. Given this contribution, several observational studies have been conducted investigating the potential of anti-inflammatory drugs in lessening the risk of AD[92]. The results of these studies suggest that long term use of non-steroidal anti-inflammatory drugs (NSAIDs) may provide some protection against AD[92]. A proposed mechanism of how this may occur is by the reduction of pro-inflammatory prostanoid synthesis, since NSAIDs inhibit cyclooxygenase activity which converts arachidonic acid to prostaglandins[93, 94]. However, some studies have proposed that NSAID-mediated reduced risk of AD may be mediated through disruptions in the proteolytic processing of APP[93].

Genome Wide Association Studies implicate microglia in late onset Alzheimer's disease

Genome wide association studies (GWAS) are commonly used to identify genomic variants (single nucleotide polymorphisms or SNPs) in tens to thousands of individuals that are associated with a risk for a gene or a particular trait[95]. GWAS can also identify regions of the genome (locus) that are associated with a trait[95]. To validate GWAS results and determine the effect of a variant on gene expression and function, it is important to follow up GWAS with computational fine mapping and functional in vitro and vivo studies[95]. These functional genomic approaches also assist in determining their contribution to disease. GWAS and gene expression network analysis have helped uncover gene networks and genetic variants that are associated with late onset AD (LOAD).

GWAS have revealed that a large proportion of genes that are present within AD-associated risk loci, are expressed preferentially in microglia compared to other brain cell types[96]. These AD risk genes that are highly expressed in microglia include: *CR1*, the *MS4As*, *TREM2*, *ABCA7*, *CD33*, and *INPP5D*. Complement receptor 1 (CR1), encoded by the *CR1* gene, plays a major role in mediating microglial activity through the complement cascade which has been shown to be activated by Aβ[97]. The membrane-spanning 4-domain subfamily A, *MS4As*, have been observed at high levels in AD brains with advanced pathology[98, 99]. Rare variants in *ABCA7* and *TREM2* have also been implicated in LOAD[95]. ATP-binding cassette transporter A7 (ABCA7), encoded by the *ABCA7* gene, has been shown to be important for the clearance of Aβ aggregates via microglia phagocytosis[95]. ABCA7 is also known to transfer phospholipids to apolipoproteins, such APOE, suggesting another route whereby mutations in this gene can affect AD[100]. Variants in *ABCA7* have been associated with the risk of LOAD in African American populations[101]. On the other hand, TREM2 is a transmembrane glycoprotein and surface receptor on microglia[102]. TREM2 activation stimulates microglia phagocytosis and mobilization, whereas absence of TREM2 in an AD mouse models (*Trem2*^{−/−} mice crossed with 5XFAD transgenic mice mice), causes defective Aβ plaque clearance due to reduced microglial activity[103, 104]. Unlike the other genes previously mentioned, *TREM2* is exclusively expressed in microglia and not in other immune cells, further implicating microglia as key player in LOAD[95]. CD33, encoded by the gene *CD33*, is a myeloid cell receptor that has also been implicated in increased Aβ plaque burden[105]. Overall, GWAS and gene expression network analyses have

helped to uncover the involvement of microglia in AD pathogenesis, with the majority of the genes correlated with disrupted phagocytic activity and clearance of Aβ plaques.

Transcriptomic diversity of microglia in murine models of Alzheimer's disease and human Alzheimer's disease

As previously alluded to, microglia are highly dynamic cells that can change their morphology and phenotype in response to changes in their environment[17]. More specifically, activated microglia have been shown to influence AD progression and pathology. To understand the transcriptomic heterogeneity of microglia at different stages of AD, Keren-Shaul et al. conducted a comprehensive single-cell RNA sequencing analysis of CNS cells in neurodegenerative conditions[106]. Using a mouse model of AD that expresses five human familial AD gene mutations (5XFAD), where AD stages are accelerated, demonstrating high levels of aggregated Aβ initiating at 1.5 months of age and Aβ plaque deposition at 2–3 months of age, they were able to understand microglia dynamics during AD progression. In these studies, they uncovered a unique subset of microglia known as "disease associated microglia" or DAM, that are conserved in mice and human[106] (**Figure 1.1**). DAM express typical microglia markers such as *Iba*, *Cst3*, and *Hexb*; however, they display a reduction in the gene expression levels of several microglia "homeostatic" genes including, *P2ry12/P2ry13*, *Cx3cr1*, *Cd33*, and *Tmem119*[15]. This is contrasted by an upregulation of genes involved in lysosomal, phagocytic, and lipid metabolism pathways, such as *Apoe*, *Ctsd*, *Lpl*, *Tyrobp*, and *Trem2*[106, 107]. Furthermore, they found that DAM associate with Aβ plaques in human AD brains[106].

Interestingly, single-cell RNA-sequencing of DAM from whole brains of *Trem2*^{+/+}5XFAD and *Trem2*^{−/−}5XFAD mice along with age matched controls, demonstrated that conversion of homeostatic microglia to DAM is a two-step process involving the microglia-specific immunoreceptor, TREM2[106, 108]. Transition from homeostatic microglia to stage 1 DAM is TREM2 independent. Stage 1 DAM signaling initiates the downregulation of homeostatic microglia genes and is associated with the upregulation of genes associated with AD progression, such as *Apoe* and *B2m*, and the TREM2 adaptor *Tyrobp*. The transition from stage 1 DAM to stage 2 DAM requires TREM2 signaling and involves upregulation of lysosomal,

phagocytic, and lipid metabolism pathways (such as *Lpl, Cst7,* and *Axl*)[106]. This two-step activation mechanism of TREM2 signaling may play a role in sustaining microglia activation[108]. Further studies that applied weighted gene co-expression analysis (WGCNA) to existing microglial transcriptomic datasets from neurodegenerative disease mouse studies, demonstrated that DAM can be resolved into two profiles: an anti-inflammatory/phagocytic profile and a pro-inflammatory profile[109]. Pro-inflammatory DAM are characterized by higher expression of CD44, CD45 and Kv1.3 channels and are regulated by NFkB, Stat1 and RelA pathways[109]. On the other hand, anti-inflammatory DAM are characterized by CXCR4 expression and are regulated by LXRα/β. The AD-associated risk gene Bin1, was highly represented within the homeostatic module, suggesting its role in regulating homeostatic microglial functions which may be impacted in early AD[109]. Outside of AD-associated pathology, there have been numerous studies that support the prevalence of DAM across various models of CNS injury, inflammation, and aging[75]. Similar to mouse models, TREM2 loss-of-function mutations in humans weakens microglia activation[110].

To investigate the extent of microglia heterogeneity in microglia, Olah et al. captured individual transcriptomes from over 16,000 microglia from human AD and nonpathological cases. In this study, they identified 9 human clusters of microglia[111]. They found that several of these clusters were enriched with genes involved in neurodegenerative disease. However only one cluster (cluster 7) contained genes that were significantly altered with pathologic diagnosis of AD in the human dorsolateral prefrontal cortex and overlapped with the mouse DAM expression profile[111]. The discordance between the transcriptome of human and rodent DAM are likely driven by a multitude of factors, including biological and experimental parameters, and further emphasize the need to perform transcriptomic analyses on both murine and human samples. Overall, data from single cell RNA sequencing, human GWAS, and WGCNAs provide a framework of microglial activation in neurodegeneration that can be used to guide future therapeutic studies.

<u>Microglia signaling in Alzheimer's disease</u>

There are several signaling cascades which enable microglia to sense and respond to their extracellular environment. As mentioned in the section above, TREM2 signaling is important for complete

transformation to DAM. Moreover, TREM2 signaling is used to detect environmental cues such as ApoE, Aβ, phospholipids, and apoptotic cells[112]. TREM2 belongs to a family of receptors referred to as the triggering receptors expressed on myeloid cells (TREM) and acts predominately through its intracellular adaptor DAP12 (DNAX-activation protein 12, also known as TYROBP)[113]. TREM2 intracellular signaling is initiated when the immunoreceptor tyrosine-based activation motif (ITAM) region of DAP12 recruits the tyrosine protein kinase, Syk[114, 115]. The recruitment of Syk activates downstream signaling components including Akt, mitogen-activated protein kinases (MAPK)[115]. Mice lacking SYK have exacerbated Aβ neuropathology and worse behavioral deficits[116]. TREM2 also associates with the adaptor DAP-10 to promote the recruitment of phosphatidylinositol 3-kinase (PI3K)[117]. TREM2 has been shown to increase the rate of phagocytosis and direct microglia to injury sites[112]. TREM2 knockout mice have decreased levels of activated microglia and less internalization of Aβ by microglia[118].

As previously mentioned, TREM2 signaling can activate MAPK cascades. MAPK cascades, including the extracellular signal-regulated kinases1 and 2 pathway (ERK1/2) regulate gene transcription to promote cell proliferation, differentiation, migration, and immune function[112, 119]. Studies have shown that the MAPK/ERK pathway is a central mechanism of AD pathogenesis. For example, in the 5XFAD mouse model of AD pathology, microglia are characterized by elevated ERK signaling[119, 120]. However, ERK inhibition reduces microglial activation and pro-inflammatory response[120]. Furthermore, in a mouse model of tauopathy, deficiency of TREM2 worsens tau pathology[121].

Another key microglial signaling pathway is the complement cascade. The complement cascade is a critical effector mechanism of the innate immune system and comprises over 40 proteins[27]. Some of the earlier components of the complement cascade are shown to be involved in synapse elimination by microglia during CNS development[20]. Moreover, the complement cascade contributes to the rapid clearance of pathogens and dead or dying cells. However, the complement cascade has also been implicated in neurodegenerative disease[27]. For example, stimulus of the C1 complex by pathological proteins such as Aβ and tau, can lead to a series of activation and cleavage steps in the complement cascade resulting in synaptic

loss or neuronal damage[27, 122]. Taken together, microglia employ several complex signaling cascades in response to changes in their environment.

Figures
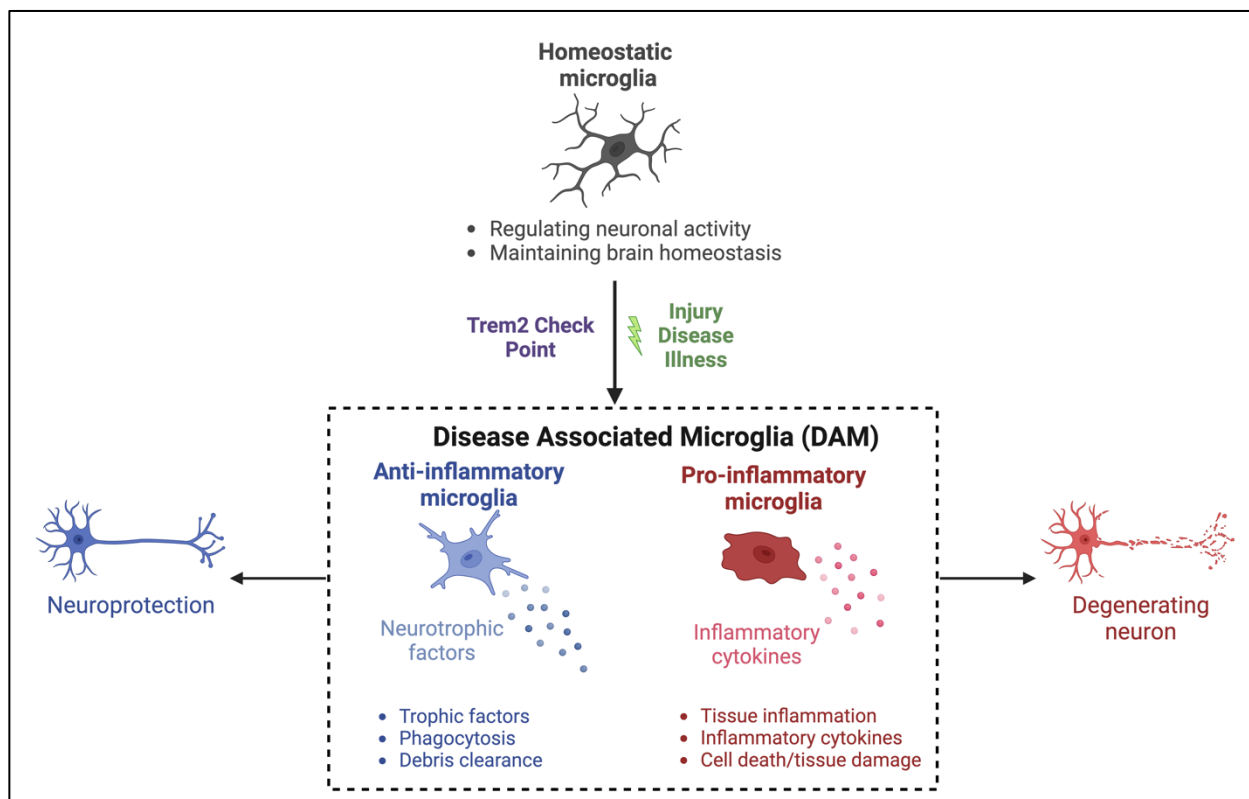
Figure 1.1: Microglial Activation. Microglia convert from a homeostatic state to a disease associated state (DAM) in response to injury, disease, or illness. Full conversion of homeostatic microglia to DAM requires Trem2 signaling. DAM can play dual roles in Alzheimer's disease (AD) pathogenesis, involving the production and release of pro-inflammatory factors including cytokines and toxic factors as well as neuroprotective, anti-inflammatory functions. This figure was created with BioRender.com.

iii.   Extracellular vesicles in neuroinflammation and neurodegeneration

As previously mentioned, the cell surface of microglia is equipped with several transporters, channels, and receptors for neurotransmitters, cytokines, and chemokines, allowing microglia to constantly survey their environment and initiate immune responses[123]. In the context of neurodegeneration, chronically activated microglia release inflammatory cytokines, such as tumor necrosis factor (TNF), IL-6, and reactive oxygen

species[124]. Furthermore, comprehensive single-cell RNA sequencing analyses have revealed novel microglia types associated with neurodegenerative diseases, also referred to as disease associated microglia (DAM)[106]. One indirect mechanism of microglia-mediated neuroinflammation may involve extracellular vesicle (EV) release, such that the molecular cargo transported by EVs can have functional effects in recipient cells by facilitating intercellular communication and influencing downstream signaling events. However, much is yet to be discovered to fully understand the role of microglia-derived EVs in neuroinflammation and neurodegeneration.

The discovery of extracellular vesicles

In the early 20th century, numerous studies came out by Erwin Chargaff and Randolph West, describing the clotting properties of platelet free-plasma, which contradicted previous work that deemed platelets necessary for blood coagulation[125, 126]. While experimenting with centrifugation methods to separate clotting factors from cells, they discovered that human plasma contains a coagulation agent that sediments at high-speed centrifugation. This was later described by Chargaff and West as a 'particulate fraction' that includes a 'thrombin agent'[125, 126]. Following this work, Hougie and O'Brien reported that platelet-rich plasma and blood serum, respectively, also contain a common coagulation agent in particulate form that sediments during high speed centrifugation[127, 128]. It would be two more decades before this particulate material would be described as the extracellular vesicle fraction that we commonly know today. In the year 1967, Peter Wolf published an article titled "The Nature and Significance of Platelet Products in Human Plasma", where he not only presented evidence supporting the work of Chargaff and West, but also introduced the term 'platelet dust'[129]. The term 'platelet dust' was used to describe the subcellular coagulant material that he observed in both plasma and serum, and originated from platelets. In this article, Wolf demonstrated that 'platelet dust' was in fact sedimented by ultracentrifugation and provided electron microscopic images of these particles[129]. Three years later, Neville Crawford furthered the work of Wolf, by publishing electron microscopy images of platelet-derived microparticles from human and animal blood[130]. He also discovered that these microparticles possess adenosine triphosphate (ATP), contractile proteins, and lipids[130]. These

groundbreaking experiments with platelets were the first to provide evidence of subcellular microparticles in plasma and blood.

Over the next several decades, scientists continued to use electron microscopy to describe these subcellular, sub-micron sized particles. H. Clarke Anderson and Ermanno Bonucci described these particles as small membrane-bound particles of different sizes and discovered them in the matrix of cartilage[131, 132]. However, Nunez et al, was the first to introduce the presence of a multivesicular body (MVB) near the plasma membrane of a cell, hinting at a subtype of extracellular vesicles that we now refer to as exosomes that are formed by the MVB fusing with the plasma membrane[133]. Simultaneously, research in the virus and cancer fields also discovered these nano-sized particles in the bodily fluids of both healthy and unhealthy patients[134-137].

Although the previously mentioned studies provided evidence for the potential existence of extracellular vesicles (EVs) in biofluids, it was not until the 1980s when the biology and characterization of EVs was interrogated. In 1983, hallmark work out of the laboratories of Phillip Stahl and R.M. Johnstone, described the formation of vesicles using a reticulocyte maturation model. Johnstone discovered that sheep reticulocytes release vesicles that are characteristic of the reticulocyte plasma membrane[138, 139]. Furthermore, it was suggested that the release of these vesicles may be by a mechanism of shedding cellular components[138]. Using the same model, Stahl's group investigated membrane trafficking and receptor-mediated endocytosis, reporting that the transferrin receptor was lost via the release of vesicles during reticulocyte maturation[139]. This seminal work led to the discovery of exosomes. For the next two decades, extracellular vesicle research expanded rapidly from beginning to characterize the proteomic cargo of EVs[140, 141] to understanding their functional role in disease and biological processes[125, 132, 142, 143]. Importantly, Ratajczak et al.[144], Skog et al.[145], and Valadi et al.[146], were the first to demonstrate that EVs can transfer nucleic acids to recipient cells as a means of intercellular communication and genetic exchange. As EV research expanded in the early 21st century, conversations regarding controversies in the field and lack of reproducibility in methods brought about the formation of the International Society for Extracellular

Vesicles (ISEV) in 2011[147]. The primary goal of the ISEV was to organize the field and establish guidelines. Despite this exponential growth in the EV community, there is still much to investigate on EV biology and their significance in disease pathogenesis and therapeutics.

Extracellular vesicles biogenesis, composition, and secretion

EVs are lipid bound vesicles that are released by cells into the extracellular space. EVs can be found in a variety of biofluids such as blood, cerebrospinal fluid, urine, breast milk, and saliva[148]. EVs are classified into three subtypes: microvesicles, exosomes, and apoptotic bodies, and differ based on their biogenesis, size, release mechanism, cargo, and function[149]. Microvesicles are 100 nanometers (nm) – 1 micrometer (μm) in size and bud directly from the plasma membrane of the cell[150]. Exosomes are 50 – 150 nm in size and come from an endocytic origin in which a multivesicular body (MVB), which contains intraluminal vesicles (ILVs), fuses to the plasma membrane, releasing the small vesicles into the extracellular space[148] (**Figure 1.2**). Vesicular apoptotic bodies are between 50 nm –2 μm in size and are released by dying cells[140]. Different EV subtypes can share similar size and density making differentiation of EV subclasses highly challenging[151]. Since EV isolation methods cannot ensure specific enrichment of only one EV subpopulation without contamination of another, the EV field collectively refers to all vesicles released by cells as EVs[151]. EVs also share comparable size and density to lipoproteins (high-density lipoprotein (HDL) and low-density lipoprotein (LDL))[152]. However, EV membranes contain a lipid bilayer unlike single layered lipoproteins[153].

In the process of exosome biogenesis, internalized cargo is sorted into early endosomes and then later into MVBs, or late endosomes, that contain ILVs which sequester cargo before being secreted as exosomes[154]. Cytosolic and microtubule proteins assist in transporting MVBs to the plasma membrane, while ESCRT machinery, SNARE proteins, and Rab GTPases, aid in ILV secretion[154, 155]. Endosomal sorting complexes required for transport (ESCRT) machinery is a multi-subunit system in the cytosol and is essential for vesicle budding and cargo sorting[155]. ESCRT machinery is dependent on ubiquitination with ubiquitin binding ESCRT proteins like STAM1 and TSG101 all having a critical role in exosome

biogenesis[156]. The loss of ESCRT subunits has been shown to reduce exosome secretion in several cell types[157]. In addition to ESCRT machinery, complex lipids such as ceramides contribute to exosome biogenesis[158]. Ceramides contribute to the inward budding process of the plasma membrane to form ILVs[158]. Sphingomyelinase is the enzyme that breaks down sphingolipid into ceramide[154]. Studies using a sphingomyelinase inhibitor, such as GW4869, reveal a reduction in exosome biogenesis and release[159]. ESCRT-dependent and ESCRT-independent ceramide mediated exosome biogenesis is cell type dependent, such that disruption of one of these pathways may not affect exosome production by a cell[154].

Apoptotic bodies are composed of DNA fragments, cytosol portions, and degraded proteins. Exosomes and microvesicles are composed of lipids, nucleic acids (messenger RNA, microRNA, non-coding RNA, DNA), and proteins. Exosomes are also comprised of multiple lipids such as cholesterol, ceramides, sphingomyelin, phosphatidylinostol, phosphatidylserine, phosphatidylcholine, phosphatidylethanolamine, and gangliosides, which contribute to exosome rigidity, structure, and secretion[153]. Typical constituent proteins of exosomes include transmembrane proteins such as tetraspanins (CD9, CD63, and CD81), antigen presenting molecules (MHC Class I and MHC Class II), glycoproteins and adhesion molecules, heat shock proteins (Hsp), cytoskeletal proteins, ESCRT components (TSG-101 and Alix), membrane transport, fusion proteins, growth factors and cytokines[148, 160] (**Figure 1.2**). Transfer of these proteins can drive phenotypic and functional changes in recipient cells. RNA species that are enriched in EVs are predominately shorter in size (< 200 nucleotides), such as microRNAs (miRNAs) and non-coding RNAs[154, 161]. However, messenger RNA (mRNA) is also enriched in EVs[154]. Interestingly, a few studies have shown that mRNAs encapsulated in EVs can be functional in recipient cells by being translated into proteins[146, 162, 163]. MiRNAs transported by EVs may regulate gene expression in recipient cells by regulating the translation of target mRNAs[161, 164]. The RNA species found in EVs originate in the nucleus of the donor cell and following enzymatic processing, they are then loaded into MVBs via ESCRT-dependent or ESCRT-independent pathways, as discussed above[161].

The cargo released by EVs can be functional and facilitate cell to cell communication and downstream signaling events in a recipient cell[154]. More importantly, EV mediated release of mRNAs and microRNAs can be a mechanism of genetic exchange between cells[146].

<u>Extracellular vesicle transport and uptake</u>

Targeting of EVs to recipient cells is primarily mediated by the surface composition of the vesicle. For example, EV transmembrane proteins such as tetraspanins, can strongly influence target cell binding through tetraspanin-integrin interaction[165]. Although uptake of EVs can be non-specific[166], studies have shown that recipient cells of the same origin as donor cells, can identify cellular signatures that are conserved in the secreted EVs, thus promoting their uptake[167]. For example, cancer cells can target other cancer cells of the same origin through the presence of mannose- and sialic acid- enriched glycoproteins on the EV surface[168]. In addition, the presence of certain receptors on the surface of EVs, such as CD47, can contribute to evasion from the host immune cells[154, 169]. This mechanism has been employed in the development of anticancer therapies by engineering EVs to display "eat me" or "don't eat me" surface receptors[169].

Once released into the extracellular space, EVs can interact with the recipient cell via different mechanisms, including phagocytosis, endocytosis, direct interaction with cell surface molecules, or fusion with the plasma membrane[149]. As previously mentioned, transmembrane ligands on the surface of the EV can directly bind with surface receptors on the recipient cell inducing a downstream signaling cascade[154]. This is commonly seen with dendritic cell derived EVs, where they can activate T lymphocytes and stimulate T cell proliferation with the expression of MHC class molecules[170, 171]. EVs can also fuse with the plasma membrane and release their contents into the cytosol of the recipient cell[154]. This process is likely mediated by SNAREs and Rab proteins that assist in mediating the fusion of the lipid bilayers and is typically adopted by tumor cells[172, 173]. The last mechanism of interaction and most common, is internalization which can occur through endocytosis or phagocytosis. EVs can be internalized by clathrin-mediated endocytosis, lipid-raft mediated endocytosis, caveolin-mediated endocytosis, phagocytosis, or micropinocytosis[149, 154]. Clathrin-mediated endocytosis involves the uptake of transmembrane receptors and

transporters and occurs via the step wise assembly of clathrin-coated vesicles[174]. Clathrin-mediated endocytosis is a common EV uptake mechanism and occurs in most cell types including macrophages, epithelial cells, and neural cells[174]. Lipid-raft mediated endocytosis is another common mechanism of EV uptake and involves complex lipids including cholesterol, sphingolipids, and glycosylphosphatidylinositol (GPI)-anchored proteins[175]. Caveolin-mediated endocytosis is similar to clathrin-mediated endocytosis such that they both involve vesicle scission following plasma membrane invagination[176]. However, caveolin-mediated endocytosis involves the integral membrane protein caveolin, which creates a small invagination in the plasma membrane known as caveolae[176]. Phagocytosis, a mechanism of EV uptake commonly used by immune cells, is where EVs are engulfed and contained by phagosomes[177]. Phagosome closure is dependent on the actin cytoskeleton and the phosphatidylinositol-3-kinase (PI3K) and phospholipase C (PLC) enzymes[177]. Lastly, micropinocytosis involves the use of lamellipodia to promote plasma membrane invagination that will get pinched off into a macropinosome[178]. Once internalized by the recipient cell, EV content is addressed into an early endosome, then MVB and can undergo multiple fates[154]. The contents of the EV can be released into the nucleus or endoplasmic reticulum (ER), leak into the cytosol, or get targeted to lysosomes for degradation[154]. The ER would be a desirable route for EVs containing mRNAs and miRNAs to facilitate translation and regulate gene expression.

Methods of isolating extracellular vesicles

There are numerous methods to isolate EVs including separation by size, charge, and affinity. As mentioned before, overlap in size and density of extracellular vesicles causes challenges in isolating specific subpopulations of EVs. However, additional steps can be added to improve isolation and characterization of EV samples. The most common isolation techniques include ultracentrifugation, size-exclusion chromatography, ultrafiltration, precipitation, and immunoaffinity capture[160]. Ultracentrifugation was the first method used to isolate EVs and is the most commonly used method. Ultracentrifugation involves separating EVs based on size and density with the use of a gradient where larger and more dense particles sediment out first[179]. Although this method can facilitate large sample volumes, purity and recovery of EVs are low due to high-speed centrifugation[180]. Size exclusion chromatography, the method the author of this

thesis used to isolate EVs (**Figure 1.3**), separates EVs based on their size. This method involves a column made of resin that is packed with a porous stationary phase in which small particles can penetrate[181]. The resin slows down the movement of the smaller particles through the tube, causing them to elute later in the gradient, and allowing larger particles to elute first. These resins come in different sizes (35nm and 75nm) to enable optimal isolation of EV subpopulations[182]. Some advantages of size exclusion chromatography include preservation of vesicle purity and quality, but this method is not easily scalable compared to ultracentrifugation[181, 182]. However, new columns being developed by iZON science may enable larger scale experiments with higher precision and isolation speed[182]. The utilization of size exclusion chromatography has rapidly increased over the past decade[152]. Another size-based technique is ultrafiltration which separates EVs based on their molecular weight. This technique filters samples using a molecular weight cut off (MWCO) where particles larger than the MWCO are retained by the filter and smaller particles are passed through[160, 183]. Ultrafiltration can be combined with size exclusion chromatography to optimize EV yield and purity[152, 183]. However, one downside to this method is loss of EVs in the filter unit due to clogging or deformation of EVs caused by harsh centrifugation[160]. Immunoaffinity capture based techniques rely on the use of an antibody that targets EVs based on the expression of an antigen on the surface of the EV[180]. Common target antigens are tetraspanins (CD9, CD63, or CD81) which are highly enriched in EVs. This method has the potential to isolate exosomes from other EV subpopulations; however, this would require using a surface protein marker that is exclusive to exosomes only[183]. This method is executed using a biotinylated antibody against the antigen of interest that can then attach to the surface of streptavidin coated magnetic beads[160, 183]. Immunoaffinity capture based isolation methods result in higher EV purity compared to other methods, but lower EV yield[183]. Lastly, another method of EV isolation is precipitation which is typically performed by introducing polyethylene glycol (PEG) into the sample causing EVs to precipitate. To avoid contamination of other precipitated materials, this method needs to be combined with other isolation techniques such as filtration or ultracentrifugation[160].

The role of extracellular vesicles in neurodegenerative disease

In the past decade, research has identified a role for EVs in disease processes such as inflammation and cell death[184]. Neurodegenerative diseases, including Parkinson's disease, Alzheimer's disease, and amyotrophic lateral sclerosis, are associated with pathological protein misfolding and deposition. A common feature among these neurodegenerative diseases is the prion-like spread of pathogenic proteins[185]. EVs have been shown to carry many different proteins associated with neurodegenerative disease, including α-synuclein in Parkinson's disease and tau and Aβ in AD[186, 187] and may be implicated in intercellular spread of these proteins[184]. In the context of AD, in vitro studies have shown that EVs can contain the neurotoxic forms of Aβ or tau and facilitate intercellular propagation of these pathogenic proteins[186, 188]. In vivo studies using the 5xFAD mouse model revealed that exosome reduction induced by inhibition of neutral sphingomyelinase 2 (nSMase2), contributes to lower amyloid plaque load[189].

To further investigate the role of EVs in neurodegenerative disease, it is critical to isolate EVs from different CNS cell types including neurons, astrocytes, microglia, and oligodendrocytes. This can be achieved by the use of immortalized or primary cell cultures and in-vivo systems. For example, Yuyama et al., reported that infusion of neuronal exosomes into the brains of APP transgenic mice decreased amyloid depositions by sequestering Aβ[190]. Additionally, collection of EVs from cerebrospinal fluid (CSF) or blood can be a suitable source of biomarkers for neurodegenerative disease diagnosis before clinical onset[191]. Clinical studies have shown that exosomes derived from the blood and CSF of AD patients contained significantly higher levels of total tau (pT181-tau and pS396-tau) and Aβ than case controls[191, 192].

EVs have also been shown to mediate inflammation which is a common pathological hallmark of most neurodegenerative diseases. EVs can transfer inflammatory molecules to recipient cells and initiate an inflammatory cascade[193]. In addition, EVs can transfer dysregulated miRNAs to recipient cells thus suppressing expression of genes that may mediate inflammatory responses[193]. For example, Alexander et al. reported that miR-155 and miR-146a released from dendritic cells and taken up by recipient dendritic cells can promote or inhibit endotoxin-induced inflammation, respectively[194]. Overall, these studies suggest

that EVs may be involved in the pathogenesis of neurodegenerative diseases and may provide novel therapeutic targets for the treatment of neurodegenerative diseases.

Microglia-derived extracellular vesicles

*This section includes a self-written section of a coauthored review publication that was published in the journal *Proteomics* on April 15th, 2023. DOI https://doi.org/10.1002/pmic.202200183.

Specific co-author contribution: writing, reviewing, and editing. Full citation below.

Sunna S, Bowen CA, Ramelow CC, Santiago JV, Kumar P, Rangaraju S. Advances in proteomic phenotyping of microglia in neurodegeneration. Proteomics. 2023:e2200183. Epub 20230415. doi: 10.1002/pmic.202200183. PubMed PMID: 37060300.

Accumulating studies have demonstrated that microglia-derived EVs can serve as key mediators in pathologies associated with neurodegenerative diseases. Proteomic analysis of exosomes derived from the N9 microglial cell line identified the composition of microglia-derived exosomes from cell culture medium[195]. Several of the proteins identified in mass spectrometry experiments were previously identified in dendritic-cell (DC) derived exosomes, such as cytoskeletal proteins, heat shock proteins, integrins, and tetraspanin proteins. Of particular interest, was the aminopeptidase N or CD13 found in microglial exosomal proteins but not in exosomes derived from B cells and DC cells. Functional assays looking at aminopeptidase activity revealed that microglia exosomal CD13 is active in neuropeptide degradation.

Yang et al. characterized microglial EV protein cargo following LPS and tumor necrosis factor (TNF) inhibitor treatment[196]. Following LPS activation of BV2 microglial cell line, EVs were found to have significantly elevated levels of pro-inflammatory cytokines TNF and interleukin (IL)-10, seen by ELISA. Furthermore, inhibition of the TNF signaling pathway resulted in a reduction of EVs released from LPS treated microglia. Mass spectrometry experiments identified 49 unique proteins in EVs derived from LPS treated microglia compared to control, with most of the proteins associated with transcription and translation. From this study, it can be inferred that microglia respond to an LPS challenge by releasing EVs with unique cargoes that may be implicated inflammatory mechanisms.

The data from both these studies suggest that microglia-derived EVs have distinct proteomic profiles which may play a role in inflammatory responses in neurodegenerative diseases. Asai et al. found that microglia-derived exosomes can release and spread pathologic tau between neurons. Furthermore, depletion of microglia and inhibition of the synthesis of exosomes in a tau mouse model of AD significantly suppressed pathologic tau propagation[186]. This study indicates the role microglia-derived exosomes may have in the pathological spread of tau. Verderio et al. found that microvesicles and exosomes derived from LPS-preactivated cultured microglia cells, induced a dose-dependent activation resting of astrocytes and microglia[197]. The findings of this study suggest that the cargo from microvesicles and exosomes can transfer an inflammatory signal to recipient cells, thus exacerbating neuroinflammatory conditions.

However, the specific cargo within microglia-derived EVs that lead to the perpetuation of AD pathology remain unknown, thus highlighting the need of omics studies on EVs. Proteomic and transcriptomic studies of microglia-derived EVs could also yield unique markers of homeostatic microglial and disease associated microglia (DAM)-derived EVs to guide exosome isolation from tissues including biofluids as disease biomarkers[198].

Figures
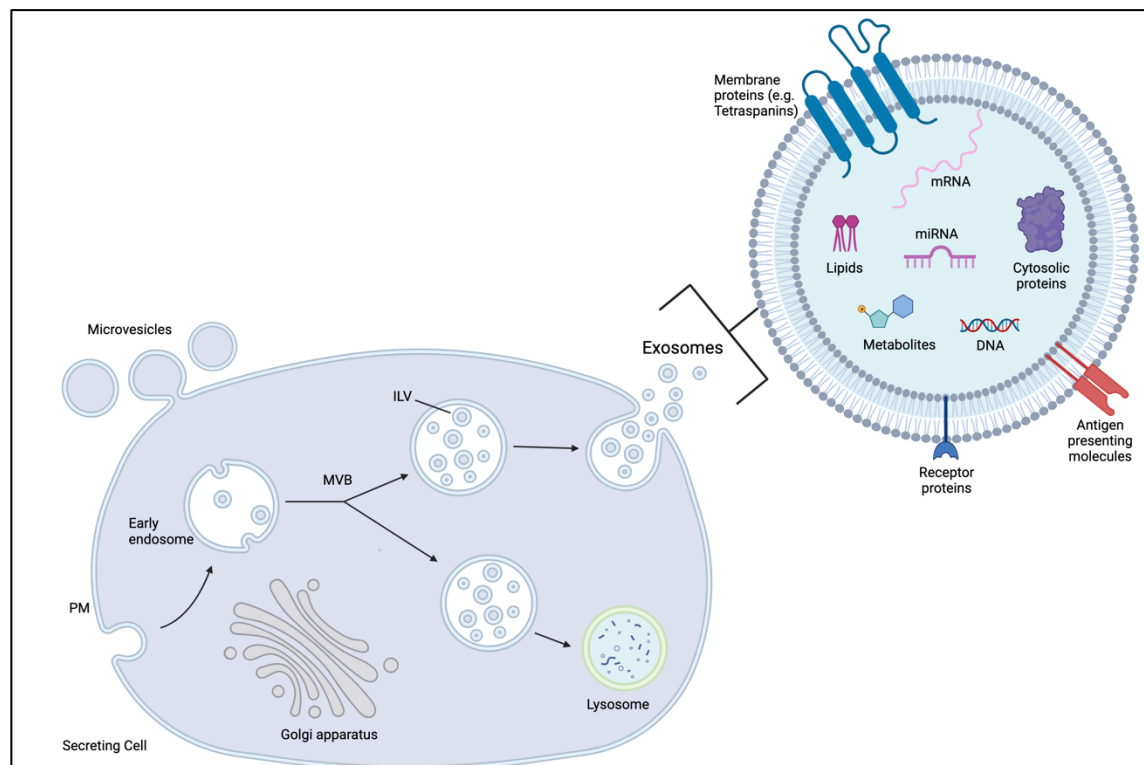
Figure 1.2. Exosome biogenesis and content. Exosomes, or small extracellular vesicles, come from an endosomal origin where multivesicular bodies (MVBs), or late endosomes, containing intraluminal vesicles (ILVs) are either targeted to the plasma membrane to be released as exosomes into the extracellular space or are targeted to the lysosome for degradation. Exosomes contain various cargo including nucleic acids, lipids, metabolites, and proteins. This figure was created with BioRender.com.
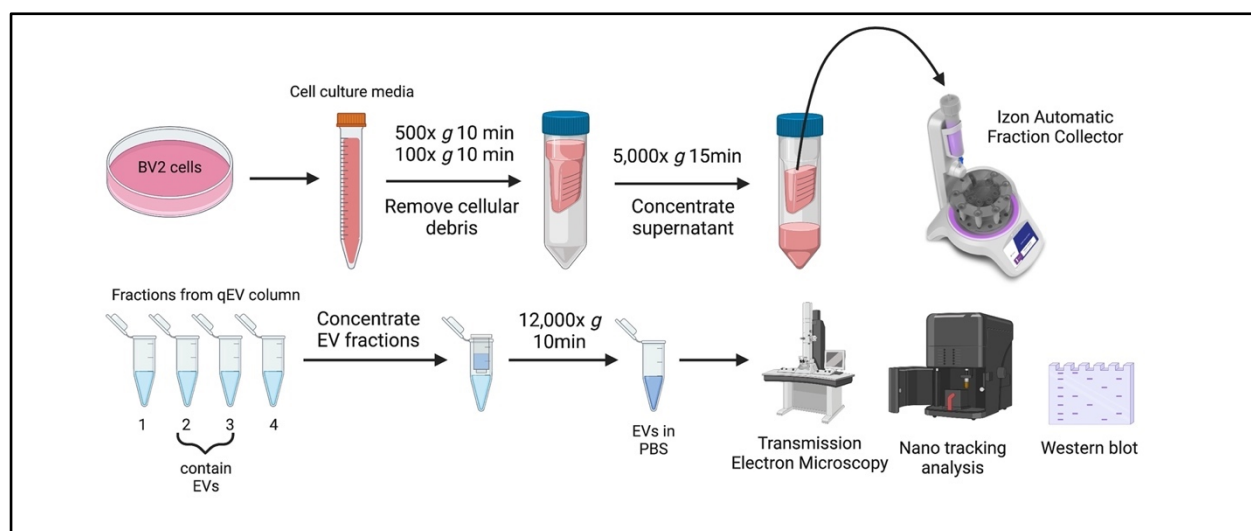
Figure 1.3. Size exclusion chromatography EV isolation strategy used to isolate EVs from cell culture medium. Serum-free cell culture media is collected and spun numerous times to remove cellular debris. The supernatant is then concentrated using an amicon filter (MWCO = 100k). The concentrated supernatant is then loaded into the column of the Izon Automatic Fraction Collector and fractionated based on size. The fractions containing EVs are then concentrated further using an amicon filter. EV size, concentration, and purity can be assessed using transmission electron microscopy, nano tracking analysis, and western blot. This figure was created with BioRender.com**.**

iv.   Proteomic interrogation of glia

Bulk brain proteomic studies

Interrogation of the molecular profile of microglia has predominately been done using transcriptomic analyses. However, it is important to note that poor concordance is observed between the transcriptome and the proteome, especially in the CNS[199]. Proteins are the biological effectors of the cell and can undergo post translation modifications (PTMs) that may regulate protein function and location, but cannot be captured by transcriptomics[119]. These challenges necessitate complimentary transcriptomic and proteomic analyses of bulk brain tissue to further understand disease processes and cellular contributions[119, 200]. Network proteomic analysis of bulk brain tissue can be achieved using quantitative mass spectrometry (MS) based approaches such as label free quantitation (LFQ) or isobaric labeling[201]. These techniques can be used for protein identification and quantification of human postmortem brain tissues, including those from control, asymptomatic AD (asymAD), and AD cases[201]. These MS based approaches are combined with bioinformatics approaches, such as WGCNA, to identify modules of co-expressed proteins and correlate module-level abundance profiles to various phenotypic traits of disease [202].

Seyfried et al. utilized these multi-network approaches across 129 human cortical tissue samples to identify protein level changes associated with asymAD and symptomatic AD[203]. Using label-free 'single shot' proteomics and WGCNA, they identified 16 modules of co-expressed proteins, 10 of which correlated with AD phenotypes. Furthermore, they observed that AD genetic risk loci were concentrated in glial-related modules in the proteome and transcriptome consistent with prior studies implicating their role in AD[203]. These approaches have also been used in large scale studies with over 2,000 brains and nearly 400 cerebrospinal fluid samples which were derived from asymAD or AD cases[204]. In this study they identified

a module of proteins (M4) that was linked to sugar metabolism and significantly associated with AD pathology and cognitive impairment. Upon further investigation, they found that this module contained several AD associated risk factors including MSN, PLEC, ITGB1, PRDX1, and CD44[204]. Moreover, glycolytic proteins including LDHB, PKM, and GAPDH, proteins associated with glycolytic flux including PRDX1, DDAH and PARK7, and glial proteins including CASP1, SPP1, and MAPK1, were also highly represented in this module[204]. They also found that both astrocytic and microglial markers present in this module are generally considered to be protective or associated with anti-inflammatory DAM[109, 204]. On the other hand, another module (M3) that was decreased in AD, was enriched in mitochondrial proteins, including electron transport activity (ATP1A3) and NADH dehydrogenase activity (NDUFA9 and NDUFA10)[204]. The observed decrease in mitochondrial proteins and increase in glycolytic proteins suggest that metabolic reprogramming in glial cells, known as the Walburg effect, is associated with AD pathology[204, 205]. This study highlights the importance of investigating microglia as a key driver in AD pathogenesis.

These network-based proteomic approaches have helped shape our understanding of protein specific pathways involved in the initiation and progress of AD. However, proteomic analysis of bulk human brain tissue has its limitations. One limitation is the inter- and intra-regional variability found throughout brain tissue, which can result in poorly representative results, especially in the context of disease pathology[206]. This challenge can be overcome with comparison to large scale system-based proteomics from a variety of brain regions and cohorts[207]. Another limitation of bulk brain proteomic studies is that they do not directly resolve cell-type specific biology. Instead, this approach indirectly infers cellular mechanisms based on cell-type specific markers. However, these cell-type specific markers may not fully reflect phenotypic shifts that cells undergo during disease processes[206].

Isolation-based proteomic strategy limitations

Isolation-based proteomic methods may resolve limitations of bulk brain proteomics studies by capturing the individual proteomes of cell populations relative to a disease state, brain region, or microenvironment. Isolation of a cell from other cell types requires fresh brain tissue that undergoes

mechanical or enzymatic dissociation followed by fluorescence-activated cell sorting (FACS), magnetic activated cell sorting (MACS), or immunopanning approaches[119, 206]. All of these methods utilize antibodies against cell-type specific surface proteins to positively identify and purify the cells. In the case of microglia, MACS isolation with CD11B+ beads typically yields between 100,000–200,000 live microglia from one adult mouse brain while FACS-based purification yields 50,000–100,000 CD11B+ CD45 intermediate microglia from one adult mouse brain[119, 206, 208]. FACS-based microglial isolation from post-mortem human brain tissue requires using a combination of markers such as CD11B and CD45, along with other lymphocytes, monocyte, and neutrophil markers[119]. Advantages of MACS include high throughput and purity and quick isolation procedure time. A disadvantage of MACS is protein contamination from other cell types[206]. Advantages of FACS include potential for simultaneous isolation of several cell types with multiple fluorescent antibodies and high sensitivity and purity. Whereas disadvantages include long isolation procedure time and high cell loss[206]. Lastly, incubation with antibody-coated plates, or immunopanning, results in high purity but also takes a long time to isolate and is expensive. Most importantly, the limitations across all three approaches are shear stress artifacts and unwanted cell activation[119, 206].

Another challenge with these methods is identifying comprehensive microglial markers since microglia are highly dynamic cells and can alter their phenotype in response to their environment. For example, under homeostatic conditions mouse microglia typically express high CD11B-positive (+) and low levels of CD45 and Ly6c on the cell surface. Whereas non-microglial macrophages express high levels of CD45 and Ly6c under homeostatic conditions[209, 210]. Furthermore, with increased pathology canonical microglia markers such as Tmem119, are decreased[211]. However despite these challenges, studies utilizing these approaches have been able to determine the relative impact of Aβ pathology and neuroinflammation on the microglial proteome in the mouse brain[119, 212, 213].

Emerging proteomic labeling strategies

Traditional isolation-based proteomic approaches require harsh reagents or mechanical dissociation that may alter the state of the cell, thus imposing artifacts in the study. These limitations along with others,

have led to the development of labeling methods that can capture the native proteomic signatures of cells in vivo. In vivo proteomic labeling strategies include bio-orthogonal non-canonical amino acid tagging (BONCAT) and proximity-dependent biotinylation methods[206].

BONCAT is a method of labeling newly synthesized proteins with a methionine (Met) analogue using a mutated Met tRNA synthetase (MetRS*, mutation L274G)[214]. In the presence of the mutant MetRS, nascent proteins incorporate azidonorleucine (ANL), a methionine analogue with a "click"-able azide residue[214]. ANL can then undergo "click" chemistry in which ANL-tagged protein residues are "clicked" with a PEG-biotin-alkyne. MetRS* labeled proteins can later be purified by means of streptavidin-based affinity capture[214]. This method can be extended in-vivo by inserting mutant MetRS (L274G or MetRS*) into the *Rosa26* locus to generate in vivo proteomic labeling in mouse models. For example, BONCAT has been successful in labeling the nascent proteome of excitatory and inhibitory neurons[215] along with astrocytes in vivo[216]. Some disadvantages of BONCAT is the cost of ANL and special diet for mouse studies and the signal-to-noise ratio between endogenously biotinylated proteins and biotin clicked ANL-tagged proteins[206].

Proximity-dependent biotinylation methods enable global labeling of a cellular proteome rather than a nascent proteome. These methods utilize biotin ligases, such as TurboID and BioID, that can efficiently label proteomes of interest in close proximity[217, 218]. More specifically, TurboID is a highly promiscuous enzyme that is engineered to biotinylate proteins within minutes and within a 10 nm radius[218]. Cytosolic proteomic labeling of cells can be achieved when TurboID is fused to a nuclear export sequence (TurboID-NES). Sunna et al. generated murine neuroblastoma (N2A) and microglial (BV2) lines stably expressing TurboID-NES to biotinylate the cytosolic cellular proteome of these cells[219]. MS analyses from this study revealed that TurboID can label endolysosome, translation, vesicle, and signaling proteins in BV2 microglia and synaptic, neuron projection, and microtubule proteins in N2A neurons, providing efficacy and biological relevance of this approach[219]. To extend this in vivo, TurboID-NES is inserted into the *Rosa26* locus of mice, for conditional TurboID expression in cell type or tissues of interest. Some

disadvantages of proximity labeling include noise introduced by endogenously biotinylated proteins and possible saturation of proximal labeling sites following biotin supplementation[206].

Cell-type specific biotin labeling in vivo

Proximity-dependent biotinylation methods can be expanded to cell-type specific in vivo biotinylation of proteins (CIBOP), by expressing TurboID under cell-type specific promoters[201]. By expressing *Cre*-recombinase under astrocyte-specific and neuron-specific promoters (*Aldh1l1* and *Camk2a*, respectively), and crossing this mouse with a *Rosa26-floxSTOP-TurboID* mouse, TurboID-NES expression was induced in *Camk2a* positive excitatory neurons and *Aldh1l1* positive astrocytes in the adult mouse brain[201]. In this study, Rayaprolu et al. successfully enriched biotinylated proteins from total brain homogenates and captured neuronal and astrocyte proteomes (>2,000 proteins in each cell type) by MS and identified >200 proteins that differentiated neurons and astrocytes[201]. The *Rosa26-floxSTOP-TurboID* mice that were generated from this study represents a promising approach for global cellular proteomics of other cell types, such as microglia, in their native state in vivo[201]. These methods could be applied for in vivo cell type-specific proteomics in animal models of neurodegeneration to complement prior studies using isolation based strategies and further elucidate the role of certain brain cells in diseases processes.

v.   Summary

In summary, studies have demonstrated that microglia play important roles in mediating inflammatory responses in several neurodegenerative diseases via direct and indirect mechanisms. One indirect mechanism of microglia-mediated neuroinflammation may involve EV release, such that the molecular cargo transported by EVs can have functional effects in recipient cells by facilitating intercellular communication and influencing downstream signaling events. Some studies have shown evidence that microglia can contain and transport pathogenic proteins (e.g. Aβ and tau) and nucleic acids that are involved in neurodegenerative disease pathogenesis. However, there is a lack of proteomic and transcriptomic characterization of EVs from distinct microglia states both in vitro and in vivo. Identification of the proteomic and transcriptomic cargo in EVs from distinct microglia states may elucidate key targets and

pathways that are involved in EV mediated neuroinflammation. With that in mind, two general questions guided my thesis work:

What is the effect of microglial state on EV composition and EV-mediated responses in vitro?

Can we label the proteome of microglia and their EVs using a cell-type specific in vivo biotinylation of proteins (CIBOP) approach by expressing TurboID under a microglia promoter?

II. Chapter 2. Identification of state-specific proteomic and transcriptomic signatures of microglia-derived extracellular vesicles

i. Abstract

Microglia are resident immune cells of the brain that play important roles in mediating inflammatory responses in several neurological diseases via direct and indirect mechanisms. One indirect mechanism may involve extracellular vesicle (EV) release, so that the molecular cargo transported by microglia-derived EVs can have functional effects by facilitating intercellular communication. The molecular composition of microglia-derived EVs, and how microglial activation states impacts EV composition and EV-mediated effects in neuroinflammation, remain poorly understood. We hypothesize that microglia-derived EVs have unique molecular profiles that are determined by microglial activation state. Using size-exclusion

chromatography to purify EVs from BV2 microglia, combined with proteomic (label-free quantitative mass spectrometry or LFQ-MS) and transcriptomic (mRNA and non-coding RNA seq) methods, we obtained comprehensive molecular profiles of microglia-derived EVs. LFQ-MS identified several classic EV proteins (tetraspanins, ESCRT machinery, and heat shock proteins), in addition to over 200 proteins not previously reported in the literature. Unique mRNA and microRNA signatures of microglia-derived EVs were also identified. After treating BV2 microglia with lipopolysaccharide (LPS), interleukin-10, or transforming growth factor beta, to mimic pro-inflammatory, anti-inflammatory, or homeostatic states, respectively, LFQ-MS and RNA seq revealed novel state-specific proteomic and transcriptomic signatures of microglia-derived EVs. Particularly, LPS treatment had the most profound impact on proteomic and transcriptomic compositions of microglia-derived EVs. Furthermore, we found that EVs derived from LPS-activated microglia were able to induce pro-inflammatory transcriptomic changes in resting responder microglia, confirming the ability of microglia-derived EVs to relay functionally-relevant inflammatory signals. These comprehensive microglia-EV molecular datasets represent important resources for the neuroscience and omics communities, and provide novel insights into the role of microglia-derived EVs in neuroinflammation.

ii.   Introduction

Microglia are the resident immune cells of the central nervous system (CNS). Given their major role in the innate immune system, the cell surface of microglia contains transporters, channels, and receptors for neurotransmitters, cytokines, and chemokines[210]. Microglia are constantly surveying their environment and can rapidly become activated to initiate immune responses[123]. Detection of immune activators and stimulating agents can cause microglia to alter their morphology and adopt heterogenous molecular profiles which can exert complex functions in different disease contexts. For example, microglia play an important role in neurodegenerative disease and neuroinflammation[96]. In the context of neurodegeneration, chronically activated microglia release inflammatory cytokines, such as tumor necrosis factor (TNF), IL-6, and reactive oxygen species. Furthermore, to detect immune activators, microglia are equipped with toll-

like receptors (TLRs). Activation of TLRs on microglia can lead to the production of pro-inflammatory cytokines and release of chemokines[124]. Comprehensive single-cell RNA sequencing analyses have revealed novel microglia types associated with neurodegenerative diseases, also referred to as disease associated microglia (DAM)[106]. This subset of microglia displays unique transcriptional features, expressing typical microglial protein markers, such as Iba1 and Hexb but with a decrease in signature microglia homeostatic genes, such as *Cx3cr1* and *P2ry12/13*, and upregulation of genes involved in lipid metabolism and phagocytic pathways, such as *Apoe, Lpl, CD9, Cst7,* and *Trem2*. Furthermore, DAM can play dual roles in Alzheimer's disease (AD) pathogenesis, involving the production and release of pro-inflammatory factors including cytokines and toxic factors as well as neuroprotective, anti-inflammatory functions[109]. While distinguishing the function of microglia as either "protective" or "detrimental" is difficult, there is accumulating evidence that microglia can dynamically switch phenotypes in response to stimuli. However, further investigation is needed to fully understand the involvement of different microglia states in CNS diseases.

A newly identified mechanism of microglia-mediated neuroinflammatory responses in neurodegenerative disease involves secretion of extracellular vesicles (EVs)[220]. EVs are lipid bound vesicles that are composed of lipids, proteins, metabolites, and nucleic acids. EVs can be classified as microvesicles, apoptotic bodies, or exosomes[160]. EV subtype is determined by biogenesis, release pathway, size, density, function, and cargo. However, due to significant overlap in protein profiles and size, along with difficulty in proving the origin of EVs, it is often preferred to refer to exosomes as EVs within a particular size range[221, 222]. Exosomes are small EVs (30-150 nm) of endocytic origin and are secreted by almost all cell types. Exosomes transport specific cargo such as proteins, messenger RNAs (mRNAs), and microRNAs (miRNAs) between cells to facilitate intercellular communication and influence downstream signaling events[148]. Exosomes can interact with recipient cells through endocytosis, fusion with the plasma membrane, or ligand receptor interaction[223]. Accumulating studies have demonstrated that microglia-derived exosomes can serve as key mediators in pathologies associated with neurodegenerative diseases. However, the molecular compositions of microglia-derived small EVs remain poorly understood.

Classical hallmarks of AD are abnormal aggregation of amyloid beta (Aβ) proteins into plaques and tau misfolding[224]. Microglia-derived exosomes in tau models of AD, release and spread pathologic tau between neurons. Recent evidence suggests that depleting microglia and inhibiting the synthesis of exosomes significantly suppresses pathologic tau propagation[186]. This study indicates the role microglia-derived exosomes may have in the pathological spread of tau. Verderio et al. found that microvesicles and exosomes derived from LPS-preactivated cultured microglial cells, induced a dose-dependent activation of resting astrocytes and microglia[197]. The findings of this study suggest that the cargo from EVs can transfer an inflammatory signal to recipient cells, thus exacerbating neuroinflammatory conditions.

Proteomic analysis of exosomes derived from the N9 microglial cell line identified the proteomic composition of microglia-derived exosomes from cell culture medium[195]. Several hallmark EV proteins previously identified from EVs derived from cell types were found in the N9-derived EV proteome; such as, cytoskeletal proteins, heat shock proteins, integrins, and tetraspanin proteins. Of particular interest, was the aminopeptidase N (CD13) found in microglial exosomal proteins but not in exosomes derived from B cells and dendritic cells. Functional assays looking at aminopeptidase activity revealed that microglia exosomal CD13 is active in neuropeptide degradation.

Yang et al. characterized microglial EV protein cargo following lipopolysaccharide (LPS) and TNF inhibitor treatment[196]. Following 12-hour LPS stimulation of BV2 microglia, EVs were found to have significantly higher levels of pro-inflammatory cytokines TNF and interleukin (IL-10), as seen by ELISA. Furthermore, inhibition of the TNF signaling pathway resulted in a reduction of EVs released from LPS activated microglia. Mass spectrometry (MS)-based experiments identified 49 unique proteins in EVs derived from LPS activated microglia compared to control, with a majority of the proteins associated with transcription and translation. From this study, it can be inferred that microglia respond to an LPS challenge by releasing EVs with unique cargoes that may be implicated in inflammatory mechanisms. The data from both these studies suggest that microglia derived EVs have distinct proteomic profiles which may play a role in inflammatory responses in neurodegenerative diseases. However, low-depth of proteomic coverage remains a limitation of these studies.

Additionally, accumulating evidence suggests that EV miRNAs have the potential to influence disease pathogenesis and treatment outcomes. MiRNAs are small non-coding RNAs that regulate the expression of specific gene targets[225]. Release of miRNAs from EVs can influence target cell function[226]. Huang et al. found that increased miR-124-3p expression in microglia-derived exosomes after traumatic brain injury can inhibit neuronal inflammation and contribute to neurite outgrowth in recipient neurons[227]. Even though miRNAs are more abundant in EVs than larger species of RNA, mRNAs have also been found to be loaded into EVs and transferred to recipient cells[146, 228]. Ratajcazk et al. provided the first evidence that mRNAs transferred to recipient cells are functional and can be translated into proteins, leading to biological changes in recipient cells[144]. Overall, several studies have highlighted that the activation of microglia can have both a direct or indirect influence on neuroinflammation and disease progression. The uptake of EVs from recipient cells appears to mediate the indirect mechanisms by which microglia can affect disease progression. However, there is a lack of proteomic and transcriptomic characterization of EVs from distinct microglia states. Identification of the proteomic and transcriptomic cargo in EVs from distinct microglia states may elucidate key targets and pathways that are involved in EV mediated neuroinflammation.

In this study, we have generated comprehensive datasets of proteomics and transcriptomics from BV2 microglia cells and BV2-derived EVs under resting states as well as following treatment with either LPS, IL-10, or transforming growth factor β (TGF-β)[15, 229, 230], which have been documented to induce distinct molecular phenotypes in vitro. Using label-free quantitative mass spectrometry (LFQ-MS) and RNA sequencing of mRNA and miRNA species, we identified unique molecular signatures of EVs at the proteomic and transcriptomic levels, including several features not previously described. We also identified unique state-dependent molecular characteristics of microglia-derived EVs, in which LPS-effects were most predominant at the level of proteins, mRNA and miRNA. Next, we asked whether EV cargo from distinct microglia states can impact the gene expression profile of resting (responder) BV2 cells. To address this, we isolated EVs from the cell culture media (CCM) of four BV2 cell conditions (control, LPS, IL-10, TGF-β) and then equally dosed individual wells of BV2 cells with those EVs to assess gene expression

changes in recipient microglia using RNA sequencing. Taken together, our study provides several comprehensive molecular datasets on microglia-derived EVs and provides novel insights into the role of microglia-derived EVs in neuroinflammation, including increased packaging of mRNAs into EVs following inflammatory activation.

iii. Results

Verification of EV purification from BV2 cell culture medium

We applied size exclusion chromatography (Izon qEV) based methods to isolate EVs from BV2 microglia culture supernatants. Prior to MS and RNA seq studies of BV2 microglia-derived EVs, we performed several quality control studies to confirm successful enrichment of EVs from cell culture media. We characterized EV morphology, size, concentration, and classical markers using transmission electron microscopy (TEM), immunogold TEM, nanoparticle tracking analysis (NTA), and western blot analyses (**Figure 2.1A**). To characterize the morphology of BV2-derived EVs, we isolated EVs and examined them using high resolution TEM following negative staining. TEM revealed vesicles with consistent round and cup-shaped morphology within ~50-150nm size range, as would be expected for EVs (**Figure 2.1B**). Immunogold-labeled TEM studies using 6nm gold particles confirmed CD9 labeling on the surface of EVs (**Figure 2.1C**). We performed NTA on our isolated EVs and found that the EVs are typically within the range of 50-200nm in diameter (mean particle size =87.9 +/- 6.1 nm, mode particle size = 44.2 +/- 9.0 nm) (**Figure 2.1D**). Lastly, we performed western blot analyses of cell lysates and EVs from BV2 microglia and found that canonical EV protein markers CD9 and TSG101 were enriched in EV lysates, in contrast with enrichment of Calnexin in BV2 cell lysates (**Figure 2.1E**). These results using complimentary validation methods as recommended by the International Society for Extracellular Vesicles[151], confirm the validity of our EV isolation approach and its suitability for subsequent molecular characterization studies.

Identification of proteomic signatures of microglia-derived EVs by quantitative mass spectrometry

We performed LFQ-MS on 16 cell lysates and 16 EV lysates derived from BV2 microglia. These included four groups of BV2 cells (n=4/group) that were treated (72 hours) with either LPS (100 ng/mL)

to polarize to a pro-inflammatory state, IL-10 (50 ng/mL) to polarize to a protective state, TGF-β (50 ng/mL) to polarize to a homeostatic state or untreated controls. Duration (72 hours) and dose of BV2 cell treatment was determined based on previous literature confirming reliable polarization of microglia and to ensure a sufficient amount of secreted extracellular vesicles[15, 229-231]. LFQ-MS identified 533 proteins in the EV proteome and 1,882 proteins in BV2 cell proteome, across all conditions (Supplemental data 3 and Supplemental data 4). To contrast the EV proteome with the whole cell proteome, we first compared BV2 EVs (n=533 proteins) with BV2 cell lysate proteomes (n=1,882 proteins). The effect of treatment was not considered when comparing all EVs to all cell lysates. Forty-six proteins were differently enriched in EVs while 1,178 proteins were differentially enriched in cell lysates (**Figure 2.2A,** Supplemental data 5). Canonical exosome/EV related proteins expected to be present in all EVs independent of cell type of origin (including SDCBP, IGSF8 and three tetraspanins namely CD9, CD81, and CD63) were significantly enriched in the EV proteome compared to the whole cell proteome (**Figure 2.2A).** In contrast, endoplasmic reticulum proteins expected to be present in cell lysates but not in EVs, namely SSR1 and Calnexin, were highly enriched in the cell proteome but not the EV proteome. Gene set enrichment (GSEA) of EV-abundant proteins showed enrichment of extracellular region (APOE, SAA), membrane organization (CD9, ITGB1, MFGE8), and localization (RAB6B, SLC1A5, SLC38A2) terms while cytosolic and intracellular organelle terms were enriched in the cellular proteomes (**Figure 2.2B**).

Next, we compared our BV2 microglia-derived EV proteome to existing lists of proteins previously detected in proteomic studies of EVs from any mouse cell types (1,015 EV proteins in ExoCarta), the Exocarta protein list for mouse microglia (56 proteins), and the Yang et al. 2018 BV2-derived EV proteome (74 proteins) (Supplemental data 6). We found that our BV2-derived EV proteome (533 proteins) shared 326 proteins with the ExoCarta protein list of 1,015 EV proteins detected across all mouse cell types (**Figure 2.2C**, 207 novel proteins). Next, we performed GSEA (Supplemental data 4) on the three groups of proteins based on these analyses (207 novel BV2 microglial EV proteins not reported in other EV proteomes, 689 proteins reported in non-microglial EV proteomes but not in our data, and 326 proteins common to both microglial and non-microglial EV proteomes). Proteins unique to BV2 microglia-derived EVs were

enriched in ontologies related to positive regulation of transporter activity, regulation of RNA splicing, cytosolic large ribosomal subunit, and aminoacyl-tRNA synthetase complex (**Figure 2.2D**). On the other hand, the 689 proteins not captured in our BV2-derived EV proteome showed enrichment of proteins related to protein heterodimerization activity, chromosome organization, and protein kinase activity (**Figure 2.2D**). We also identified networks of known direct (protein-protein) and indirect (functional) interactions (STRING) within these core protein signatures related to RNA metabolism and protein translation, that are unique to our BV2 microglia-derived EVs as compared to other cell type-derived EVs (**Figure 2.2E**). Finally, we compared our BV2-derived EV proteome (533 proteins) with the Exocarta protein list of 56 mouse microglia and identified 494 novel proteins (**Figure 2.2F**) and to the Yang et al. 2018 BV2-derived EV proteome list of 74 proteins and identified 489 novel proteins (**Figure 2.2G**).

Taken together, these analyses verify the validity of our EV proteomes by confirming enrichment abundances of canonical EV markers, highlight the increased depth of our EV proteome as compared to prior microglial studies, and identify novel proteomic characteristics of microglia-derived EVs that are distinct from non-microglial EVs which may have functional implications.

Microglial activation impacts proteomic characteristics of EVs

Three groups of BV2 cells (n=4/group) were treated with either LPS (100 ng/mL) to polarize to a pro-inflammatory state, IL-10 (50 ng/mL) to polarize to a protective state, or TGF-β (50 ng/mL) to polarize to a homeostatic state (**Figure 2.3A**). Untreated BV2 cells served as a control group. To ensure that any state-related differences in EV proteomes are not related to impacts of EV yield, we used NTA to compare EV concentrations across treatment conditions and observed no significant differences across treatment groups (**Figure 2.3B**). To confirm that in vitro conditions induced distinct microglial activation states, we analyzed BV2 cell LFQ-MS proteomes and 334 differentially enriched proteins (DEPs) across polarization states, as compared to control (one-way ANOVA FDR-adjusted $p<0.05$ & $\log_2$FC>0) (**Supplemental Figure 2.1,** Supplemental data 3). Principal component analysis (PCA) using these DEPs showed that 56% of variance was explained by 2 principal components (PCs), of which PC1 explained 33% of variance while PC2 explained 23% of variance. Notably, the PCA identified four distinct proteomic clusters (Figure 3B).

As compared to untreated control BV2 microglia, LPS treatment increased levels of several pro-inflammatory proteins (e.g., OAS1L, IRG1, ACSI1) (**Supplemental Figure 2.1A**). For the BV2 cell proteome, GSEA using the generated up and down lists for each treatment against the background list (1,882 proteins) showed unique enrichment patterns across treatment groups (**Supplemental Figure 2.1B**). For example, LPS treated cells demonstrated an enrichment in proteins related to antigen processing, defense response, and immune response, whereas there was an observed decreased abundance in proteins lipid binding and phospholipase inhibitor activity. These results agree with prior proteomic studies of BV2 microglia using similar in vitro conditions, thereby confirming successful polarization of BV2 microglia to distinct molecular states[219, 232]. We also found that TGF-β treated cells demonstrated an enrichment in proteins related to positive regulation of homeostatic regulation and gluconeogenesis following, while IL-10 treated cells showed enrichment of proteins related to lipid binding and lipase inhibitor activity.

We next examined BV2-derived EV proteomes to determine whether microglial polarization state impacts proteomic composition of EVs. To account for unequal protein loading per sample, we performed our analyses of EV proteomes after normalizing MS data to total protein content in each sample, based on sum intensities across all quantified proteins. Our analyses of EV proteomes also accounted for batch effects since 4 different batches of experiments were performed, each with 1 replicate per condition (**Supplemental Figure 2.2**). We identified 83 DEPs across microglia states compared to control ($p<0.05$ & $\log_2FC>0$) (Supplemental data 4). PCA based on these DEPs identified four clusters among EVs (**Figure 2.3C**). Interestingly, all polarized BV2 microglia-derived EVs clustered away from control BV2-derived EVs and majority of these DEPs showed lower levels in polarized conditions as compared to the control group. Distinct signatures across polarization states compared to control are shown in **Figure 2.3D and 2.3E**.

We performed GSEA based on the DEPs for each treatment (compared to the control group), against the background list of 533 proteins identified in the EV proteome. We identified "Biological processes" and "Molecular function" terms along with KEGG pathways (**Figure 2.4A-C**) enriched in EV signatures from distinct BV2 microglial polarization states. GSEA of increased DEPs were limited due to small numbers of proteins that showed increased levels. EVs derived from BV2 cells treated with LPS

demonstrated an enrichment in proteins related to proteasome activity (e.g., PSMB3) and reduction in proteins related to chromosomal organization (e.g., CLTC, HIST2H2AA1,TCP1), and clathrin/receptor mediated endocytosis (e.g., CLTC, DNM2). Conversely, EVs derived from BV2 cells treated with IL-10 and TGFβ demonstrated a reduction in cytosolic chaperonin Cct ring complex proteins (e.g., CCT3, CCT4), microtubule related proteins and ATP/nucleotide binding (e.g., CCT4, TCP1, TUBA1B). EVs derived from BV2 cells treated with TGFβ showed enrichment of proteins related to membrane bound vesicle and receptor binding (CD9 and SDCBP). These proteomic analyses of EVs confirm that microglial activation states can determine the proteomic compositions of EVs.

Novel transcriptomic signatures microglia-derived EVs in resting and pro-inflammatory states

Beyond proteins, EVs carry mRNA and miRNA cargo which may be important mediators of microglia-mediated mechanisms of neuroinflammation. It is also possible that microglia state-dependent effects on EVs are more likely to be more pronounced at the levels of mRNA and miRNA levels. Therefore, we performed RNA seq to quantify mRNA and miRNA compositions of EVs and their corresponding cell lysates, after polarizing stimuli. Three groups of BV2 cells (n=3/group) were treated with either LPS (100 ng/mL), IL-10 (50 ng/mL) or TGF-β (50 ng/mL) to mimic conditions used for proteomic studies. Untreated BV2 cells served as a control group. Following 72 hours of treatment, whole cells and EVs were isolated from cell culture media, lysed in Trizol, followed by RNA extraction, purification and quality control steps. To assess length of RNA from BV2 cells and their EVs, RNA was characterized through capillary electrophoresis using two separate analyses kits: Pico and small RNA kits for bioanalyzer. These analyses (Supplemental data 7) revealed that cells display peaks at the ~2,000 nt (18s) and ~4,000 nt (28s), while EVs displayed peaks predominately between ~20-100 nt which correspond to small RNAs. To characterize the different subtypes of RNAs in EV and whole cells, we proceeded with mRNA sequencing and small RNA sequencing. We first discuss our mRNA sequencing results.

Sequencing of mRNAs identified over 12,000 mRNA species (transcripts) in EVs and cells across all conditions. As we observed at the proteomic level, different polarizing conditions induced distinct transcriptomic states in BV2 microglial cells, as evidenced by PCA in which PC1 explained 73% of

variance while PC2 explained 19% of variance (**Figure 2.5A**). Similarly, PCA revealed a large effect of LPS on EV transcriptomic composition as compared to other polarizing stimuli (**Figure 2.5B**). We first assessed unique transcriptomic signatures of EVs as compared to whole cells (control BV2 microglia only) (**Figure 2.5C**). EVs contain higher levels of over 1,000 mRNA species, including *Pak7, Arhgef40, and Saa3*. In contrast, cellular transcriptomes had higher expression of over 1,500 mRNAs including *Cebpb, Prkaca, and Pip5k1c*. Interestingly, *Cebpb* is a transcription factor known to regulate immune genes including genes critical for microglia switch from homeostatic to DAM[233]. GSEA of highly-enriched mRNAs (>=2-fold change in EVs or whole cells) showed enrichment of translation, ribosome, and cytokine activity in EVs, while we observed enrichment of terms such as ion binding and homeostasis and transmembrane receptor activity (**Figure 2.5D,** Supplemental data 8).

Pro-inflammatory genes (e.g., *Il1b, Il6*) and ontologies related to defense and immune response were increased in LPS-treated BV2 microglia. Interestingly, genes (e.g. *G3bp2*) and ontologies related to mRNA transport were also enriched in LPS treated cells (**Figure 2.5E**). TGF-β increased expression of several genes (e.g., *Cx3cr1, Flt1*) and ontologies related to homeostatic microglial function and biological regulation. IL-10 also increased expression of genes (e.g., *C1qc, Saa3*) and ontologies related to protein activation cascade and response to wounding and other organisms (Supplemental data 9).

Transcriptomic analyses of EVs identified over 3,000 differentially expressed genes (DEGs - mRNA species) across treatment groups (Supplemental data 10). As compared to TGF-β and IL-10, LPS polarization had the strongest impact on BV2 microglia-derived EV transcriptomes; therefore, we focused on LPS effects on the whole cell and EV transcriptomes. As discussed above, LPS polarization resulted in enrichment of pro-inflammatory genes (e.g., *Il1b, Il6)* related to immune response (**Figure 2.5E**). EVs from LPS-treated BV2 microglia showed increased levels of 2,949 mRNAs and decreased levels of 413 mRNAs (**Figure 2.5F**). Interestingly, transcriptomic alterations induced by LPS (DEGs upregulated with LPS, $p<0.05$, >1-fold change) on the whole cell (n=1,040) and EVs (n=2,949) showed modest overlap, with only 10% of EV transcriptomic changes overlapping with cellular changes (**Figure 2.5G**). 359 mRNAs showed shared differential expression in whole cells and EVs (**Figure 2.5G**) and majority of these DEGs were

related to lipopolysaccharide-mediated signaling pathway, positive regulation of cell activation, and regulation of immune response. The 2,591 DEGs related to EV only showed enrichment of RNA metabolic process and nucleic acid binding terms. While the 682 DEGs related to cell only showed enrichment of terms such as cell cycle and mature B cell differentiation (**Supplemental Figure 2.3**).

To take a deeper look at LPS effects on the cellular and EV transcriptomes, we performed GSEA based on identified DEGs. We found that LPS treated BV2 cells showed enrichment in immune response, RNA binding, and metabolism, whereas we observed a decreased expression in signal transduction and GTPase activity (**Figure 2.5H**). In contrast, EV transcriptomes from LPS treated BV2 cells, showed enrichment in terms such as signaling and ion channel activity (**Figure 2.5I**). Conversely, the downregulated DEGs in EVs from LPS treated BV2 cells showed enrichment in terms such as ATPase activity and transmembrane activity.

Furthermore, we found that the majority of EV transcriptomic changes induced by LPS are not observed in the whole cell transcriptomes. This suggests that pro-inflammatory activation of microglia not only induces whole cell gene expression changes, but also likely impacts mechanisms that govern mRNA export into EVs, consistent with our observation of LPS-induced altered expression of genes involved in mRNA transport at the whole cell level.

Taken together, these analyses identify novel transcriptomic signatures of EVs that are distinct from whole cell transcriptomes. Our studies also reveal distinct effects of pro-inflammatory activation on EV transcriptomic signatures, confirming microglial state-dependent effects on EV composition at the mRNA level, many of which do not occur at the whole-cell level.

Integrative proteomic and transcriptomic analysis of BV2-dervied EVs reveal enrichment of pathways involved in RNA binding and translation

Next, we were interested in contrasting our BV2-derived EV proteomics dataset to our BV2-derived EV mRNA transcriptomic dataset (Supplemental data 11). We compared the 533 proteins in the EV proteome to the 9,151 transcripts (mRNA) in the EVs using GSEA. We found that the EV transcriptome is enriched in ontologies related to ribosome, RNA binding, and metabolic and catabolic processes

(**Supplemental Figure 2.4A**). The pathway enrichment results of the EV proteome, interestingly, also revealed enrichment of ontologies related to ribosome, structural molecule activity, and translation (**Supplemental Figure 2.4B**). Taken together, we found that the major overlapping molecular pathways between the EV proteome and transcriptome are RNA binding, ribosomal large and small subunit binding and biogenesis, extracellular region part, and translation (**Supplemental Figure 2.4C**). Overall, these analyses suggest that BV2-derived EV cargo contains ribosomal proteins and mRNAs that can encode ribosomal proteins. This correlation further highlights the point that EVs can transport cargo that may regulate translation in a recipient cell, a hypothesis that needs future investigation. Furthermore, it also suggests that there is an inter-relationship between the RNA and protein cargo in EVs that may work together to achieve a regulatory function, which has been previously suggested in prior studies[234].

Microglia-derived EVs exhibit unique microRNA signatures under resting and LPS-treated conditions

We obtained sufficient RNA for sequencing of small RNA species from BV2 whole cell and EV RNA extracts. Small RNA sequencing identified ~100 miRNAs in EVs and ~270 miRNAs in whole cells (Supplemental datasheets 12 and 13). In addition to miRNA, we also identified other small RNA species (circRNA, piRNA, snoRNA, snRNA, and tRNA), included in Supplemental data 14. PCA of post-filtered, lowly expressed miRNA molecules in the whole cell (PC1 63%, PC2 12% of variance) (**Figure 2.6A**) identified four distinct clusters based on polarization state, with the LPS effect showing the strongest effect (along PC1), a pattern similar to our mRNA-based results. PCA of post-filtered, lowly expressed miRNA molecules in the EVs (PC1 43%, PC2 16% of variance) (**Figure 2.6B**) also showed group-based clustering primarily based on LPS treatment.

When comparing the whole cell and EV miRNA transcriptomes (**Figure 2.6C,** Supplemental data 15), we found that EVs contained very high levels of miRNAs mmu-mir-6240, mmu-mir-1983, and mmu-mir-1896. Interestingly, mir-6240 has been previously reported to be found at higher than expected levels in EVs compared to cell, in both human and mouse samples[235].

Focusing on LPS treatment effects, we observed that LPS-treated BV2 cells and their EVs enrich for unique miRNA signatures (**Figure 2.6D and 2.6E**). More specifically, we see increased expression of mmu-mir-320, mmu-mir-5126, and mmu-mir-466h. Interestingly, mir-320 has been found to be upregulated in plasma EVs from individuals at high risk of lung cancer[236]. Furthermore, one study found that mmu-mir-5126 was dysregulated in IFN-γ primed mesenchymal stromal/stem cells (MSC) and mmu-mir-466q found in MSC-derived exosomes modulated the pro-inflammatory phenotype of activated N9 microglia cells[237]. Overall, these results implicate that miRNAs in EVs from LPS treated BV2 cells could play a role in modulating inflammation.

Given that miRNA binds with target mRNA to direct gene silencing via mRNA cleavage or translation[238], we used the miRDB[239] online database to generate a list of predicted targets from our differentially expressed miRNAs in EVs following LPS treatment. We found that significantly enriched miRNAs that are increased with LPS treatment in EVs (mir-664, mir-5126, and mir-320) had 462 predicted targets (target prediction score > 80) which showed an enrichment in ontologies related to androgen and corticosteroid receptor signaling pathway and cytoplasmic mRNA processing pathway (**Figure 2.6F**). On the other hand, we found that significantly enriched miRNAs that are decreased with LPS treatment in EVs (mir-6240, mir-5108, mir-5119, and mir-6345) had 487 predicted targets (target prediction score > 80) which showed an enrichment in ontologies related to regulation of cell proliferation, chromatin remodeling structure and regulation of glycolysis. Overall, these results demonstrate that EVs from LPS activated BV2 cells could contain a set of miRNAs that target distinct mRNAs, thus modulating gene expression in a responder cell.

EVs derived from LPS-treated microglia induce pro-inflammatory changes in responder microglia

Our results from proteomic and transcriptomic characterization of microglia-derived EVs demonstrate EV-specific molecular changes induced by microglial polarization state, particularly by LPS induced pro-inflammatory activation. Since EVs carry these protein and RNA cargo to other cells, we hypothesized that state-dependent alterations in EV composition by LPS can relay inflammatory signals to responder cells and impact their transcriptomic state. To accomplish this, we isolated EVs from untreated

and LPS-treated BV2 microglia, estimated EV concentration by NTA, and then dosed resting responder BV2 microglia with equal amounts of EVs and assessed the transcriptomic alterations induced by EVs using RNA seq (**Figure 2.7A**). To ensure that LPS (endotoxin) contamination of EV preparations does not confound these EV transfer assays, we measured endotoxin levels in cell culture supernatants as well as in EV preparations. Cell culture supernatants from LPS-treated BV2 microglia contained 80-90 ng/mL of LPS, consistent with the dose of 100 ng/mL that was added. EV preparations from control and LPS-treated BV2 cells had equal endotoxin levels (approximately 4ng/mL, p=0.511060, not significant), confirming that prior to addition to responder cells, any endotoxin contamination in the EV preparations was equal in both groups. EVs were dosed at 2,000,000 EVs/well (2mL of media/well) across all conditions, and the estimated final endotoxin concentration added to responder cells was minimal (p=0.103, not significant) and also similar in control and LPS-treated conditions (**Figure 2.7B**). These results confirm that any potential effects of EVs in our transfer experiments cannot be explained by spurious endotoxin contamination of EV preparations.

PCA of post-filtered, lowly expressed genes showed 74% of variance was explained by 2 PCs, of which PC1 explained 57% of variance while PC2 explained 17% of variance (**Figure 2.7C**). The PCA identified two distinct clusters. RNA sequencing analyses of responder BV2 microglia exposed to control or LPS-treated BV2-derived EVs identified 148 genes that were differently expressed at the FDR<0.10 level (n=71 increased DEG including *Ddx54* and *Mllt1*; n=73 decreased DEGs including *Atp6v1e2* and *Cd72*) (**Figure 2.7D,** Supplemental data 16). GSEA revealed enrichment of terms such as G-protein coupled receptor protein signaling and regulation of synaptic plasticity for the down list; whereas, there was enrichment of GTPase activity for the up list (**Figure 2.7E**).

We also conducted Fisher's exact test (FET) analyses to determine whether gene expression changes induced by transfer of EVs from pro-inflammatory microglia overlap with specific homeostatic, pro-inflammatory and disease-associated microglial gene signatures previously identified by weighted gene co-expression network analyses of microglial transcriptomes[109] (**Figure 2.7F**). We found that genes that were increased in responder cells following exposure to EVs from LPS-polarized microglia were enriched

(unadjusted FET p=0.005) in a LPS-induced pro-inflammatory gene module (Red Module), including genes *4932438A13Rik, Dst, Fyb, Gnai, Heatr6, Slc25a22, and Tmem72*. These results from EV transfer experiments demonstrate the ability of EVs to relay the inflammatory state of microglia of origin to responder microglia.

iv.   Discussion

Microglia, the resident immune cell type of the brain, play an essential role in mediating inflammatory responses in the CNS. Microglia can alter their morphology, molecular profile, and function in response to immune activators, thus exerting different functions in different diseases[123]. Microglia-mediated neuroinflammation is a key pathological component of several neurodegenerative diseases[96]. Compelling evidence has suggested that EVs can have an indirect role in regulation of inflammatory signals and propagation of pathogenic cargo[186, 240]. Since microglia demonstrate heterogenous states in response to stimuli and signals from other brain cell types, it is possible that microglia-derived EVs may also exhibit state-related heterogeneity. However, the characterization of microglia-derived EVs at the proteomic and transcriptomic level, and how these are impacted by microglial state, have not been well studied. In the present study, we have characterized the proteomic and transcriptomic signatures of EVs from distinct microglia states using in vitro models. Our results demonstrate that upon treatment with LPS, TGF-β, or IL-10 to elicit distinct microglial states, BV2 cells and their EVs indeed demonstrate unique proteomic and transcriptomic signatures; indicating polarization of BV2 cells impacts the cargo of EVs. LPS treatment, in particular, had the most profound impact on transcriptomic compositions of microglia-derived EVs, and interestingly, these changes in EV mRNA cargo were not apparent at the whole cell level, suggesting unique effects of LPS on mechanisms that direct mRNA to EVs. Lastly, EVs derived from LPS-activated microglia were able to induce pro-inflammatory transcriptomic changes in resting responder microglia, confirming the ability of microglia-derived EVs to relay functionally-relevant inflammatory signals. Collectively, our results provide a critical resource of microglia-specific EV signatures, many of which are distinct from EVs from other cell types. State-specific EV signatures at the levels of proteins, mRNA, miRNA as well as other

non-coding RNA species, will serve as important resources for the fields of EV biology as well as neuroscience.

The microglial EV proteomes in our study are also deeper than current microglial EV proteomes, identifying 494 proteins not previously reported. Over 207 proteins in microglia EVs were also identified that have not been reported in proteomic studies of EVs from other cell types. This increased depth of the microglia EV proteome was not due to non-EV contamination, because we verified EV enrichment via several complimentary methods, including TEM, Western blotting, as well as high-level enrichment of canonical EV surface proteins such as CD9. Our proteomic studies of EVs identified unique functional groups of proteins as compared to the whole cell proteome of BV2 microglia. We found that BV2 microglia-derived EVs were enriched in ontologies related to positive regulation of transporter activity, regulation of RNA splicing, cytosolic large ribosomal subunit, and aminoacyl-tRNA synthetase complex in comparison to non-microglial EV proteomes. This suggests that proteins contained within microglia-derived EVs could play a role in mRNA processing as well as protein synthesis in the recipient cell. Furthermore, Oh et al. 2022 reported that Aminoacyl tRNA synthetase (ARS) complex-interacting multifunctional protein 1 (AIMP1), a structural component of the multienzyme ARS complex, can induce microglial activation and has been associated with several inflammatory diseases[241]. Based on this, microglia specific-EV signatures could be related to protein-synthesis machinery and influence activation of recipient cells.

Another major finding in our study is that microglial state influences EV proteomic composition. Specifically, we show that EVs derived from BV2 cells treated with IL-10 and TGF-β demonstrated a reduction in cytosolic chaperonin Cct ring complex proteins (e.g., Cct3, Cct4). Given that IL-10 is supposed to induce a protective response in microglia cells and TGF-β a homeostatic response, we would expect a decrease abundance in proteins related to pathogenic pathways. Previous studies have shown that chaperonins Cct subunits show increased quantities in disease states. For example, studies with glioblastomas have demonstrated an increase in the Cct subunits in EVs derived from tumor tissues[242]. Since Cct proteins (as part of the TRiC complex) also participate in the regulation of protein folding of actin and tubulin as well as pathological protein aggregation, it is also plausible that CCT changes in microglia-

derived EVs could impact pathogenic mechanisms of neurodegeneration[243]. The results of these studies align well with the reduction in Cct ring complex proteins following treatment with IL-10 and TGF-β. Furthermore, we found that EVs derived from LPS activated BV2 microglia demonstrated an enrichment in proteins related to proteasome activity (e.g., PSMB3). Prior work has demonstrated that proteasome systems are involved in regulating pro-inflammatory pathways[244]. Thus, EVs derived from LPS-activated microglia can potentially enhance inflammation through enrichment of proteasomes. These findings together with our results suggest that microglial EVs from distinct microglia states have unique proteomic profiles.

Beyond elucidating proteomic features of microglia-derived EVs, we also comprehensively characterized RNA cargo of microglia-derived EVs and the corresponding RNA content from whole cells as well. Our RNA sequencing studies (mRNA and miRNA) showed that microglia-derived EVs had a relatively larger number of miRNA species relative to mRNA, when compared to whole cell mRNA and miRNA profiles. This aligns with the general consensus that smaller RNAs are more abundant than mRNAs in exosomes. Interestingly, following LPS activation of BV2 cells we noticed an increase in mRNA transcripts in EVs compared to cells. Furthermore, we found that LPS activated BV2 microglia demonstrated an enrichment in genes related to mRNA transport and RNA binding. Given the accumulating evidence showing that mRNAs in EVs could serve as templates for novel protein translation in recipient cells[162, 245], it is possible that there is a specific mechanism involved in the shuttling of mRNAs into EVs that is increased following LPS microglial activation. We also found that a majority of EV transcriptomic changes induced by LPS activation are not observed in the whole cell transcriptomes. This suggests that pro-inflammatory activation of microglia not only induces whole cell gene expression changes, but also likely impacts mechanisms that govern mRNA export into EVs. However, further investigation is necessary to determine whether these mRNAs in EVs are translated into proteins in responder cells thereby influencing the phenotype of the cell.

Upon comparing the EV proteome with the EV mRNA transcriptome, we discovered overlapping molecular pathways between the EV proteome and transcriptome are involved in RNA binding, ribosomal

subunits, translation, and extracellular region and vesicles. This correlation suggests that BV2-dervied EVs contain mRNA and protein cargo that may influence translation and downstream regulatory functions in a recipient cell.

Next, we sought to explore the miRNA contents of microglia-derived EVs given their role in regulating the expression of specific gene targets[225]. In our studies, we observed that LPS-treated BV2 microglia and their EVs bear unique miRNA signatures that may be important in modulating inflammation. Specifically, mir-320, which was increased in EVs from LPS-treated BV2 cells, has been previously found to be upregulated in the cortex of human sporadic AD cases[246]. Furthermore, we identified several miRNAs that are contained at very high levels in EVs but not cells (e.g. mir-6240 and mir-6236). Focusing on the miRNAs that are differentially expressed in EVs from the LPS treated group versus control, we found that miRNAs in the EVs from LPS treated group target unique mRNAs compared to control, which are involved in androgen and corticosteroid receptor signaling pathway and the cytoplasmic mRNA processing pathway. By targeting distinct mRNAs, the miRNA cargo in these EVs could impact gene expression and modulate inflammation in a recipient cell. However, further mechanistic studies are needed to test this hypothesis.

The complementary multi-omics characterization of microglia-derived EVs and microglial state-dependent effects on EVs suggest that EVs from distinct microglia states have unique protein and RNA cargo, which may be able to impact other cells. Therefore, we hypothesized that state-dependent alterations in EV composition by LPS can relay inflammatory signals to responder cells and impact their transcriptomic state. To accomplish this, we dosed resting responder BV2 microglia with equal amounts of EVs from untreated and LPS-treated BV2 microglia and then assessed the transcriptomic alterations induced by EVs using RNA seq. Our RNA sequencing analyses revealed that responder BV2 microglia exposed to LPS-treated BV2-derived EVs display upregulation of genes related to GTPase activity and downregulation of genes related to G-protein coupled receptor protein signaling and regulation of synaptic plasticity. Mukai et al. reported that LPS stimulation significantly increased Rho-GTPase activity levels in microglia[247]. These results from EV transfer experiments demonstrate the ability of EVs to relay the inflammatory state of microglia of origin to responder microglia. Although these transcriptomic effects were not very large,

the overall effect of LPS-microglia-derived EVs on responder microglia was consistent with a pro-inflammatory profile previously reported in mouse microglia. Importantly, we confirmed that the observed effects of EVs cannot be explained by passive transfer of LPS itself. We attribute the smaller effect size on responder transcriptomes to dosing of EVs and duration of exposure.

Despite the strengths of our in vitro studies, some limitations of our work should be considered. For our study we chose to use BV2 microglia cells, a well characterized immortalized murine microglial cell line[248], because of their ability to capture major cellular phenotypes of microglia, suitability as an alternative model for primary microglia culture[249], and feasibility with obtaining sufficient EVs for EV proteomics and transcriptomics analyses. However, it should be noted that BV2 cells represent transformed cells which could change their phenotype compared to primary microglia cells in the central nervous system[250]. Therefore, further studies will be needed in either human iPSC-induced microglia cells or primary mouse microglia to confirm that there are similar proteomic and transcriptomic changes as observed in our BV2 cell studies. While we chose untreated BV2 microglia as responder cells for our EV dosing studies, other cell types (e.g. neurons and astrocytes) may be considered in future studies to understand the effects of microglia-derived EVs on non-microglial cellular phenotypes. Another potential limitation of our study is the sensitivity to detect low quantities of protein, mRNA, and miRNAs from EVs; however, we employed several steps in our experimental design and data analysis pipeline to account for low input.

v.   Conclusion

To conclude, our findings suggest EVs from distinct microglia states have unique proteomic and transcriptomic profiles. Furthermore, we have identified novel EV proteins in microglia not seen in other EVs, thereby increasing the depth of the microglia-derived EV proteome that has not been previously reported on. Through our transcriptomic analysis, we discovered that LPS activation of BV2 cells has the strongest impact on EV composition, possibly increasing the amount of mRNAs transported and packaged into the EVs. Lastly, our data suggests that EVs from LPS-activated microglia can elicit a transcriptomic

change in resting recipient microglia that mimics that of a pro-inflammatory response. Our study highlights the value of characterizing the cargo of EVs from distinct cell types. EVs are a promising therapeutic as well as diagnostic tool for neurodegenerative disease. Given that microglia are highly dynamic cells and can polarize to multiple phenotypes in response to their environment, it is to be inquired if their EVs might have distinct functions and contents. Therefore, the uptake of microglia-derived EVs by other cells could mediate indirect downstream signaling events. More research is needed to understand the mechanisms of microglia-derived EVs in neurodegenerative disease, specifically whether the presence or absence of certain cargo can impact disease progression.

vi.   Materials and Methodology

Antibodies, buffers, and reagents

A complete table of antibodies & reagents are provided (Tables 1 & 2).

Table 1. Antibodies used and their corresponding dilutions

Antibody	Manufacturer	Catalog #	Dilution/ Duration
Anti-CD9 Antibody	System Biosciences	EXOAB-CD9A-1	1:500 / overnight
Anti-CD9 Antibody	Abcam	ab223052	1:500 / overnight
Anti-TSG101 Antibody	Abcam	ab30871	1:500 / overnight
Anti-Calnexin (AF18)	Santa Cruz	sc-23954	1:200 / 1 hour
Donkey anti Rabbit 800	Invitrogen	A11374	1:10,000 / 1 hour
Goat Anti-Rabbit IgG H&L (6nm Gold)	Abcam	ab41498	

Table 2. Reagents used and their manufacturer and catalog numbers

Reagent	Manufacturer	Catalog #
StartingBlockT20	Thermofisher	37543
HALT protease & phosphatase inhibitor cocktail	Thermofisher	78446
Dulbecco's Modified Eagle Medium (DMEM)	Gibco	11965-092

Penicillin-Streptomycin	Gibco	15140-122
Fetal Bovine Serum (FBS)	Gibco	26140-079
Lipopolysaccharide (LPS)	Sigma-Aldrich	L4391, 1 mg
Recombinant Mouse IL-10 Protein	R&D Systems	417-ML-005, 5 ug
Recombinant Mouse TGF-beta 1 Protein	R&D Systems	7666-MB-005, 5 ug
0.05% Trypsin-EDTA	Gibco	253000054
Reagent A	Thermofisher	23222
Reagent B	Thermofisher	23224
Bovine Serum Albumin Standards	Thermofisher	23208
qEVoriginal / 35 nm Gen 2 Column	Izon	ICO-35
Amicon Ultra-2 Centrifugal Filter Units	Millipore	UFC210024, 100 KDa
Amicon Ultra-15 Centrifugal Filter Units	Millipore	UFC910024, 100 KDa
Pierce Protein Concentrator PES, 100K MWCO, 2-6 mL	Thermofisher	88524
Lys-C	Wako	127-06621
Trypsin	Thermofisher	90058
HLB columns	Waters	186003908
Carbon Film Grids 400 Mesh-copper-thick	Electron Microscopy Sciences	CFU400-CU-TH
miRNeasy Mini Kit	Qiagen	217004

Experimental Procedures

Cell culture studies

BV2, an immortalized murine microglial cell line, was cultured in filtered Dulbecco's Modified Eagle Medium (DMEM) supplemented with high glucose and L-glutamine containing 1% penicillin/streptomycin, and 10% Fetal Bovine Serum (FBS). All media was vacuum-filtered with 0.2 μm filters. The cells were incubated at 37 degrees Celsius (°C) and 5% CO2 until reaching 80% confluency.

The splitting regimen took place twice weekly, plating one million cells onto a 100 mm culture plate to a final volume of 12 mL culture media. In preparation for experiments, one million cells were plated in 100 mm plates with 12 mL of media. 24 hours after plating, existing media was swapped for filtered serum-free media (DMEM containing 1% penicillin/streptomycin) and BV2 cells were treated with either TGF-β (50 ng/mL), IL-10 (50 ng/mL), and LPS (100 ng/mL) for 72 hours[15, 229-231]. Control cells were left untreated. BV2 cells were treated for 72 hours to ensure a sufficient amount of secreted extracellular vesicles. For dosing resting recipient cells, EVs were isolated from cell culture media following treatment of BV2 as described above. The concentration of isolated EVs for each sample were determined using NTA. Recipient BV2 cells (n=3/condition) in a 6 well plate were dosed for 24 hours with 2 million EVs/well from either TGF-β, IL-10, or LPS treated BV2 cells. Cell culture media in 6 well plates was swapped with serum-free media prior to dosing recipient cells with EVs. After 72 hours in culture, cell culture medium was collected from the plates, transferred into 15 mL tubes, and placed on ice. Next, the plates were washed twice with ice-cold 1x phosphate buffer saline (PBS). Cell pellets were harvested in 500 μL Urea lysis buffer (8 M Urea, 10 mM Tris, 100 mM NaH2PO4, pH 8.5) with 1x HALT protease & phosphatase inhibitor cocktail without EDTA. Cell lysates were then sonicated at 30% amplitude thrice in 5-second on-off pulses to disrupt nucleic acids and cell membrane. All cell lysates were centrifuged at 4°C for 2 minutes at 12,700 rpm. The supernatants were transferred to a fresh 1.5 mL LoBind Eppendorf tube. The protein concentrations of whole cell lysates were determined by Bicinchoninic acid (BCA) assay reagents using Bovine Serum Albumin Standards.

EV isolation

EV isolation was conducted as per Izon manufacturer's protocol[251]. Cell culture media underwent several centrifugation steps to remove cellular debris (10 min at 500xg and 10 min 10,000xg). After each spin, the supernatant was collected and subjected to the subsequent spin. The final supernatant was collected and added to an Amicon Ultra-15 Centrifugal Filter (molecular weight cut-off 100 kDa) to concentrate the sample and then was added to a qEV column resin column for size exclusion chromatography using the Izon qEV system with a qEVoriginal / 35 nm Gen 2 Column. Sterile PBS was used as the flushing buffer.

The second fraction containing the most abundant amount of EVs was then concentrated using a Amicon Ultra-2 Centrifugal Filter (molecular weight cut-off 100 kDa) or Pierce Concentrator 0.5mL, PES (molecular weight cut-off 100 kDa). The resulting concentrate was used for any downstream analysis (TEM, immunoblotting, NTA, proteomics, or transcriptomic analyses).

Transmission Electron Microscopy (TEM) of EVs

For electron microscopic analysis, 5 µL from the EV samples were loaded onto the carbon side of charged copper/carbon-coated electron microscopic grids. After 5 minutes, sample loaded grids were washed 3 times in distilled water and then stained with 1-3% uranyl acetate for 1 minute in the dark. Once grids were dry, EVs were observed under TEM at 80 kV. TEM grids were stored in the appropriate grid storage boxes for future use. Hitachi HT7700 transmission electron microscope operating at 80 kV was used for imaging.

<u>Immunogold labeling of EVs with CD9</u>

For the preparation of samples for immunogold electron microscopy, purified EVs were fixed for 1 hour in a mixture of 0.1% glutaraldehyde, 2.5% paraformaldehyde, 0.03% picric acid, and 0.03% CaCl2 in 0.01 M cacodylate buffer at a pH of 7.2. Fixed samples were then adsorbed for 1 hour to freshly glow discharged copper Formvar-coated grids. For immunogold staining, grids with adsorbed EVs were incubated sample-side down on drops of blocking buffer for 30 minutes (a mixture of 0.1% BSA and 0.01 M glycine in 0.01 M PBS). They were then transferred to drops containing rabbit polyclonal antibody to CD9 (Abcam ab223052) diluted in diluent buffer (1% BSA in 0.01 M PBS) at a dilution of 1:20 and incubated for 1 hour at room temperature and then overnight at 4°C. Next, grids were washed through a series of drops of blocking buffer and subsequently transferred to drops containing gold-labeled secondary antibodies. Secondary antibodies were goat polyclonal antibody to rabbit IgG labeled with 6-nm gold particles (Abcam ab41498), at a dilution of 1:20 in diluent buffer. After EVs were incubated with secondary antibodies for 1 hour at room temperature, they were once again washed by transferring them through a series of drops of blocking buffer, then through a series of drops of 0.01 M PBS, and finally, through a series of drops of deionized water. Grids were then fixed for 15 min on drops of 2.5% aqueous glutaraldehyde. EVs were

subsequently negatively stained with 2% aqueous uranyl acetate and examined in a JEOL JEM 1400 transmission electron microscope operated at 80 kV.

Nano tracking Analysis (NTA) of isolated EVs

The size and total number of EVs were measured by using NanoSight NS300 (Malvern, UK) with the technology of Nanoparticle Tracking Analysis (NTA). Size distribution and concentration of EVs in an aqueous buffer was obtained by utilizing Brownian motion and light scattering properties[252]. Samples were diluted with 1X PBS to obtain optimal concentration for detection (10^6–10^9 particles/ml) and injected with a continuous syringe system for 60 s × 3 times at speed 100 μl/min. Data acquisition was undertaken at ambient temperature and measured 3 times by NTA. Data were analyzed with NTA 3.2 software (Malvern, UK) with minimum expected particle size 10 nm.

Immunoblotting studies

In each well, 15 μg of protein from cell lysates and 21 μL of EV lysate resolved in a 4-12% polyacrylamide gel and transferred onto iBlot 2 Transfer Stack containing nitrocellulose membrane using the BOLT transfer system. The membranes incubated for 1 hour at room temperature in StartingBlockT20 before receiving rabbit anti CD9 primary antibody overnight at 4 °C. After primary antibody incubation, the membranes underwent three 5-minute washes with 1x TBS-T. The membranes were then further incubated for 1 hour at room temperature in a secondary antibody cocktail of donkey anti rabbit 800 (1:10,000 dilution). The membranes were then washed again as previously described before undergoing imaging via the Odyssey infrared Imaging System (LI-COR Biosciences).

Experimental Design and Statistical Rationale

The sample conditions were prepared as follows: BV2 cells or BV2-derived EVs and treatment (TGF-β, IL-10, LPS, or control). For each individual sample condition, there were four biological replicates for proteomic studies and three biological replicates for transcriptomic studies. For proteomics studies, there were a total of 16 cell samples and 16 EV samples analyzed and described in the results. For transcriptomic studies, there were a total of 12 cell samples and 12 EV samples analyzed and described in the results. The

maximum number of biological replicates was chosen within budgeted allowance; an a priori power analysis was not performed. Statistical rationale for each analysis is described below in the "Proteomic studies of BV2 microglia and EVs" and "Transcriptomic studies of BV2 microglia and EVs" sections.

Proteomic studies of BV2 microglia and EVs

Protein digestion

Sample preparation for MS was performed according to our laboratory protocols modified from previous publications[203, 212, 253]. To prepare enriched samples for mass spectrometry analysis, EV fractions and cells were lysed in 8M urea containing protease and phosphatase inhibitors. 100 μg of protein from the cell lysates and the entire volume of the EV lysates were then reduced with 1 mM dithiothreitol (DTT) at room temperature for 30 min and alkylated with 5 mM iodoacetamide (IAA) in the dark for 30 min with rotation. Proteins were digested overnight with 2 μg of lysyl (Lys-C) endopeptidase (Wako, 127-06621) at RT on shaker. Samples were then diluted (7-fold) with 50 mM ammonium bicarbonate (ABC) to bring the urea concentration to 1 M. Samples were then digested overnight with 2 μg of trypsin (Thermo, 90058) at RT on shaker. The resulting peptide solutions were acidified to a final concentration of 1% formic acid (FA) and 0.1% triflouroacetic acid (TFA), desalted with a HLB columns (Waters, 186003908), and dried down in a vacuum centrifuge (SpeedVac Vacuum Concentrator).

Mass spectrometry (MS)

Dried peptides were resuspended in 15 μL of loading buffer (0.1% FA and 0.03% TFA in water), and 7–8 μL was loaded onto a self-packed 25 cm (100 μm internal diameter packed with 1.7 μm Water's CSH beads) using an Easy-nLC 1200 or Dionex 3000 RSLCnano liquid chromatography system. The liquid chromatography gradient started at 1% buffer B (80% acetonitrile with 0.1% FA) and ramps to 5% in 10 s[254]. An Orbitrap Fusion Lumos Tribrid mass spectrometer with a high-field asymmetric waveform ion mobility spectrometry interface was used to acquire all mass spectra at a compensation voltage of –45V[254]. The spectrometer was operated in data dependent mode in top speed mode with a cycle time of 3 s. Survey scans were collected in the Orbitrap with a 60,000 resolution, 400 to 1600 m/z range, 400,000 automatic gain

control (AGC), 50 ms max injection time and RF lens at 30%. Higher energy collision dissociation (HCD) tandem mass spectra were collected in the ion trap with a collision energy of 35%, an isolation width of 1.6 m/z, AGC target of 10000, and a max injection time of 35 ms. Dynamic exclusion was set to 30 s with a 10 ppm mass tolerance window.

<u>Protein identification and quantification</u>

MS raw files were searched using the search engine Andromeda, integrated into MaxQuant, against 2020 mouse Uniprot database (91,441 target sequences). Methionine oxidation (+15.9949 Da) and protein N-terminal acetylation (+42.0106 Da) were variable modifications (up to 5 allowed per peptide); cysteine was assigned as a fixed carbamidomethyl modification (+57.0215 Da). Only fully tryptic peptides were considered with up to 2 missed cleavages in the database search. A precursor mass tolerance of ±20 ppm was applied prior to mass accuracy calibration and ±4.5 ppm after internal MaxQuant calibration. Other search settings included a maximum peptide mass of 4600 Da, a minimum peptide length of 6 residues, 0.05 Da tolerance for orbitrap and 0.6 Da tolerance for ion trap MS/MS scans. The false discovery rate (FDR) for peptide spectral matches, proteins, and site decoy fraction were all set to 1 percent. Quantification settings were as follows: re-quantify with a second peak finding attempt after protein identification has completed; match MS1 peaks between runs; a 0.7 min retention time match window was used after an alignment function was found with a 20 min RT search space. Quantitation of proteins was performed using summed peptide intensities given by MaxQuant. The quantitation method only considered razor plus unique peptides for protein level quantitation.

The MaxQuant output data were uploaded onto Perseus (Version 1.6.15) for analyses. The categorical variables were removed, and intensity values were log (base 2) transformed. The data were filtered based on 50% missingness values and missing values were further imputed from normal distribution (width: 0.3, down shift: 1.8). The MaxQuant output data (LFQ intensities) from the EV samples were first normalized based on column sum weight (column sum of given sample divided by average sum across all samples) for

each sample to account for volumetric loading of EV samples. The data was then processed as described above with Perseus.

Data Analysis related to proteomic studies

Proteomic data analysis involved several approaches including differential expression analysis, gene ontology (GO) analysis, principal component analysis (PCA), and hierarchical clustering using the average linkage method with one minus Pearson correlation. To visualize the data, heat maps of the normalized data were generated using Morpheus from the Broad Institute (https://software.broadinstitute.org/morpheus), and additional graphical representations were created using R software (version R-4.2.0) and Prism (GraphPad, version 9) software.

Cell Proteome: Data Normalization, Log Transformation, and Filtering

LFQ intensities and raw intensity values were uploaded onto Perseus (version: 1.6.15) for analyses. Categorical variables were removed, LFQ intensity values were log-2 transformed, and data were in general filtered based on 50% missingness across the group of samples that were selected for each analysis. Missing values were imputed from normal distribution.

Cell Proteome: PCA and Differential Expression Analysis

The inputted data was then preprocessed to remove duplicates. The code used for this preprocessing is referenced from the Supplemental materials. Post processing, the inputted data file from the cell proteome contained 1882 proteins. To identify patterns, relationships, and important variables in the dataset and gain insight into the main sources of variation, we performed principal component analysis (PCA), a widely used statistical technique for analyzing high-dimensional datasets. To identify significantly differentially enriched proteins (with an unadjusted p-value ≤ 0.05), we conducted an unpaired t-test comparing the treatment groups against the control group. Furthermore, to identify proteins of interest that were differentially expressed, we performed a one-way analysis of variance (ANOVA) on all samples (n = 16), comparing the control, LPS, IL-10, and TGF-β groups (n = 4 each). The code for the one-way ANOVA analysis was adapted from the "parANOVA" repository on GitHub (https://github.com/edammer/parANOVA). Based on the one-way ANOVA calculation, we calculated the

PCA (https://rdrr.io/bioc/M3C/src/R/pca.R) for the differentially expressed gene "cleanDat." To determine whether a gene was differentially expressed, we used a threshold of a p-value < 0.05 in the one-way ANOVA analysis. Out of the 1882 proteins in cleanDat, we identified 333 proteins that met this criterion. Additionally, we generated one-way ANOVA significant proteins and created heatmap (https://nmf.r-forge.r-project.org/aheatmap.html) and PCA plots to identify patterns in the dataset. Differentially enriched proteins were presented as volcano plots. Overall, these methods allowed us to analyze the proteomic data, identify differentially enriched and differentially expressed proteins, and gain insights into the underlying structure and variation within the dataset.

EV Proteome: Data Normalization, Log Transformation, and Filtering Missingness

Before conducting any analysis, protein abundances in the EV samples were normalized. This involved calculating the column sum (LFQ intensities) for each sample in the raw file and determining weights by dividing the column sum of a given sample by the average sum across all samples. The LFQ data was then normalized to the column sum weight for each sample.

Following normalization, LFQ intensities and raw intensity values were uploaded onto Perseus (version: 1.6.15) for analyses. Categorical variables were removed, LFQ intensity values were log-2 transformed, and data were in general filtered based on 50% missingness across group of samples that were selected for each analysis. Missing values were imputed from normal distribution.

EV Proteome: Batch Regression, Differential Expression Analysis, and PCA

The EV analysis involved 533 proteins divided into Control, TGF-β, IL10, and LPS groups, each with four samples. For statistical analysis, batch regression was performed using bootstrap regression to minimize the impact of batch on sample variance. Variance partitioning was employed to generate violin plots illustrating the contributions of treatment and batch to the observed variance in the data. The primary objective was to reduce the variance caused by batch and eliminate the batch effect. Volcano plots were then generated to visualize the differentially enriched or depleted proteins. The regressed data, obtained after applying batch regression, was used in an unpaired t-test comparing the control group to the treatment groups. The top proteins identified from the volcano plots were further examined for their ontologies.

Principal component analysis (PCA) was conducted, incorporating one-way ANOVA (P < 0.05) and batch regression. Throughout the EV analysis, the "parANOVA" repository on GitHub (https://github.com/edammer/parANOVA) was referenced for the one-way ANOVA code. These analyses allowed for a comprehensive investigation of the proteomic data, encompassing normalization, statistical tests, visualization, ontological analysis, and enrichment analysis, providing valuable insights into the characteristics and differential expression patterns of the proteins under study.

Gene Set Enrichment Analysis (GSEA)

Gene set enrichment analysis (GSEA) was conducted using AltAnalyze (http://altanalyze.org) (Version 2.0). Three treatment groups were compared to the Control group. Specific parameters were employed for the analysis. Additionally, differentially enriched proteins with unadjusted p-values ≤ 0.05 and fold change ≥ 2 from the differential analyses were included in the input lists. The background gene list consisted of unique gene symbols for all proteins identified and quantified in the mouse brain.

Transcriptomic studies of BV2 microglia and EVs

RNA extraction, library prep, and RNA sequencing

Total RNA was extracted from BV2 cells and BV2 cell-derived extracellular vesicles using the Qiagen miRNeasy Mini Kit (Cat. No. 217004). 20 μL of EV fraction was resuspended in 700 μL of TRIzol lysis buffer. BV2 cell pellets were harvested in 700 μL of TRIzol lysis buffer. Added 140 μL of chloroform was added to each sample and shook vigorously. Samples were then centrifuged for 15 min at 12,000 x g at 4°C. After centrifugation, the sample separated into 3 phases: an upper, colorless, aqueous phase containing RNA; a white interphase; and a lower, red, organic phase. The top aqueous phase was carefully isolated without disturbing the other phases. The top aqueous phase was transferred to a new collection tube and 1.5 volumes of 100% ethanol was added and mixed by pipetting up and down. 700 μL of the sample was added to the provided spin column in collection tubes. Samples were spun at ≥8000 x g for 15 s at room temperature and the flow-through was discarded. This was repeated for the rest of the sample.

Bound RNA was washed 2 times using the included wash solution (Buffer RPE). Finally, elution solution (RNase-free water) was used to elute the RNA in 40 μL volume for cells and 20 μL for extracellular

vesicles. RNA was stored at -80°C and RNA quality was assessed by Bioanalyzer (Agilent 2100 Bioanalyzer, RNA 6000 Nano Kit for cells, RNA 6000 Pico Kit for EVs, Agilent Technologies).

cDNA Libraries were prepared for small RNAs using the SMARTer smRNA-seq kit and for mRNAs using the SMART-Seq v4 and Nextera XT kit. A total of 18 cycles of PCR were carried out to obtain a good yield of cDNA from cells and EVs. Final library quality was verified with Qubit and Bioanalyzer. Negative (no RNA) and positive controls provided the expected results. Next-generation RNA sequencing was performed using a HiSeq X Illumina 2x150, 40M total reads per sample (20M in each direction) at Admera Health.

Data Analysis related to RNA seq studies of BV2 microglia and EVs: mRNA and non-coding RNA RNA sequencing analysis was conducted to identify genes exhibiting differential expression. The counts data provided information on the abundance of reads mapped to the reference genome or the number of fragments assigned to each gene. The primary objective was to identify systematic changes between the conditions of interest, specifically Control vs Treatment. The analysis utilized the DESeq2 package, developed by Michael I. Love, Simon Anders, and Wolfgang Huber (Package Authors). A DESeq2DataSetFromMatrix object was created, and the design parameter was set to ~Treatment, which captured the information on how the traits file was structured. For instance, in the case of n=4 Control vs n=4 LPS, the design matrix reflected these conditions. To ensure data quality, the raw counts data were aligned to the traits file, following the documentation guidelines. Lowly expressed genes were filtered out based on the criterion of rowSums(counts(dds)) ≥ 30, meaning that only genes with 30 reads in total across all samples (5 X 6 samples = 30) were retained. This step was performed to remove genes with insufficient expression levels. Additionally, if required by the dataset, Ensembl IDs were converted to gene names for ease of downstream analysis. The control condition was designated as the reference for comparison, and genes exhibiting differential expression were identified using the criteria of adjusted p-value < 0.05 and log2 fold change (LFC > 0 for upregulated genes and LFC < 0 for downregulated genes). It should be noted that in the comparison of Bulk RNA-seq on responder BV2 cells, the LPS samples were contrasted against the control (n = 4), deviating from the general protocol. Principal component analysis (PCA) (https://www.rdocumentation.org/packages/netresponse/versions/1.32.2/topics/plotPCA) was employed as

an initial analysis step to identify patterns, relationships, and important variables in the high-dimensional dataset.

The RNA-seq analysis, utilizing the DESeq2 package, allowed for the identification of differentially expressed genes, subsequent gene enrichment analysis, and visualization of the results through various plots. This comprehensive approach provided valuable insights into the expression patterns and functional characteristics of the genes under investigation.

GSEA of transcriptomic data

Gene enrichment analysis was performed on the lists of differentially expressed genes using AltAnalyze, with specific parameters specified. Volcano plots (https://github.com/kevinblighe/EnhancedVolcano) and heatmaps (https://cran.r-project.org/web/packages/pheatmap/index.html)based on the top 50 genes with adjusted p-values were generated to visualize the results of the differential expression analysis. For gene enrichment analysis of the predicted targets for specific miRNAs, we used miRDB[239] and MirTarget[255]. Input lists were relaxed to an adjusted p-value of 0.10, as opposed to the usual 0.05, in order to enhance the coverage of genes for Bulk RNA-seq on responder BV2 cells, and the LPS samples were contrasted against the control (n=4). To assess the statistical significance between two categorical variables, a Fisher's exact test was conducted.

Data availability

R code associated with the data analyses for the manuscript are published to GitHub (https://github.com/adityanatu1/proteomic-and-transcriptomic-signatures-of-microglia-derived-extracellular-vesicles-)

The mass spectrometry proteomics data have been deposited to the ProteomeXchange Consortium via the PRIDE partner repository with the dataset identifier PXD04395.

The RNA sequencing data (including raw files) have been deposited to the NCBI Gene Expression Omnibus (GEO). GEO accession number is GSE240295 (Public as of August 12, 2023).

Supplemental datasets supporting the conclusions of this article are included within the article as Supplemental data (16).

ExoCarta[256] (http://www.exocarta.org) was used for lists of proteins previously identified in EVs from different mouse tissues and cell types.

Rangaraju et al. 2018[109] was used for WGCNA module membership data used for analyses comparing the transcriptomes of responder BV2 microglia to known microglial transcriptomic profiles.

vii.   Chapter II Figures
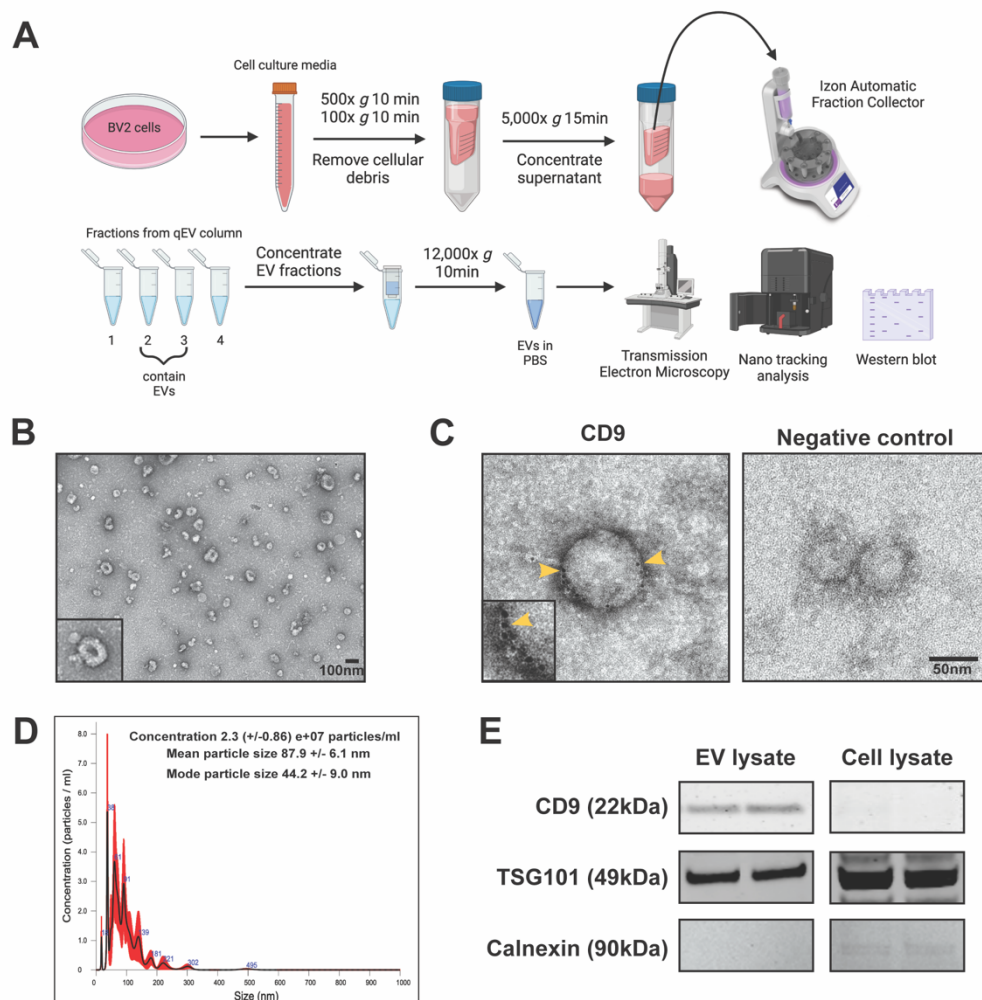
Figure 2.1: Purification of BV2 microglia-derived extracellular vesicles (EVs). A. Illustration outlining the process for isolating EVs from cell culture media. This figure was created with BioRender.com. **B.** Transmission electron microscopy (TEM) image of isolated EVs from BV2 cells. Scale bar is 100nm. **C.** TEM immunogold labeling of EVs (6nm gold particles) shows CD9 protein on the surface of EVs. CD9 is a canonical EV surface marker. **D.** Nanoparticle tracking analysis (NTA) shows size and concentration of isolated EVs from BV2 cell culture media. **E.** Western blot analyses of EVs and cell lysate, probed with antibodies to detect EV-enriched and cytosolic markers. CD9 and TSG101 are positive EV markers and Calnexin is a negative EV marker. Two biologically-independent experimental samples were blotted for each condition.
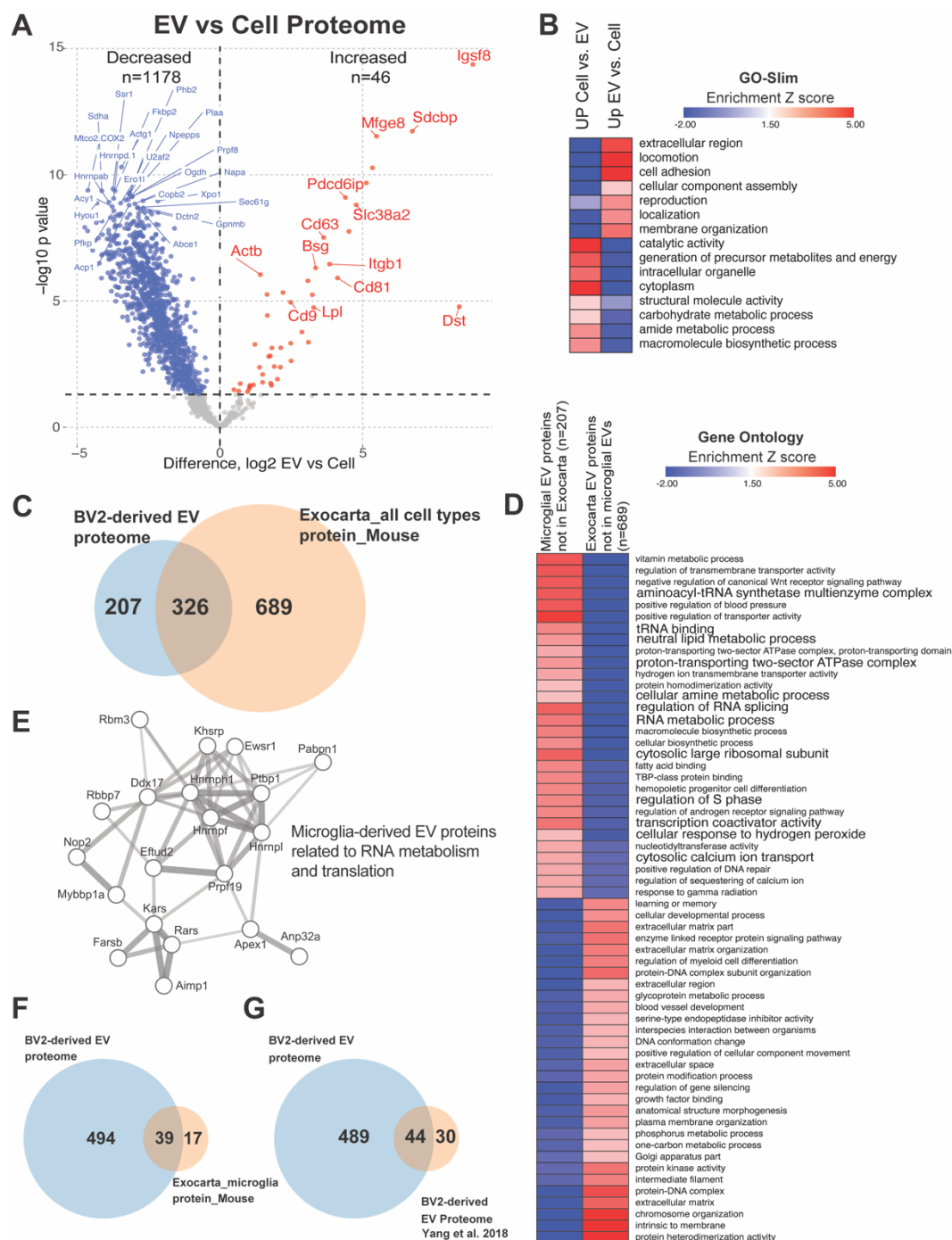
Figure 2.2: Comparison of BV2 whole-cell proteome and BV2-derived EV proteome. A. Enrichment of EV related proteins in EV proteome compared to BV2 cell proteome. Red labeled circles are in the Exocarta top 100 list. **B.** Heatmap representation, based on enrichment Z-scores, of GOSlim for list of differentially enriched proteins (DEPs) from Figure 2A. **C.** Comparison of 533 identified proteins from BV2-derived extracellular vesicles across all conditions to online database Exocarta mouse, all cell types, protein. **D.** Heatmap representation, based on enrichment Z-scores, of Gene Ontology for list of 207 proteins and list of 689 proteins from Figure 2B. **E.** STRING protein-protein-interaction network highlighting protein groups related to RNA metabolism and protein translation, that are unique to BV2 microglia-derived

EVs as compared to other cell type-derived EVs. Edges represent protein-protein associations. Line thickness represents edge confidence. **F.** Comparison of 533 identified proteins from BV2 derived extracellular vesicles across all conditions to online database Exocarta mouse, microglia, protein. **G.** Comparison of 533 identified proteins from BV2 derived extracellular vesicles across all conditions to Yang et al. 2018 BV2-derived EV proteome.
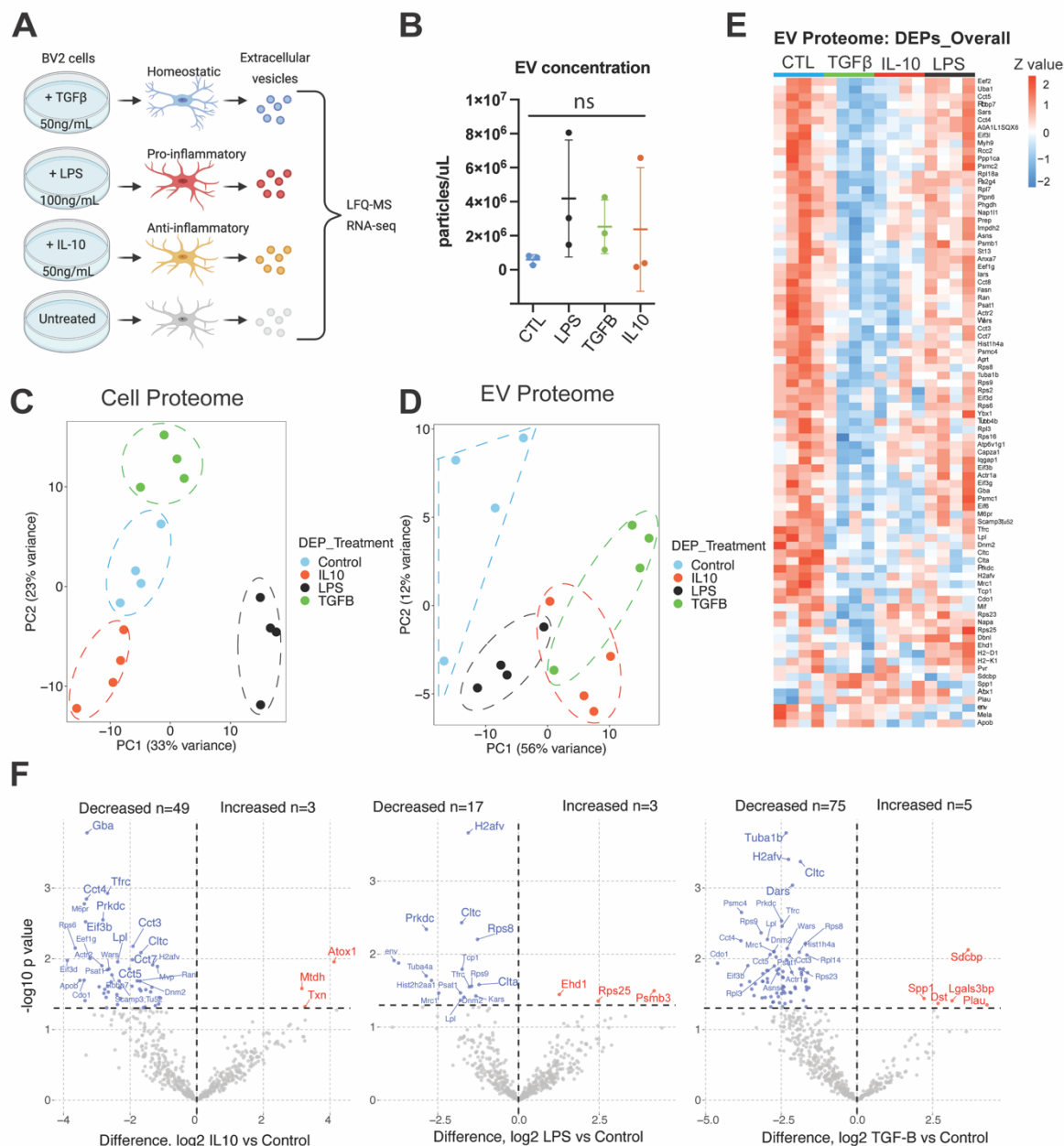
Figure 2.3: BV2 cells of distinct states and their EVs have unique protein signatures. A. Illustration outlining the experimental setup. This figure was created with BioRender.com. **B.** Comparison of EV yield from BV2 cell culture media, across different treatment conditions. One-way ANOVA, p-value is not significant (p=0.4684). **C.** Principal component analysis (PCA) plot of BV2 cell proteome – p<0.05, one-

way ANOVA (n=333 proteins). **D.** PCA plot of BV2-derived EV proteome – p<0.05, one-way ANOVA (n=84 proteins)**. E.** Heatmap of DEPs – p<0.05, one-way ANOVA (n=84 proteins). **F.** Volcano plots showing DEPs in EV proteome comparing each treatment group to the control group (p<0.05).
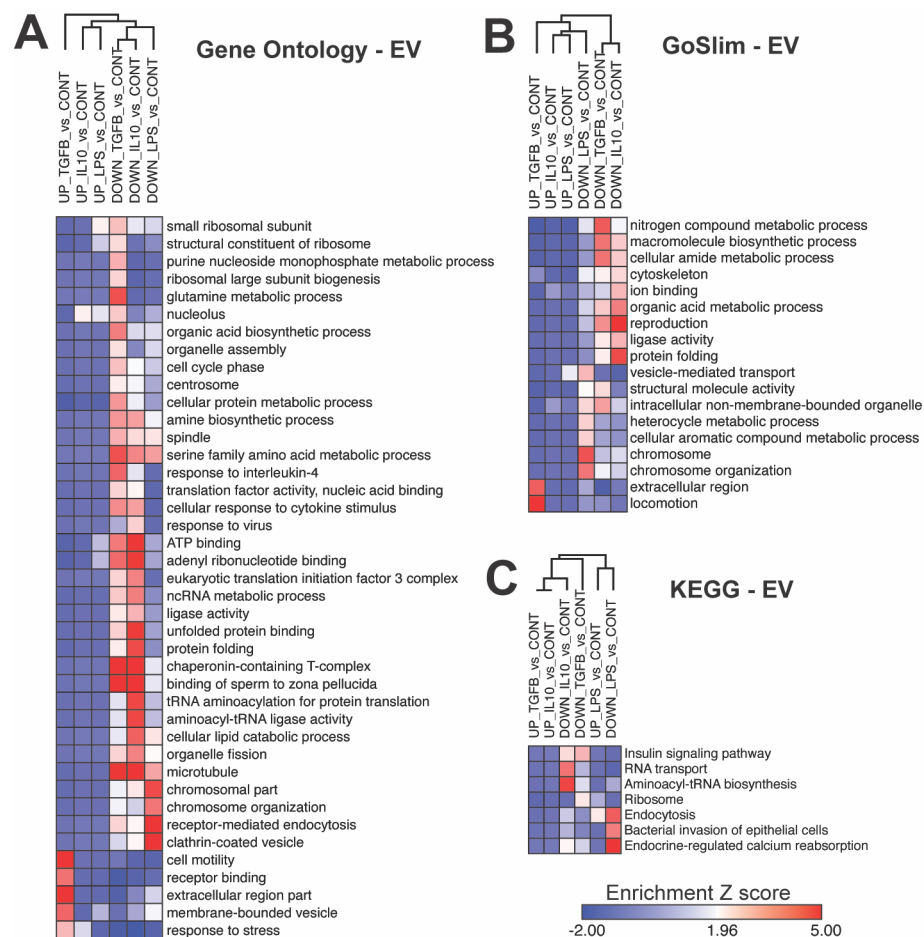
Figure 2.4: Gene ontology (GO) analysis of identified proteins in EVs from distinct microglia states. A. Heatmap representation, based on enrichment Z-scores, of Gene Ontology for EVs from polarized BV2 cells (p<0.05). **B.** Heatmap representation, based on enrichment Z-scores, of GO Slim for EVs from polarized BV2 cells (p<0.05). **C.** Heatmap representation, based on enrichment Z-scores, of KEGG for EVs from polarized BV2 cells (p<0.05).
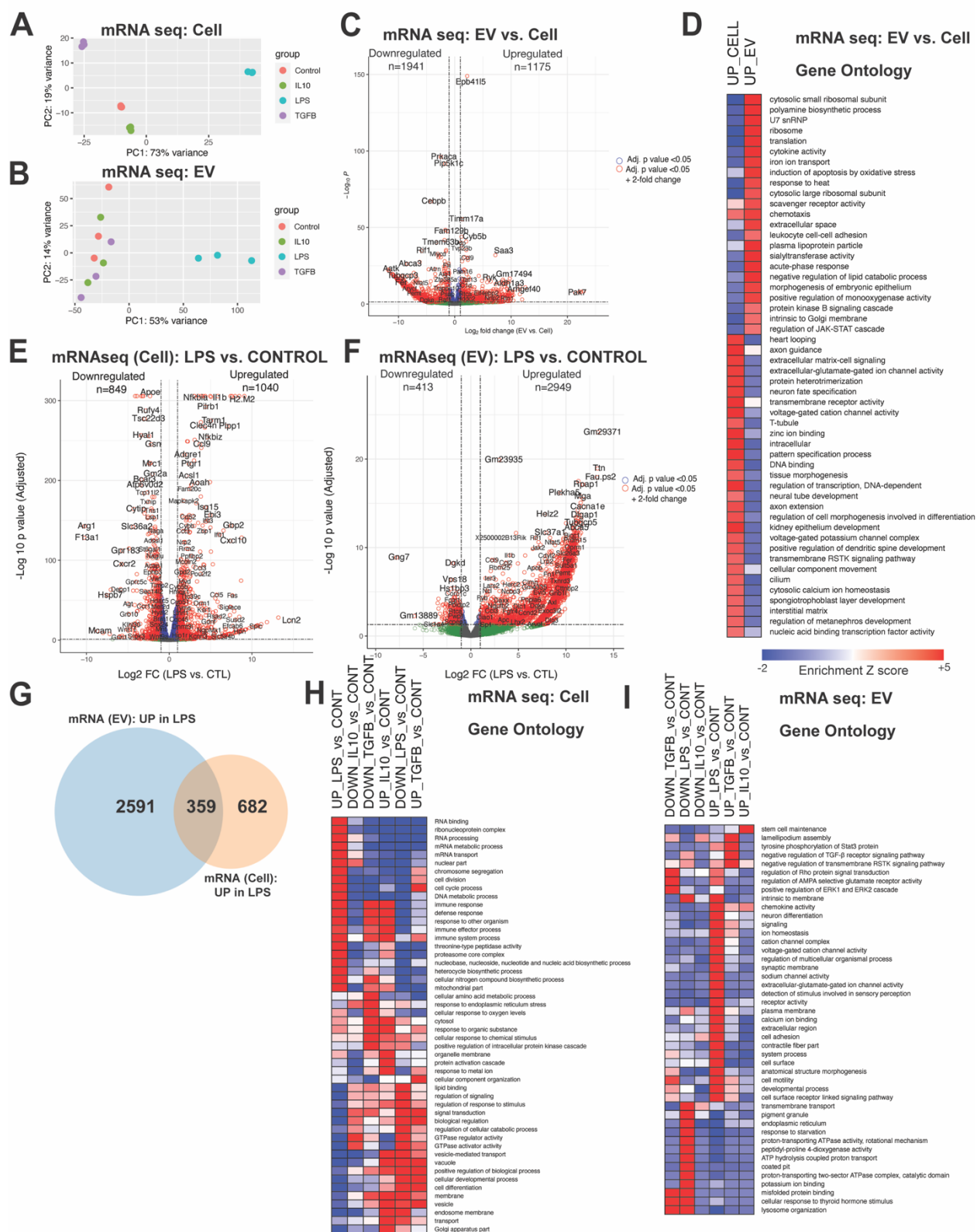
Figure 2.5: BV2 cells of distinct states and their EVs have unique mRNA signatures. A. PCA plot on mRNA seq data from BV2 cells – p<0.05, one-way ANOVA. **B.** PCA plot on mRNA seq data from BV2-

dervied EVs – p<0.05, one-way ANOVA. **C.** Volcano plot showing differentially expressed genes (DEGs – mRNA species) in EVs compared to BV2 cells (p <0.05). Upregulated and downregulated numbers correspond to red dots (p< 0.05 and log2 fold change LFC>1 for upregulated genes and LFC<-1 for downregulated genes). **D.** Heatmap representation, based on enrichment Z-scores, of Gene Ontology for highly enriched mRNAs (>=2-fold change) in EVs or whole cells. (p<0.05). **E.** Volcano plots showing DEGs in cell mRNAseq data – LPS vs Control (p<0.05). Upregulated and downregulated numbers correspond to red dots (p-value < 0.05 and log2 fold change LFC > 1 for upregulated genes and LFC<-1 for downregulated genes). **F.** Volcano plots showing DEGs in EV mRNAseq data – LPS vs Control (p<0.05). Upregulated and downregulated numbers correspond to red dots (p<0.05 and log2 fold change LFC>1 for upregulated genes and LFC<-1 for downregulated genes). **G.** Comparison of 1,040 upregulated mRNAs from BV2 cells treated with LPS to 2,949 upregulated mRNAs from LPS treated BV2-derived EVs. **H.** Heatmap representation, based on enrichment Z-scores, of Gene Ontology for BV2 cells (p<0.05). **I.** Heatmap representation, based on enrichment Z-scores, of Gene Ontology for BV2-dervied EVs (p<0.05).
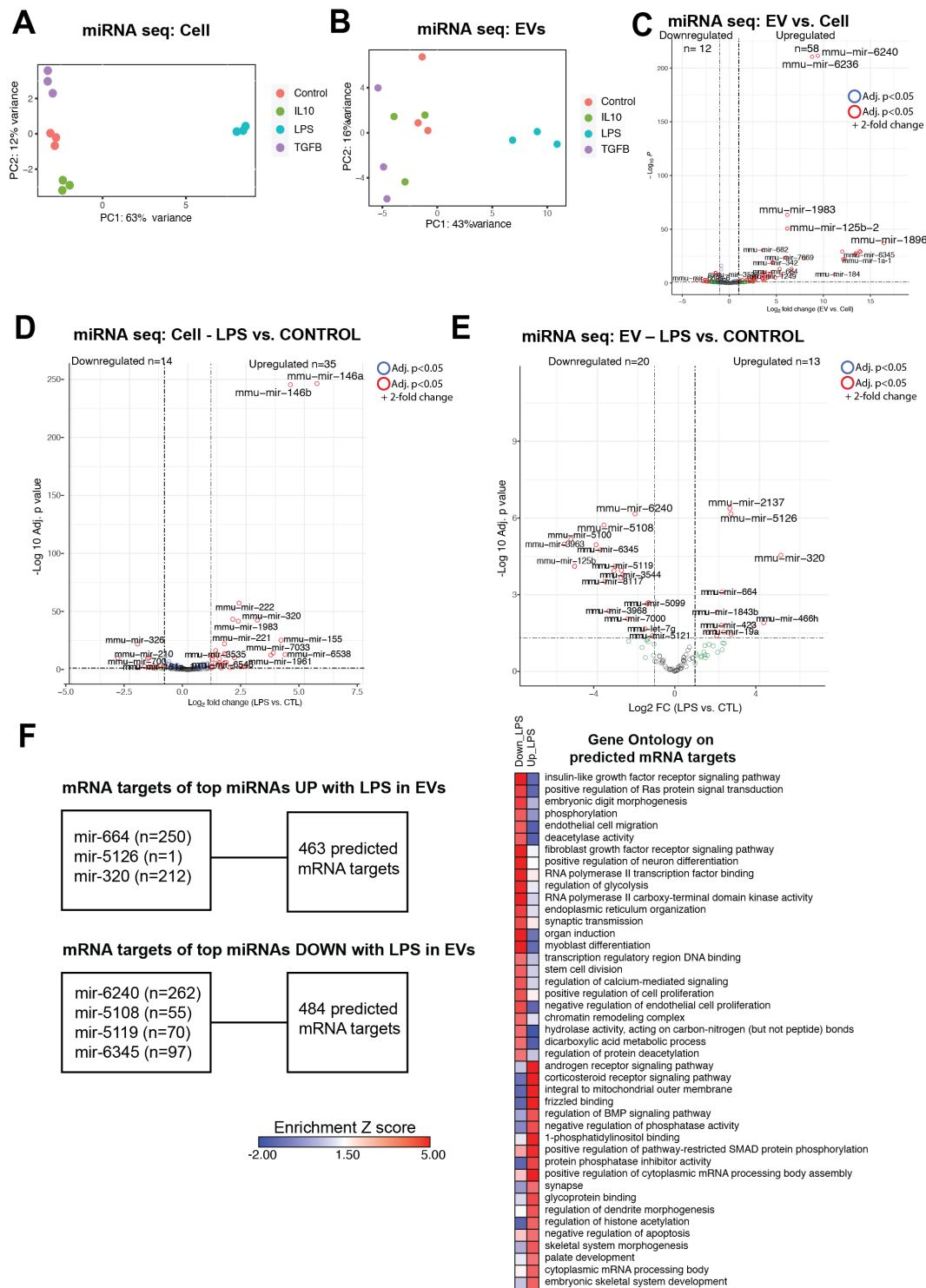
Figure 2.6: BV2 cells of distinct states and their EVs have unique microRNA signatures. A. PCA plot miRNA seq data from BV2 cells – p<0.05, one-way ANOVA. **B.** PCA plot miRNA seq data from BV2-dervied EVs – p<0.05, one-way ANOVA. **C.** Volcano plot – EV differentially expressed (DEX) miRNAs vs. Cell DEX miRNAs (p<0.05). Upregulated and downregulated numbers correspond to red dots (p<0.05 and log2 fold change LFC>1 for upregulated genes and LFC<-1 for downregulated genes). **D.** Volcano plot

– Cell miRNAs: LPS vs. CTL (p<0.05). Upregulated and downregulated numbers correspond to red dots (p<0.05 and log2 fold change LFC>1 for upregulated genes and LFC<-1 for downregulated genes). **E.** Volcano plot – EV miRNAs – LPS vs. CTL (p<0.05) Upregulated and downregulated numbers correspond to red dots (p<0.05 and log2 fold change LFC>1 for upregulated genes and LFC<-1 for downregulated genes). **F.** Top DEX miRNAs in EVs comparing LPS vs. CTL (p<0.05 and log2 fold change LFC>2 or LFC<-2) and the number of mRNA targets (target prediction score > 80 on miRDB) for those miRNAs. Heatmap representation, based on enrichment Z-scores, of Gene Ontology for mRNA targets.
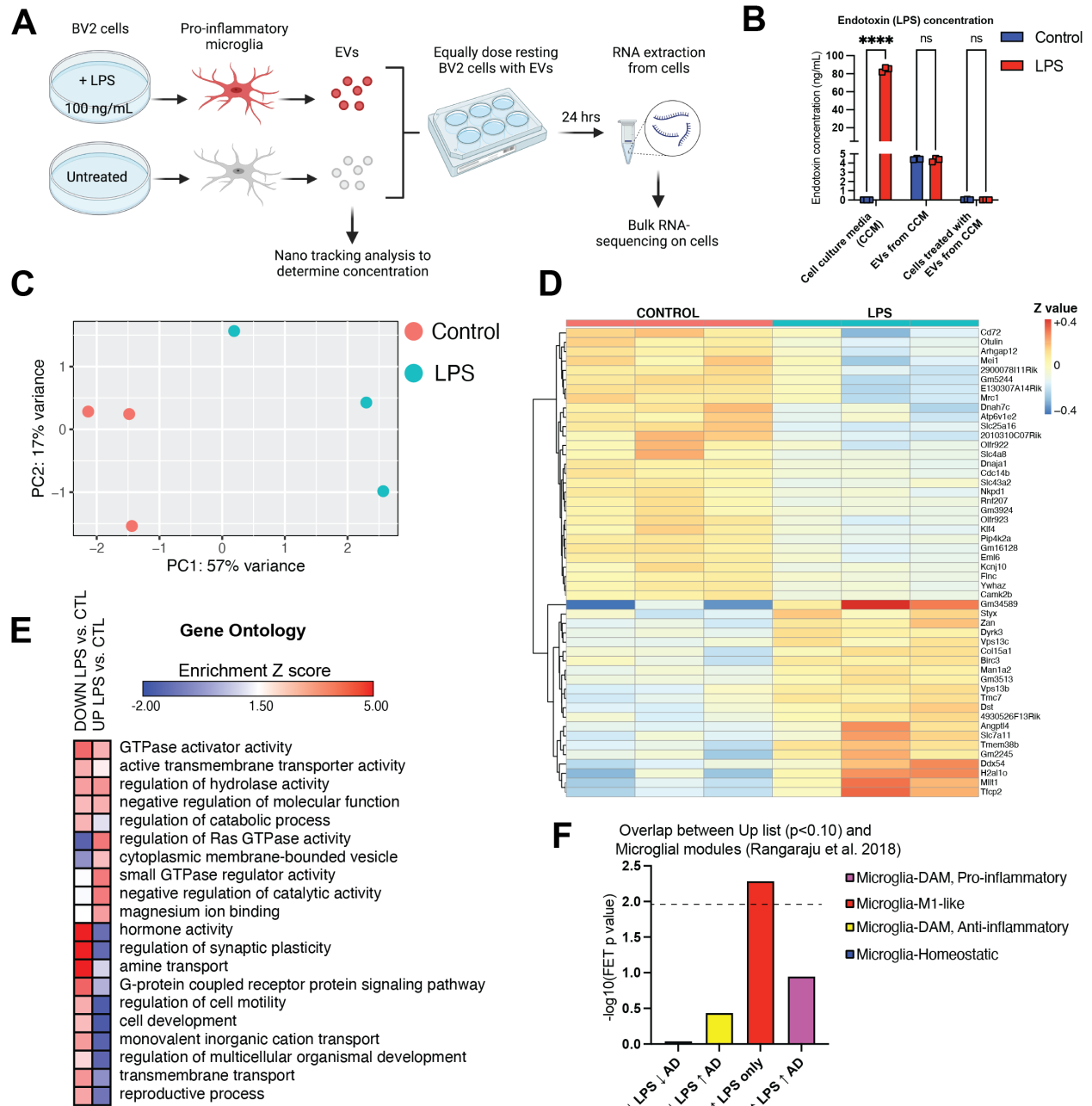
Figure 2.7: State specific effects of LPS treated microglia-derived EVs on resting BV2 cells. A. Illustration outlining experimental setup. This figure was created with BioRender.com. **B.** The endotoxin concentrations (ng/mL) of cell culture media (untreated and treated with LPS 100ng/mL) p<0.000001, significant, EVs from CCM (untreated and treated with LPS) p=0.511, not significant, and cells treated with EVs from CCM (untreated and treated with LPS) p=0.103, not significant. **C.** PCA plot on bulk RNA seq data from responder cells dosed with EVs derived from LPS treated BV2 cells or Control BV2 cells – p value <0.05, one-way ANOVA. **D.** Heatmap of DEGs in responder cells (LFC < or >0, p<0.05). **E.** Heatmap representation, based on enrichment Z-scores, of Gene Ontology in responder cells (LFC < or >0, p<0.10). **F.** FET Analysis demonstrating overlap between Up list (p<0.10) and microglia microarray analysis in Rangaraju et al. 2018. Bar color indicates microglial module color from referenced paper.
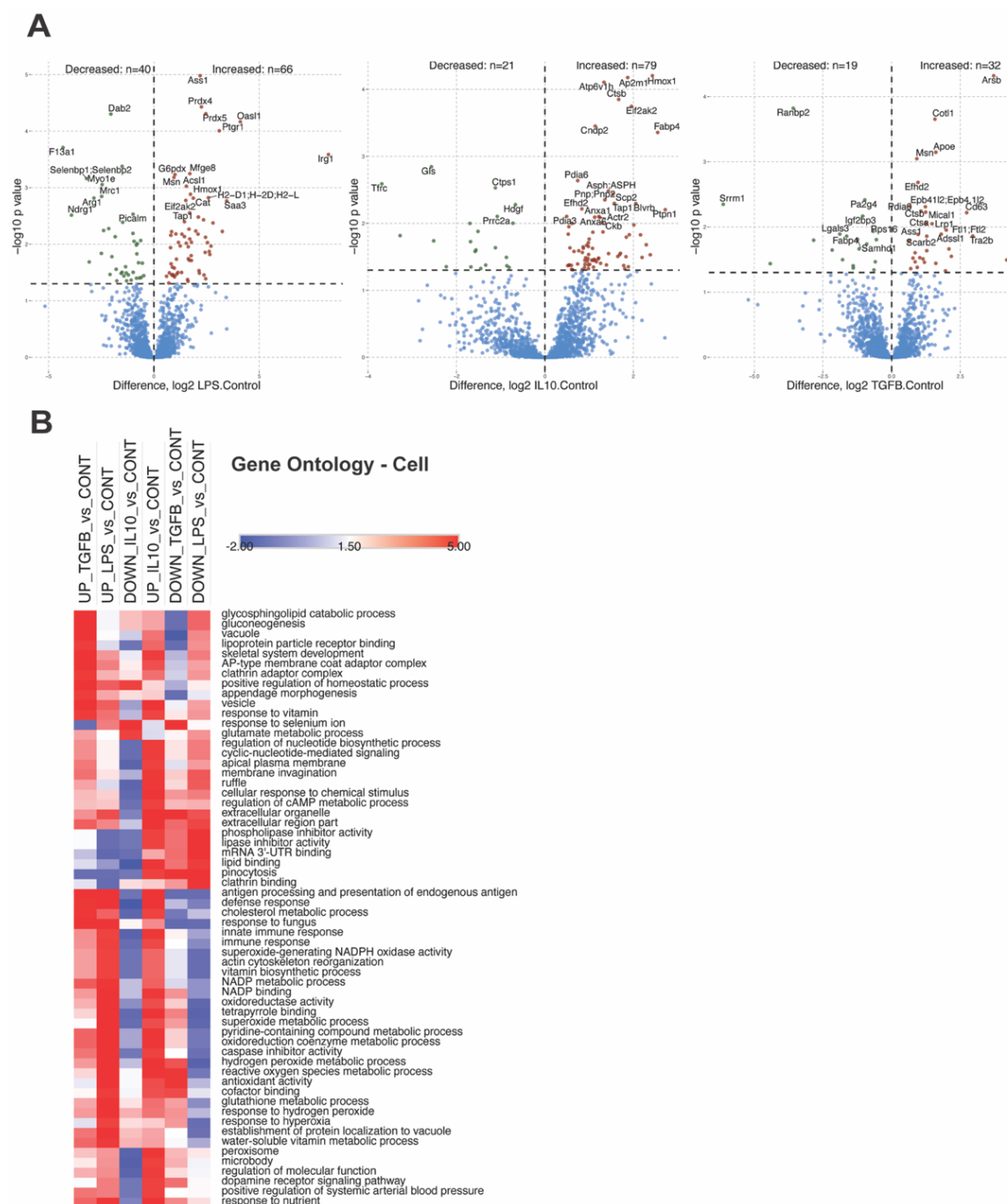
Supplemental Figure 2.1: BV2 Cell Proteome. A. Volcano plots showing differentially enriched proteins in EV proteome – IL10-CTL , LPS-CTL, TGF-β-CTL. **B.** Heatmap representation, based on enrichment Z-scores, of Gene Ontology for polarized cells (padj.<0.05).
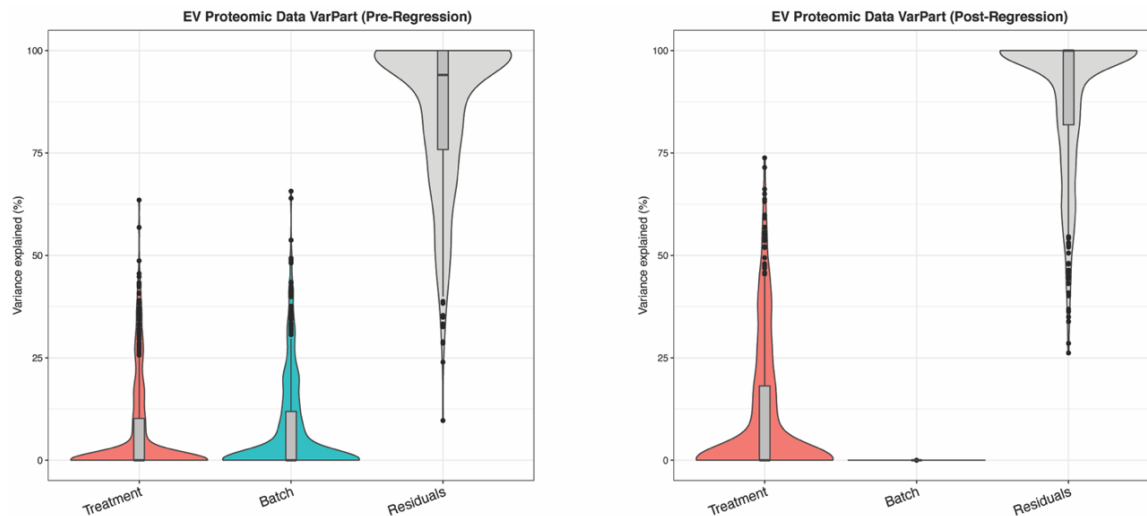
Supplemental Figure 2.2: Pre and Post Regression Variance Partition Plots for BV2 EV Proteome
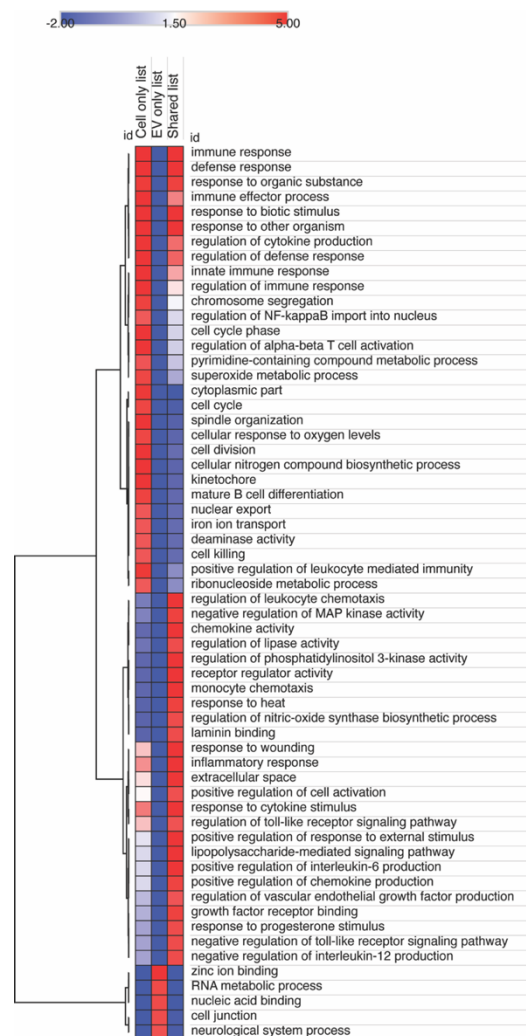
Supplemental Figure 2.3: Heatmap representation, based on enrichment Z-scores, of Gene Ontology from comparison of 2,949 upregulated mRNAs from BV2 cells treated with LPS to 1,040 upregulated mRNAs from LPS treated BV2-derived EVs (Figure 2.5F).
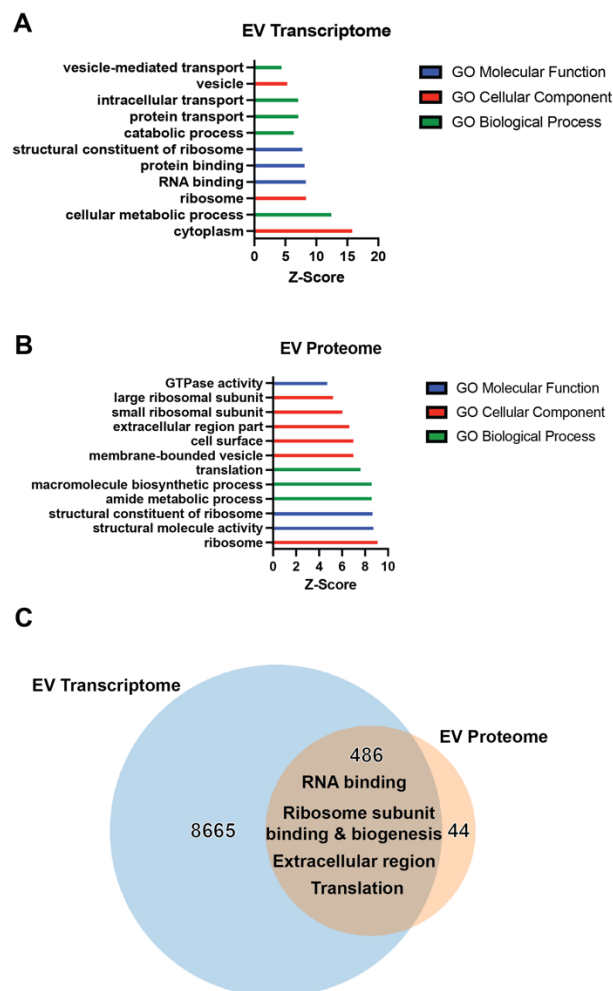
Supplemental Figure 2.4: Integrative analysis of EV proteomics and EV transcriptomics reveal common enrichment of RNA subunits, RNA binding, and translation. **A.** Top enriched pathways in the EV transcriptome. **B.** Top enriched pathways identified in the EV proteome. **C.** Venn diagram showing overlapping proteome and transcriptome pathways enriched in EVs.

III. Chapter 3. Cell-type specific biotin labeling in vivo to resolve glial-derived extracellular vesicle proteomes in the mouse brain

*Chapter III contains modified excerpts of findings and methodologies originally published in a coauthored publication in *Nature Communications* on May 25th, 2022. DOI: https://doi.org/10.1038/s41467-022-30623-x. Specific co-author contribution: methodology, writing, reviewing, and editing. Full citation below.

Rayaprolu S, Bitarafan S, Santiago JV, Betarbet R, Sunna S, Cheng L, Xiao H, Nelson RS, Kumar P, Bagchi P, Duong DM, Goettemoeller AM, Olah VJ, Rowan M, Levey AI, Wood LB, Seyfried NT, Rangaraju S. Cell type-specific biotin labeling in vivo resolves regional neuronal and astrocyte proteomic differences in mouse brain. Nat Commun. 2022;13(1):2927. Epub

i. Introduction

Different cell types, including neurons and glia, play distinct roles in brain development and disease processes. For example, a key causal pathological hallmark of neurodegenerative disease is chronic neuroinflammation which is primarily mediated by immune cells of the brain called microglia[96]. In AD, Aβ and tau pathologies promote microglia transformation from homeostatic to disease-associated states[257]. Genome-wide association studies have revealed that a large proportion of AD-associated risk genes are expressed preferentially in microglia compared to other brain cell types[96]. Disease-associated-microglia (DAM) play dual roles in AD pathogenesis, involving the production and release of pro-inflammatory factors including cytokines and toxic factors as well as neuroprotective, anti-inflammatory functions[109]. In addition, microglia depletion has been shown to increase Aβ plaque size in a mouse model of AD[258]. These findings confirm causal roles for microglia-mediated neuroinflammation in AD pathogenesis. While the molecular landscape of microglia in the AD brain has been investigated using omics-based tools, it is well known that transcriptomic data are poorly reflective of protein changes which are ultimately the effectors

of biological functions[200]. Therefore, there is a need to define microglial proteomic changes in AD to provide insight into microglia-mediated mechanisms of AD pathogenesis.

There is increasing evidence that pro-inflammatory subsets of DAM can mediate synapse loss[109], release neurotoxic factors, and secrete extracellular vesicles (EVs), including exosomes[96]. A newly identified mechanism of microglia-mediated neuroinflammatory responses in AD involves EV secretion and uptake. EVs contain proteins, mRNA, and microRNA and are secreted by several cell types[220]. EVs transport macromolecules between cells to facilitate intercellular communication and influence downstream signaling events as well as gene expression profiles in distant cells[148]. For example, in AD, DAM release small EVs (exosomes) containing pathologic tau that can be spread between neurons via endocytosis[186]. Furthermore, depleting microglia and inhibiting the synthesis of exosomes significantly suppresses propagation of pathogenic tau[186]. However, the specific proteins within microglia-derived EVs that lead to the perpetuation of AD pathology remain unknown. Thus, there is a need to identify the proteins that are transported by microglia-derived EVs in the context of neuroinflammation and neurodegenerative diseases, such as AD. Previous work conducted by the author of this thesis (*Chapter 2*), demonstrated that polarized BV2 microglia derived EVs display unique proteomic and transcriptomic signatures. Furthermore, the study demonstrated that LPS activated BV2-derived EVs can induce pro-inflammatory transcriptomic changes in receipt microglia, thus emphasizing the importance of microglia-derived EV cargo (*Chapter 2*). However, the proteomic cargo of microglia in vivo, across disease states is yet to be explored. Proteomic studies of microglia-derived EVs in vivo may yield unique markers of homeostatic microglial and DAM-derived EVs to guide EV purification from tissues including biofluids as disease biomarkers[198].

Microglia-specific proteomic studies have traditionally required isolation of microglia from the brain. Despite high purity of microglia, the resulting proteomes using these approaches are still contaminated by proteins from other cell-types. Furthermore, cell enrichment methods result in low yield, sampling bias, and artefactual cellular activation which lead to proteomes that are poorly-representative of the native state of microglia in vivo[206, 212, 259]. Cell-type specific in vivo proteomic labeling approaches, particularly biotinylation of proteins with a biotin ligase, TurboID, represent a promising approach to

overcome these scientific and technical gaps (*section 1.4*)[260]. Our laboratory has developed a novel approach that employs in-vivo TurboID to achieve <u>C</u>ell type-specific <u>I</u>n vivo <u>B</u>iotinylation <u>O</u>f <u>P</u>roteins or CIBOP. In this chapter, the author discusses in detail how we approached labeling the proteome of microglia in vitro and in vivo using the CIBOP approach. Furthermore, the author discusses ongoing efforts to label the EVs from specific cell types in vivo using the CIBOP approach.

ii. Paving the way to in vivo extensions of TurboID to label microglia and extracellular vesicles proteomes

Prior to developing an in vivo method of proximity labeling cell-type specific proteomes, our lab generated murine neuroblastoma (N2A) and microglial (BV2) lines stably expressing cytosolic TurboID (TurboID Nuclear Export Sequence or TurboID NES) to biotinylate the cellular proteome of these cells for downstream purification and analysis using mass spectrometry (MS)[219]. The purpose of this work was to establish the effects of global expression of cytosolic TurboID and biotinylation on mammalian cells and determine the breath of proteomic labeling using this approach. Sunna et al. reported that cytosolic TurboID biotinylates >50% of the proteome in microglia and neuronal cells and that these proteomes differ by about 1340 proteins[219]. Among these proteomes, TurboID-NES biotinylated several subcellular compartments within microglia and neuronal cells including neurodegenerative disease-relevant proteins. Moreover, using the lipopolysaccharide (LPS) model of acute inflammation, they showed that TurboID proteomic profiling captures microglial activation through the enrichment of immune-relevant proteins in microglia. The results from this study not only demonstrated the efficacy of TurboID-based proximity labeling to label cytosolic proteins in vitro, but also showed that TurboID-NES has minimal impacts on cellular proteomic composition and function which important for future applications[219].

Following foundational in vitro studies proving the efficacy of TurboID-based proximity labeling, we began developing in vivo proximity labeling applications of TurboID-NES for cell type–specific proteomics. Our first application was a stereotaxic injection AAV mediated delivery (AAV-CIBOP) of Cre recombinase under the human synapsin (hSyn1) promoter for pan-neuronal labeling of proteins in the

hippocampus[201]. Following 4 weeks after stereotaxic injection, mice received biotin supplementation in water (37.5 mg/L) for 2 weeks to induce biotin labeling. Label-free quantitation via mass spectrometry (LFQ-MS) of enriched biotinylated proteins from the forebrain lysates of *Rosa26^TurboID/wt*/hSyn1 mice and control mice (un-injected) revealed robust pan-neuronal labeling of proteins in the hippocampus by TurboID in vivo compared to control[201]. Furthermore, proteomic analysis of biotinylated proteins confirmed neuron-specific labeling with enrichment of neuronal and synaptic proteins.

Our second application involved a transgenic approach (Tg-CIBOP) by crossing *Rosa26-floxSTOP-TurboID* mice with *Camk2a-CreERT2* mice to label neurons and with *Aldh1l1-CreERT2* mice to label astrocytes[201]. The following section validating the neuronal-specific and astrocytic-specific biotinylation of proteins includes excerpts from our co-authored publication, Rayaprolu et al. 2022[201]. All experimental studies shown in **Figure 3.1** were reported in a prior collaborative publication from our group and these data have been included here as they were instrumental in establishing feasibility for proceeding experiments in this thesis[201]. Camk2a (Ca2+/calmodulin-activated protein kinase 2A) is an abundant serine-threonine kinase highly expressed by excitatory neurons, particularly in the synapse, where it regulates synaptic transmission, excitability, and long-term potentiation[261]. Aldh1l1 (aldehyde dehydrogenase 1 family member L1) converts 10-formyltetrahydrofolate to tetrahydrofolate and CO_2 together with the reduction of NADP and is regarded a pan-astrocyte marker[262]. To achieve astrocyte specific and neuronal specific labeling, we bred *Rosa26-floxSTOP-TurboID* mice with well-validated inducible Cre mouse lines, *Aldh1l1-CreERT2* and *Camk2a-CreERT2* mice, to express TurboID in an inducible manner (**Figure 3.1A**)[261, 262]. Conditional gene expression with the *Rosa26* vector was achieved by insertion of a *Lox*P flanked STOP element between the promoter (CAG) and the coding region. We inserted the V5-TurboID-NES construct into the *Rosa26* locus using restriction enzyme ligation resulting in *Rosa26-floxSTOP-TurboID* mice. *Rosa26-floxSTOP-TurboID* mice were then crossed with *Camk2a-CreERT2* or *Aldh1l1-CreERT2* to obtain heterozygous *Camk2a-CreERT2*, *Rosa26-floxSTOP-TurboID;Camk2a-CreERT2* , *Aldh1l1-CreERT2*, and *Rosa26-floxSTOP-TurboID;Camk2a-CreERT2* mice. Littermate *Rosa26-*

floxSTOP-TurboID control mice were also used for experiments. When *Camk2a-CreERT2* or *Aldh1l1-CreERT2* transgenic mice are bred with the *Rosa26-floxSTOP-TurboID* mice containing *LoxP*-flanked sequences, tamoxifen-inducible Cre-mediated recombination results in deletion of the floxed sequences allowing the system to turn on so TurboID is expressed in *Camk2a* or *Aldh1l1*expressing cells. Mice were treated with tamoxifen (i.p. 75mg/kg x 5 days) followed by 3 weeks and then 2 weeks of biotin water. After 2 weeks of biotinylation, brain regions (cortex, hippocampus, striatum/thalamus, pons/medulla, cerebellum, and spinal cord) were dissected from one hemisphere for proteomic studies, while the other hemisphere was used for immunohistochemical studies (**Figure 3.1A**). Western blot analysis of lysates from different brain regions of *Rosa26-floxSTOP-TurboID*;*Aldh1l1-CreERT2* and *Rosa26-floxSTOP-TurboID*;*Camk2a-CreERT2* mice confirmed biotinylation of proteins with distinct patterns of biotinylation between the two mouse lines, with few endogenously biotinylated proteins observed in control mice (**Figure 3.1B**). Qualitatively, *Rosa26-floxSTOP-TurboID*;*Camk2a-CreERT2* brain regions displayed a higher degree of labeling compared to *Rosa26-floxSTOP-TurboID*;*Aldh1l1-CreERT2* brain regions. We also confirmed TurboID protein expression via detection of V5 (**Figure 3.1B**). Immunofluorescent imaging of brain sections from these mice demonstrated biotinylation, as detected by Streptavidin-488, in *Rosa26-floxSTOP-TurboID*;*Camk2a-CreERT2* and *Rosa26-floxSTOP-TurboID*;*Aldh1l1-CreERT2* brains while control brains lacked any biotinylation (**Figure 3.1C**). *Rosa26-floxSTOP-TurboID*;*Aldh1l1-CreERT2* brains co-localized with Gfap- and Ndrg2- positive astrocytes with a preponderance of labeled blood vessels in the hippocampus (**Figure 3.5D**) as well as other brain regions, with no evidence of gliosis (**Figure 3.5E**). Furthermore, biotinylation was not observed in βIII-tubulin-positive neurons or Iba1-positive microglia, confirming astrocyte specificity in the *Rosa26-floxSTOP-TurboID*;*Aldh1l1-CreERT2* brains (**Figure 3.5D**). We next compared the proteomes from *Rosa26-floxSTOP-TurboID*;*Camk2a-CreERT2* and *Rosa26-floxSTOP-TurboID*;*Aldh1l1-CreERT2* brain regions and identified 1061 proteins with cell type-specific differences ($\geq$ 2-fold change and $p \leq 0.05$, **Figure 3.1F**), including 925 proteins more highly abundant in astrocytes and 136 proteins more highly abundant in neurons. We performed cell type enrichment analysis

of these differentially expressed proteins using protein marker lists derived from existing reference proteomes of brain cell types[263]. We found astrocytic proteins such as Gfap, Fbxo2, and Hepacam enriched in *Rosa26-floxSTOP-TurboID*;*Aldh1l1-CreERT2* proteome (**Figure 3.1F**, dark red dots) while neuronal proteins such as Syngap1, Camk2a, and Nptxr1 enriched in *Rosa26-floxSTOP-TurboID*;*Camk2a-CreERT2* proteome (**Figure 3.1F**, dark blue dots). GSEA of the differentially expressed cell type-specific protein lists revealed enrichment of metabolic terms, including lipid metabolism, in astrocytes, while receptor (ionotropic and metabotropic), synaptic and signal transduction terms were enriched in neurons (**Figure 3.1G).** Finally, we used the adapted Luminex approach to measure biotinylated signaling phosphoproteins from *Rosa26-floxSTOP-TurboID*;*Camk2a-CreERT2* and *Rosa26-floxSTOP-TurboID*;*Aldh1l1-CreERT2* brain homogenates. In comparison to *Rosa26-floxSTOP-TurboID*;*Camk2a-CreERT2* brain, levels of astrocyte-derived signaling phospho-proteins in the *Rosa26-floxSTOP-TurboID*;*Aldh1l1-CreERT2* brains were significantly lower even after accounting for differences in efficiency of TurboID labeling across cell types (**Figure 3.1H**). This suggests that basal MAPK and Akt/mTOR signaling activity is higher in Camk2a neurons compared to astrocytes under homeostatic conditions in the mouse brain. To summarize, these findings demonstrate the ability of CIBOP to resolve proteomic differences between two brain cell types, neurons and astrocytes, and identify regional molecular differences at the proteomic level in their native state, without the need for isolation[201].

Given the success of the *Rosa26-floxSTOP-TurboID*;*Camk2a-CreERT2* and *Rosa26-floxSTOP-TurboID*;*Aldh1l1-CreERT2* mice to label neurons and astrocytes in an inducible manner, we generated *Rosa26-floxSTOP-TurboID*;*Tmem119-CreERT2* mice to characterize the proteome of microglia using the CIBOP approach. Our goal is that when expressed, TurboID biotinylates microglial proteins that can be affinity captured by streptavidin coated beads for MS experiments. Furthermore, we hypothesized that the TurboID proximity labeling approach will not only label the proteomes of microglia but also microglia-derived EVs, thus allowing them to be traced back to their cell origin in proteomic studies.

iii.   **Preliminary Results**

TurboID labels extracellular vesicles derived from TurboID transduced BV2 cells

We applied size exclusion chromatography (Izon qEV) based methods to isolate EVs from BV2 microglia culture supernatants. We characterized EV morphology, size, concentration, and classical markers using transmission electron microscopy (TEM), nanoparticle tracking analysis (NTA), and western blot analyses. NTA verified that BV2-derived EVs are typically within the range of 50-200nm in diameter (mean particle size = 90nm) (**Figure 3.2A**). To characterize the morphology of BV2-dervied EVs, isolated EVs were examined using high resolution TEM following negative staining. TEM revealed vesicles with consistent round and cup-shaped morphology within ~50-150nm size range, as would be expected for EVs (**Figure 3.2B**). Western blot analyses of EV lysates from BV2 TurboID transduced microglia and BV2 untransduced control microglia found that the canonical EV protein markers CD9 is present (**Figure 3.2C**). Furthermore, preliminary data demonstrates robust biotinylation (streptavidin 680) in TurboID BV2 cellular and EV lysates (stably transduced to express V5 tagged TurboID with a nuclear export sequence or V5-TurboID-NES) compared to control BV2 cells **(Figure 3.2C)**. The two upper bands on the western blot represent endogenously biotinylated carboxylases that are enriched in control samples. These experiments provide the first data to demonstrate that TurboID proximity labeling can label extracellular vesicles derived from TurboID-NES transduced BV2 cells, as evidenced by streptavidin 680 western blot probing.

Rosa26-floxSTOP-TurboID;Tmem119-CreERT2 mice reveal insufficient biotin labeling of microglia

We used *Rosa26-floxSTOP-TurboID;Tmem119-CreERT2* mice to characterize the molecular composition of microglia by using a Cre/flox approach to express a biotin ligase, TurboID, in an inducible manner (**Figure 3.3A**). For this approach, we inserted a *Loxp-STOP-Loxp-V5-TurboID-NES* cassette into the *Rosa26* locus similar to previous CIBOP approaches as described above (**Figure 3.3B**)[201]. These *Rosa26-floxSTOP-TurboID* mice (heterozygous or homozygous) when bred with Cre mice, leads to the expression of TurboID causing biotinylation of the proteome outside the nucleus. *Tmem119-CreERT2* knock-in mice (JAX:031820) have the endogenous transmembrane protein 119 (Tmem119) promoter/enhancer sequences that direct the expression of tamoxifen-inducible Cre recombinase in

microglia. To validate the microglial Cre line and confirm that the Rosa26 locus is active in microglia, *Tmem119-CreERT2* mice were crossed with green fluorescent protein (GFP) reporter mice, *Rosa26-EGFP^f* mice (JAX:004077). Expression of the EGFP gene is blocked by a *lox*P-flanked STOP fragment placed between the EGFP sequence and the Gt(ROSA)26Sor promoter. However, once crossed with the *Tmem119-CreERT2* mice, successful *Cre* excision can occur by EGFP expression in *cre*-expressing microglia. We then treated these mice with tamoxifen (i.p. 75mg/kg x 5 days) and euthanized them after 3 weeks of recombination. IF of fixed brain confirmed cell type specific GFP expression (**Figure 3.3C**).

Before we processed any brains for EV isolation, we wanted to ensure that our cell type specific protein labeling technique was successful in labeling microglia. To assess this, we analyzed biotinylated proteins from *Rosa26-floxSTOP-TurboID;Tmem119-CreERT2* mice using western blot, immunofluorescence (IF), and flow cytometry (**Figure 3.4A**). For our first cohort, we followed the traditional CIBOP protocol which includes 1 week of tamoxifen followed by a 3 week period and then 2 weeks of biotin water. In this cohort, we found that *Rosa26-floxSTOP-TurboID;Tmem119-CreERT2* mice (n=5) and control *Tmem119-CreERT2* mice (n=2) showed no difference in biotin labeling by western blot analysis with streptavidin 680 **(Figure 3.4B)**. Overall the level of biotinylation in brain lysates (regardless of the brain region) from *Rosa26-floxSTOP-TurboID;Tmem119-CreERT2* mice was underwhelming compared to control mice. These results vary significantly from the robust biotinylation we observed with our *Rosa26-floxSTOP-TurboID;Camk2a-CreERT2* (neuronal) and *Rosa26-floxSTOP-TurboID;Aldh1l1-CreERT2* (astrocytic) mice **(Figure 3.1C).**

Given these results, we decided to set up several experimental timelines that differ from our standard protocol to determine if biotin labeling of microglia can be improved. We extended the time between tamoxifen (75mg/kg x 5 days) and biotin water (37.5 mg/L) from 3 weeks to 6 weeks. In addition, we attempted a longer period of biotin water treatment, trying out 4 weeks instead of 2 weeks. And lastly, we treated mice with LPS (10 µg/dose/day) for the five days prior to the sac to determine if an inflammatory challenge and microglia activation would increase uptake of biotin and improve biotinylation levels.

Western blot (probed for streptavidin 680) of regional brain lysates from mice that underwent these different experimental paradigms, demonstrated that there was no difference in the level of biotinylation between *Rosa26-floxSTOP-TurboID;Tmem119-CreERT2* mice and control *Tmem119-CreERT2* mice (**Figure 3.4C**). These results were also confirmed by immunofluorescence (IF) in the hippocampal brain region with DAPI (nuclear marker), Iba1 (microglia marker) and streptavidin-488 (biotin detector). IF images confirmed that there is no observed biotinylation of *Rosa26-floxSTOP-TurboID;Tmem119-CreERT2* mouse microglia. These IF studies were conducted across all mice and brain regions and the results were the same.

These negative qualitative results from IF and western blot studies, led us to conduct flow cytometric based approaches to assess biotinylation levels and confirm that recombination at the *Rosa26* locus occurred. For flow cytometry experiments, mononuclear cells isolated from the fresh brains of *Rosa26-floxSTOP-TurboID;Tmem119-CreERT2* (n=2) and *Tmem119-CreERT2* control mice (n=2) were fixed, permeabilized, and stained with Cd11b, Ly6c, and streptavidin to determine the percentage (if any) of the microglia population that is labeled by biotin. Using Cd11b$^+$ and Ly6c^{low} we gated for our microglia population among mononuclear cells (**Figure 3.5**). Next, we used streptavidin-488 to gate for our biotinylated microglia population. Our results demonstrated that 47% of microglia from *Rosa26-floxSTOP-TurboID;Tmem119-CreERT2* mice are biotinylated compared to 1.5% in *Tmem119-CreERT2* control mice (**Figure 3.5**). These results demonstrating biotinylation in 47% of microglia from *Rosa26-floxSTOP-TurboID;Tmem119-CreERT2* mice confirms that recombination at the *Rosa26* locus occurred. However, this labeling is still significantly lower than the labeling we observe by flow cytometry in our other cell type specific TurboID mouse models (neuronal and astrocyte). Furthermore, although the biotinylation percentage of microglia from *Rosa26-floxSTOP-TurboID;Tmem119-CreERT2* is larger than that of *Tmem119-CreERT2* control mice as evidenced by flow cytometry, this is still not robust enough to be detected by IF, western blot analyses, or mass spectrometry. Since *Rosa26-floxSTOP-TurboID;Tmem119-CreERT2* mice reveal insufficient biotin labeling of microglia, we decided to assess biotin labeling of brain-derived EVs with the validated *Rosa26-floxSTOP-TurboID;Aldh1l1-CreERT2* mice.

<u>*Rosa26-floxSTOP-TurboID;Aldh1l1-CreERT2* mice reveal sufficient biotin labeling of astrocytes and</u>

<u>brain derived-EVs</u>

Given the success of labeling the astrocytic proteome with the *Rosa26-floxSTOP-TurboID;Aldh1l1-CreERT2* mice[201], we isolated EVs from the brains of these mice to see if the CIBOP method is successful in labeling the proteome of EVs as well. We applied enzymatic digestion of tissue and size exclusion chromatography based methods to isolate EVs from frozen mouse brain. Given the novelty of this approach to the lab, we once again characterized the EV morphology, size, and concentration using TEM and NTA. NTA verified that brain-derived EVs are typically within the range of 50-200nm in diameter (mean particle size =126nm) (**Figure 3.6A**). TEM revealed vesicles with consistent round and cup-shaped morphology within ~50-200nm size range, as would be expected for EVs (**Figure 3.6B**). Using the established CIBOP protocol from our lab[201], we treated *Rosa26-floxSTOP-TurboID;Aldh1l1-CreERT2* mice (n=3) and control *Aldh1l1-CreERT2* mice (n=3) with 1 week of tamoxifen followed by a 3 week period and then 2 weeks of biotin water (**Figure 3.6C**). In this cohort, we found that the brain lysates and brain-derived EV lysates from *Rosa26-floxSTOP-TurboID;Aldh1l1-CreERT2* mice demonstrated robust biotin labeling compared to control *Aldh1l1-CreERT2* mice, based on western blot analyses probing with streptavidin 680 (**Figure 3.6D**). It is important to note that biotinylation levels are far more robust in brain lysates compared to EV lysates due to the larger amount of input protein. These results demonstrate a promising approach to labeling the EV proteome of specific cell types in vivo.

iv. Preliminary conclusions and study limitations

This study represents the first effort to label the proteome of microglia in vivo by applying the CIBOP approach to *Rosa26-floxSTOP-TurboID;Tmem119-CreERT2* mice. Using western blot analysis, IF, and flow cytometry to visualize biotinylation levels, we determined that *Rosa26-floxSTOP-TurboID;Tmem119-CreERT2* mouse microglia, regardless of experimental timelines, do not robustly label compared to previous CIBOP models (*Rosa26-floxSTOP-TurboID;Aldh1l1-CreERT2* and *Rosa26-floxSTOP-TurboID;Camk2a-CreERT2*) and control mice. Although there was modest biotinylation of microglia

(47%) from *Rosa26-floxSTOP-TurboID;Tmem119-CreERT2* mice compared to control (1%), this percentage is not enough for detection via western blot analysis, IF, and LFQ-mass spectrometry. On the other hand, as previously discussed and demonstrated, BV2 cells transduced with TurboID-NES demonstrate robust labeling compared to control cells. However, this mechanism of biotin labeling by TurboID is somehow ineffective in vivo compared to in vitro approaches. These results spark the conversation regarding why microglia are resistant to TurboID labeling in vivo. One idea is that small molecule transporters that transport vitamins including biotin (ex. Slc5a6/SMVT) may be less abundant or active in microglia in vivo. Studies have shown that the expression of Na(+)-dependent multivitamin transporter (SLC5A6/SMVT) is critical to transport of biotin, pantothenate, and lipoic acid into the brain via the blood-brain barrier[264]. However, Slc5a6/SMVT levels in microglia compared to other cell types have not been previously reported. Some ways to address this question would be to delete Slc5a6 globally in our microglia Cre/TurboID system to see if biotinylation decreased or to modify the dose of biotin (not the duration) to see if that improves transporter activity. Limitations to these approaches are that deletion of Slc5a6 may induce a metabolic disorder and increased biotin dose may cause toxicity. If it is in fact an issue with less active or less abundant Slc5a6 in microglia, we can attempt to over express Slc5a6 in our mouse microglia model to see if microglia biotinylation can be achieved. Potentially in vitro BV2 microglia cells are oversaturated with biotin that there is passive transport, whereas transport of biotin in vivo is transporter dependent. However, future experiments similar to those outline above will need to be performed to understand the biological or mechanistic reason behind microglia resistant to TurboID labeling in vivo.

The CIBOP approach can be a powerful approach to investigate molecular changes occurring at the proteomic level while retaining the native state of the cell. More importantly, the CIBOP approach may elucidate cargo proteomic differences of EVs from specific cell types which may be helpful in understanding disease pathogenesis. To understand the potential of TurboID-proximity labeling to label the proteomes of EVs, we first utilized an in vitro approach with BV2 transduced (TurboID NES) cells. Our results demonstrated that TurboID proximity labeling can label EVs derived from TurboID-NES transduced BV2 cells, as evidenced by western blot analysis. After validating this in vitro, we decided to utilize the

well characterized *Rosa26-floxSTOP-TurboID;Aldh1l1-CreERT2* astrocytic mouse model to determine the efficacy of labeling brain derived-EVs using the CIBOP approach. Following successful isolation of EVs from frozen mouse brain, we were able to demonstrate that the brain and EV lysates from *Rosa26-floxSTOP-TurboID;Aldh1l1-CreERT2* demonstrate robust labeling compared to control mice as seen by western blot. To further validate this labeling, mass spectrometry based approaches need to be performed. However, a difficult aspect of the affinity purification of biotinylated proteins using streptavidin beads is the requirement for a large amount of protein (~1mg), as demonstrated in previous studies in our lab[201, 219]. Given that EV protein abundance is much smaller than brain protein abundance, there needs to be adaptations to existing pipelines so that biotin labeled proteins in EVs can be properly enriched. First, the ratio of magnetic streptavidin coated beats to protein must to be scaled appropriately to reflect the smaller amount of protein in EVs. Furthermore, samples should be run on more sensitive mass spectrometry instruments such as the Thermal Ionization Mass Spectrometry (TIMS), which allows for highly sensitive detection of specific peptides and proteins in complex biological sample[265].

However, it is important to consider that the CIBOP approach using the TurboID nuclear export sequence may not be the best way to label the proteomes of extracellular vesicles. This year, Li et al. published their study on "TurboID-EV" system[266]. They developed the TurboID-EV system with the TurboID tethered to the EV membrane, which allowed them to track the footprints of EVs during and after EV uptake by the proximity-dependent biotinylation of recipient cellular proteins. By combining TurboID-EV biotinylation with stable isotope labeling with amino acids in cultured cells (SILAC), fluorescence-activated cell sorting (FACS), and spintip-based affinity purification of biotinylated proteins, they successfully identified TurboID-EV proteins themselves and recipient cell proteins proximal to TurboID-EVs[266]. This TurboID-EV system applied with cell type specificity, could potentially elucidate various EV subtypes and recipient cell types, providing a tool to further dissect the role of EVs in cellular communication and disease processes.

v.   Methodology

Creating a stably transduced TurboID BV2 cell line

BV2 cells were transduced with a puromycin-resistant lentivirus construct of a V5-TurboID-NES containing an NES (V5-TurboID-NES) and a GFP connected via a T2A linker. Constructs were generated in Emory University's Viral Vector Core. Given a titer of 1.5×10^9 I.U./ml, we experimented with multiplicities of infection (MOIs) 5 and 10. In biological triplicates, three wells of each cell type received the lentivirus at either an MOI of 5 or 10 or received no virus (untransduced control). About 48 h following transduction, half of the media was replaced with fresh media, and the cells were split 1:3 on 72 h following transduction. Puromycin selection began 96 h after transduction, half of the media were replaced with 2 μg/ml of puromycin for a final concentration of 1 μg/ml. For the following week, half of the media were replaced every other day with fresh puromycin-containing media to remove nonadherent cells. After this, the cells were split twice weekly and maintained with media containing 1 μg/ml of puromycin. We validated the puromycin screening procedure by assessing the percentage of GFP-positive cells with a fluorescent microscope and flow cytometry. A majority of cells were GFP positive 3 days after addition of puromycin selection. After >90% of the cells were GFP positive, the cells were maintained in 10 cm dishes in media containing 1 μg/ml of puromycin. Cells receiving the lentivirus at an MOI of 5 reached confluency sooner, and we did not observe a difference in transduction efficacy between MOIs 5 and 10. Successfully transduced BV2 cells were frozen as stocks in the liquid nitrogen tank for future use.

Cell culture studies

Transduced (V5-TurboID-NES) and untransduced (control) BV2 cells were cultured in Dulbecco's modified Eagle's medium (DMEM) supplemented with high glucose and L-glutamine containing 1% penicillin/streptomycin, and 10% FBS. All media was vacuum-filtered with $0.2\,\mu$m filters. The cells were incubated at 37 degrees Celsius (°C) and 5% CO_2 until reaching 80% confluency. The splitting regimen took place twice weekly, plating one million cells onto a 100 mm culture plate to a final volume of 12 mL culture media. In preparation for experiments, one million cells were plated in 100 mm plates with 12 mL

of media. 24 hours after plating, existing media was swapped for filtered serum-free media (DMEM containing 1% penicillin/streptomycin) and transduced (V5-TurboID-NES) and untransduced BV2 cells were treated with 200 μM of Biotin. After 72 hours in culture, cell culture medium was collected from the plates, transferred into 15 mL tubes, and placed on ice. Next, the plates were washed twice with ice-cold 1x phosphate buffer saline (PBS). Cell pellets were harvested in 500 μL Urea lysis buffer (8 M Urea, 10 mM Tris, 100 mM NaH_2PO_4, pH 8.5) with 1x HALT protease & phosphatase inhibitor cocktail without EDTA. Cell lysates were then sonicated at 30% amplitude thrice in 5-second on-off pulses to disrupt nucleic acids and cell membrane. All cell lysates were centrifuged at 4°C for 2 minutes at 12,700 rpm. The supernatants were transferred to a fresh 1.5 mL LoBind Eppendorf tube.

EV isolation from cell culture media

EV isolation from cell culture media is the same as described in *Chapter 2.6 Methods & Methodology*. Cell culture media underwent several centrifugation steps to remove cellular debris (10 min at 500xg and 10 min 10,000xg). After each spin, the supernatant was collected and subjected to the subsequent spin. The final supernatant was collected and added to an Amicon Ultra-15 Centrifugal Filter (molecular weight cut-off 100 kDa) to concentrate the sample and then was added to a qEV column resin column for size exclusion chromatography using the Izon qEV system with a qEVoriginal / 35 nm Gen 2 Column. Sterile PBS was used as the flushing buffer. The second fraction containing the most abundant amount of EVs was then concentrated using a Amicon Ultra-2 Centrifugal Filter (molecular weight cut-off 100 kDa) or Pierce Concentrator 0.5mL, PES (molecular weight cut-off 100 kDa). The resulting concentrate was used for any downstream analysis.

Transmission Electron Microscopy (TEM) of EVs

For electron microscopic analysis, 5 μL from the EV samples were loaded onto the carbon side of charged copper/carbon-coated electron microscopic grids. After 5 minutes, sample loaded grids were washed 3 times in distilled water and then stained with 1-3% uranyl acetate for 1 minute in the dark. Once grids were dry, EVs were observed under TEM at 80 kV. TEM grids were stored in the appropriate grid storage boxes for future use. Hitachi HT7700 transmission electron microscope operating at 80 kV was used for imaging.

Nano tracking Analysis (NTA) of isolated EVs

The size and total number of EVs were measured by using NanoSight NS300 (Malvern, UK) with the technology of Nanoparticle Tracking Analysis (NTA). Size distribution and concentration of EVs in an aqueous buffer was obtained by utilizing Brownian motion and light scattering properties. Samples were diluted with 1X PBS to obtain optimal concentration for detection (10^6–10^9 particles/ml) and injected with a continuous syringe system for 60 s $\times$ 3 times at speed 100 µl/min. Data acquisition was undertaken at ambient temperature and measured 3 times by NTA. Data were analyzed with NTA 3.2 software (Malvern, UK) with minimum expected particle size 10 nm.

Confirming protein biotinylation with western blot analysis

Protein concentration was determined by bicinchoninic acid (BCA) assay (Thermo, 23225). To confirm protein biotinylation, 15 µg of cell lysates or 20 ul of EV lysate were resolved on a 4–12% Bris-Tris gel, transferred onto a nitrocellulose membrane, and probed with streptavidin-Alexa680 (Thermo, S32358) diluted 1:10 K in Start Block (Thermo, 37543) for 1 h at room temperature. Subsequently, the membrane was washed in 1X tris buffered saline containing 0.1% Tween20 (TBS-T) and imaged using Odyssey Infrared Imaging System (LI-COR Biosciences).

Animal studies

Approval from the Emory University Institutional Animal Care and Use Committee was obtained prior to all animal-related studies. All mice used in the present study were housed in the Department of Animal Resources at Emory University under a 12 h light/12 h dark cycle with ad libitum access to food and water. Animals were housed in the vivarium under standard conditions for mice (temperature 72 F, humidity range 40–50%). All procedures were approved by the Institutional Animal Care and Use Committee of Emory University and were in strict accordance with the National Institute of Health's "Guide for the Care and Use of Laboratory Animals."

Transgenic approach for microglial Cre recombinase expression in *Rosa26-floxSTOP-TurboID* mice

Rosa26-floxSTOP-TurboID mice were crossed with *Tmem119-CreERT2* (Jackson Labs, Strain #:031820, RRID:IMSR_JAX:031820) to generate heterozygous *Tmem119-CreERT2* and *Rosa26-floxSTOP-TurboID;Tmem119-CreERT2* littermate mice. For the standard protocol, mice were given tamoxifen (75 mg/kg) intraperitoneally for 5 days at 6 weeks of age. After 3 weeks, mice were given water supplemented with biotin (37.5 mg/L) for 2 weeks until euthanasia at 3 months of age. After biotin supplementation (37.5 mg/L) for 2 weeks (standard protocol), mice were anesthetized with ketamine (ketamine 87.5 mg/kg, xylazine 12.5 mg/kg) followed by transcardial perfusion with 30 mL of ice-cold PBS. The brain was immediately removed and hemi-sected along the mid-sagittal line. The left hemisphere was fixed in 4% paraformaldehyde (PFA) for 24 h and then transferred to 30% sucrose after through washes in PBS.

Transgenic approach for astrocytic Cre recombinase expression in *Rosa26-floxSTOP-TurboID* mice

Rosa26-floxSTOP-TurboID were crossed with *Aldh1l1-CreERT2* mice (Jackson Labs, Stock No. 012362) to generate heterozygous *Aldh1l1-CreERT2* and *Rosa26-floxSTOP-TurboID;Aldh1l1-CreERT2* littermate mice. For the standard protocol, mice were given tamoxifen (75 mg/kg) intraperitoneally for 5 days at 6 weeks of age. After 3 weeks, mice were given water supplemented with biotin (37.5 mg/L) for 2 weeks until euthanasia at 3 months of age. After biotin supplementation (37.5 mg/L) for 2 weeks (standard protocol), mice were anesthetized with ketamine (ketamine 87.5 mg/kg, xylazine 12.5 mg/kg) followed by transcardial perfusion with 30 mL of ice-cold PBS. The brain was immediately removed and hemi-sected along the mid-sagittal line. The left hemisphere was fixed in 4% paraformaldehyde (PFA) for 24 h and then transferred to 30% sucrose after through washes in PBS. The right hemisphere of the brain was used for EV isolation (if performed) and downstream western blot analysis.

EV isolation from mouse brain

Frozen brain tissue samples (~400-500 mg) was enzymatically digested with 75U/ml of collagenase type 3 in Hibernate-E (at a ratio of 800 μl per 100 mg of brain). Tissue was incubated at 37°C for a total of 20 min. After 5 min passed in the incubation, the tube was swirled gently and inverted to mix tissue and

digestion solution and then returned to the incubator. After 10min passed in incubation, tissue was gently pipetted twice up and down before incubating for the remaining time. After incubation was complete, tissue was returned to ice immediately and HALT phosphatase and protease inhibitors were added to a final concentration 1x. Next, samples underwent a series of centrifugation steps (5 min at 300xg, 30 min at 2,000xg, and 30 min at 10,000xg). Supernatants were collected after every spin and transferred to a fresh tube before next spin. Steps following centrifugation are the same as EV isolation from cell culture media (see above).

Confirming protein biotinylation with western blot analysis

Protein concentration was BCA assay (Thermo, 23225). To confirm protein biotinylation, 10 μg of cell lysates or 20 ul of EV lysate were resolved on a 4–12% Bris-Tris gel, transferred onto a nitrocellulose membrane, and probed with streptavidin-Alexa680 (Thermo, S32358) diluted 1:10 K in Start Block (Thermo, 37543) for 1 h at room temperature. Subsequently, the membrane was washed in 1X tris buffered saline containing 0.1% Tween20 (TBS-T) and incubated over-night with mouse anti-V5 (1:250; Thermo, R960-25) diluted in Start Block. After washes in TBS-T, membranes were incubated with goat anti-mouse 700 (1:10 K) and imaged using Odyssey Infrared Imaging System (LI-COR Biosciences).

Immunofluorescence (IF) studies

Brains were fixed in 4% PFA and cut into 30μm sections. Sections were rinsed in TBS 3 times for 5 minutes. Then sections were incubated in TBS/ 0.25% Triton TX-100 / 5% serum at room temperature for 1 hour. Primary antibody Iba1 (microglia marker, 1:500 rabbit anti-Iba1, Abcam, ab178846) was diluted in TBS/ 0.25% Triton TX-100 /1% serum. Sections were incubated overnight at 4 degrees Celsius with primary. The following day samples were rinsed in TBS/1% Serum Solution 3 times for 10 minutes. Secondary antibodies (anti-rabbit Rhodamine-red ThermoFisher, R6394; Streptavidin Alexa flour 488 1:500, ThermoFisher, S11223) were diluted in TBS/1% serum solution. Sections were incubated in secondary antibodies for 1 hour at room temperature in the dark. Stained sections were rinsed in TBS 3 times for 10 minutes. sections were mounted on slides with mounting media containing DAPI (Sigma Aldrich, F6057)

for nuclear staining. Representative images of the same regions across all samples were taken using the Keyence BZ-X810 and all image processing.

Acute isolation of adult mice CNS cells for flow cytometry

Experimental mice were anesthetized with isoflurane and euthanized by cardiac perfusion with ice-cold 1xPBS. Whole brain was removed and immediately dissociated over a 40μM sterile cell strainer to obtain single cell suspension in 30mL of 1xPBS. The suspension was centrifuged at 800 x g for 5 min at 4 degrees Celsius to obtain a cell pellet. Supernatant was discarded and the cell pellet was re-suspended in 6 mL of fresh 35% Stock Isotonic Percoll (SIP), transferred to a 15mL conical, and 2mL of 70% SIP was carefully under-laid. SIP was prepared as 90% percoll + 10% 10xHBSS. The established gradient was centrifuged for 25 min at 800 x g at 15 degrees Celsius with no brakes. Subsequently, 3mL of the layer between the 35-70% SIP layers were collected, washed with ice-cold 1xPBS, and centrifuged at 800 x g for 5 min at 4 degrees Celsius. The cell pellet containing microglia was resuspended in cold 1xPBS and transferred into 5mL round-bottom tubes for downstream experiments.

Flow cytometry

Acutely isolated cells were stained with surface flow cytometry antibodies along with appropriate negative and positive controls as previously described[267]. Briefly, isolated cells were washed with 1mL of 1xPBS, centrifuged at 2200 rpm for 2.5 min at 4 degrees Celsius, and re-suspended in 100μL of 1xPBS. The cell were then fixed with 100μL of fixation buffer (cat# 00-8222-49, 2X) and incubated for 25 minutes on ice. Following incubation the cells were centrifuged at 2200 rpm for 2.5 min at 4 degrees Celsius and the supernatant was discarded. Fixed cells were then washed with 100μL at 2200 rpm for 2.5 min at 4 degrees Celsius. Next, cells were permeabilized by adding 200μL of 1x permeabilization buffer (cat# 00-8333-56; 10X) and incubated for 30 minutes. Each step following this was performed with 1x permeabilization buffer. 40 μl of sample was taken out as a control. At this point, unstained cells were collected by centrifuging the cells at 2200 rpm and adding 300μL PBS and left a 4 degrees Celsius until flow experiment. For the remaining samples, cells were centrifuged the tubes at 2200 rpm for 2.5 minutes; X2 and 90 μl of permeabilization buffer was added to each tube. Next 10 μl of primary antibody cocktail (for multiple

antigens) was added into vial and incubated for 30 minutes in the dark on ice. The cells were stained with the following fluorophore-conjugated flow-cytometric antibodies: CD11b- APC-Cy7 (1:100, ThermoFisher), Anti-Ly6c-PE (1:100, ThermoFisher), and Streptavidin 488 (1:500, ThermoFisher). Subsequently, the cells were washed 3X at 2200 rpm for 2.5 minutes, re-suspended in 100μL 1xPBS, and placed at 4 degrees Celsius until flow cytometry. For all experiments, compensation controls were prepared with OneComp eBeads stained with appropriate fluorophore-conjugated antibodies and unstained beads. Data were collected on a BD LSR II flow cytometer. Flow data were further analyzed using FlowJo v10. After gating for single mononuclear cells (FSC and SSC), live cells were selected and CNS mononuclear cells were sub-gated into CD11b+/Ly6c low and then further gated based on streptavidin 488 expression.

vi. Figures
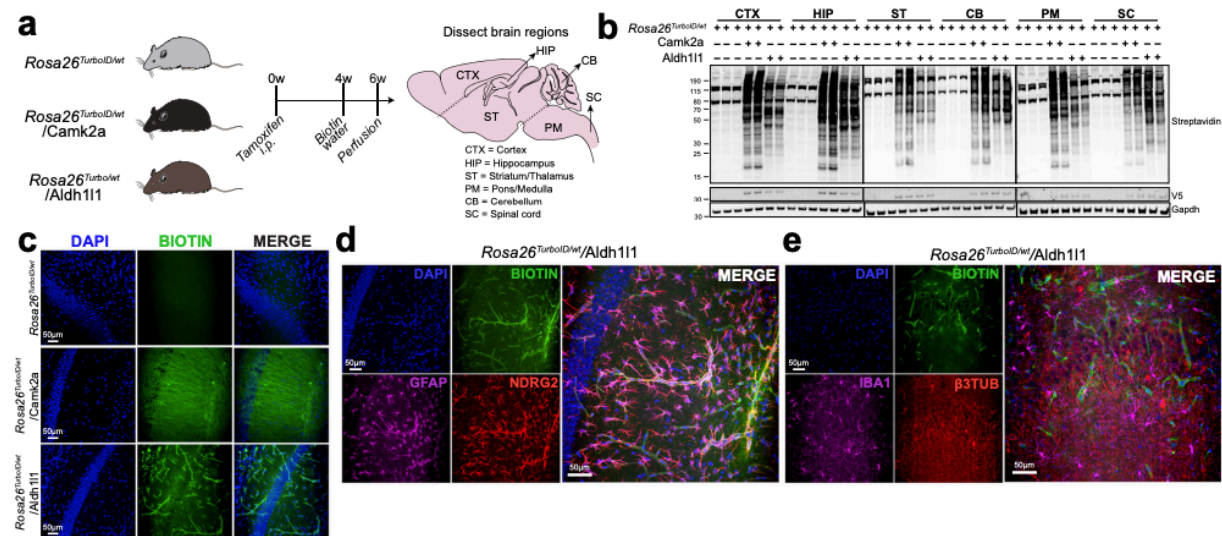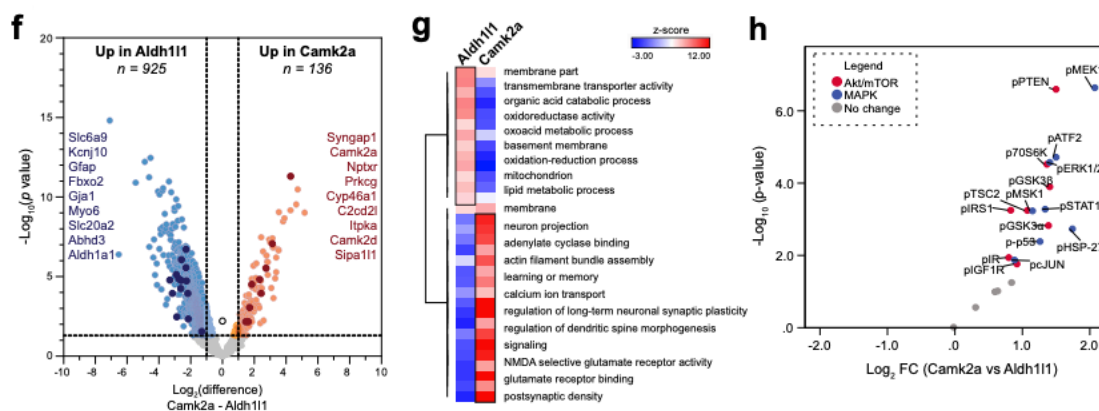
Figure 3.1: **CIBOP approach for labeling neuron-specific and astrocyte-specific proteomes. A:** *Rosa26-floxSTOP-TurboID*, *Rosa26-floxSTOP-TurboID;Camk2a-CreERT2*, *Rosa26-floxSTOP-TurboID;Aldh1l1-CreERT2* mice received tamoxifen intraperitoneally for 5 days. After 4 weeks, mice received biotin water for 2 weeks. **B:** Representative Western blots from brain region lysates (n = 2 mice/group), probed for biotin (streptavidin Alexa488), V5 and Gapdh are shown. **C:** Representative images (n = 2 mice/group) showing biotinylation in the hippocampus. **D:** Representative immunofluorescence images (n = 2 mice/group) showing overlap between astrocytic biotinylation (streptavidin Alexa488), Gfap, and Ndrg2 in the hippocampus region from *Rosa26-floxSTOP-TurboID;Aldh1l1-CreERT2* mice. **E:** Representative immunofluorescence images (n = 2 mice/group) showing no overlap between biotinylation, Iba1, and βIII-tubulin in astrocytes and blood vessels in the hippocampus region from *Rosa26-floxSTOP-TurboID;Aldh1l1-CreERT2* mice. **F:** Volcano plot showing differentially enriched proteins comparing *Rosa26-floxSTOP-TurboID;Aldh1l1-CreERT2* and *Rosa26-floxSTOP-TurboID;Camk2a-CreERT2*. For this analysis, all six brain regions were combined for both groups. Orange symbols (two-tailed T test unadjusted p ≤ 0.05 and ≥ 2-fold change) represent biotinylated proteins enriched in Camk2a neurons with neuron-specific proteins highlighted. Blue symbols (two-tailed T test unadjusted p ≤ 0.05 and ≥ 2-fold change) represent biotinylated proteins enriched in Aldh1l1 astrocytes and examples of astrocyte-specific proteins are highlighted in dark blue. **G:** GSEA showing over-represented ontologies within neuronal-enriched proteins and astrocyte-enriched proteins. Representative gene ontology terms are highlighted. **H:** Volcano plot showing enrichment (two-tailed T test unadjusted p ≤ 0.05) of MAPK and Akt/mTOR phospho-proteins in *Rosa26-floxSTOP-TurboID;Camk2a-CreERT2* compared to *Rosa26-floxSTOP-TurboID;Aldh1l1-CreERT2*. ***** This figure was derived from a coauthored publication in Nature Communications on May 25th, 2022 (2927). Methods can be found at DOI: https://doi.org/10.1038/s41467-022-30623-x.
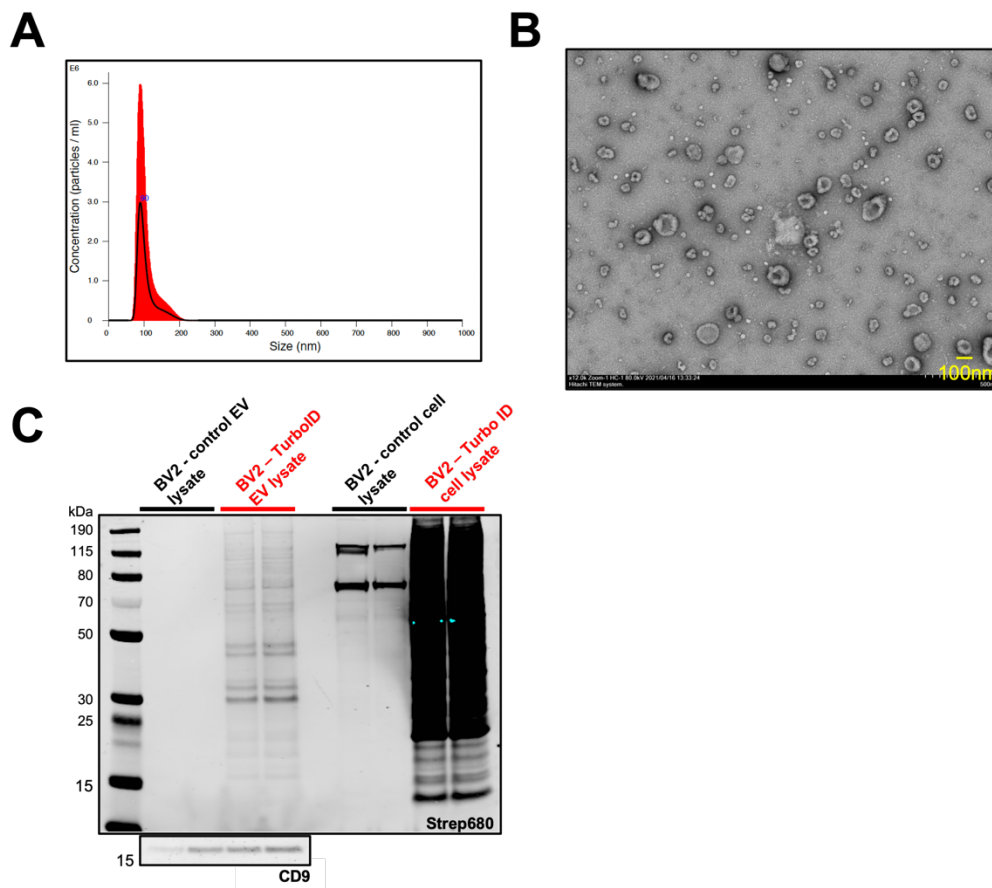
Figure 3.2. Validation of microglia and microglia-derived EVs TurboID labeling in vitro. A: Nanoparticle tracking analysis (NTA) shows size and concentration of isolated EVs from BV2 cell culture media. **B:** Transmission electron microscopy (TEM) image of isolated EVs from BV2 cells. Scale bar is 100nm. **C:** Western blot (left) of EV lysates derived from BV2 cells probed for CD9 (EV marker) and streptavidin (to detect biotin) confirms increased biotinylation in TurboID EV lysates compared to control and EV purity. Western blot (right) confirming robust biotinylation of proteins in TurboID-NES expressing BV2 cell lysates as compared to endogenous biotinylation in controls.
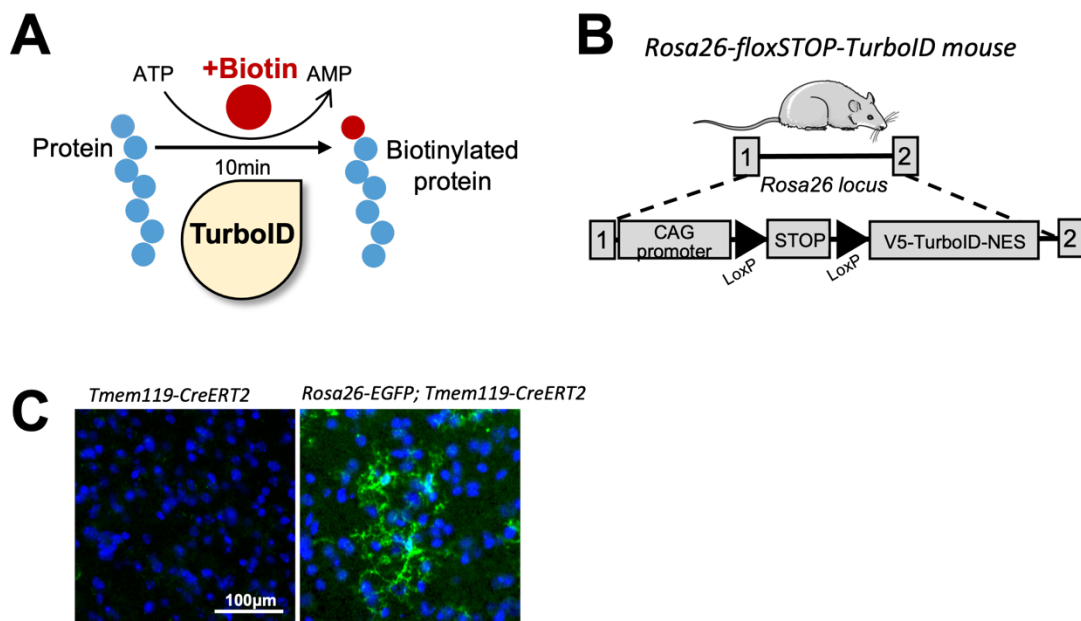
Figure 3.3. TurboID-mediated proteomic labeling approach. A: Schematic of in-vivo protein proximity labeling with TurboID. **B:** Genetic strategy for targeting TurboID (V5-TurboID-NES) to the *Rosa26* locus under the CAG promoter to develop *Rosa26-floxSTOP-TurboID*. **C.** Validation of microglial Cre line: *Tmem119-CreERT2* mice were crossed with *Rosa26-EGFP^f* reporter mice, treated with tamoxifen (i.p. 75mg/kg x 5 days), and euthanized after 3 weeks of recombination. IF of fixed brain confirmed cell type specific GFP expression.

C

— 2 weeks biotin water
— 4 weeks biotin water
— 4 weeks biotin water + 5 days of LPS

All: 6 weeks post Tmx injections
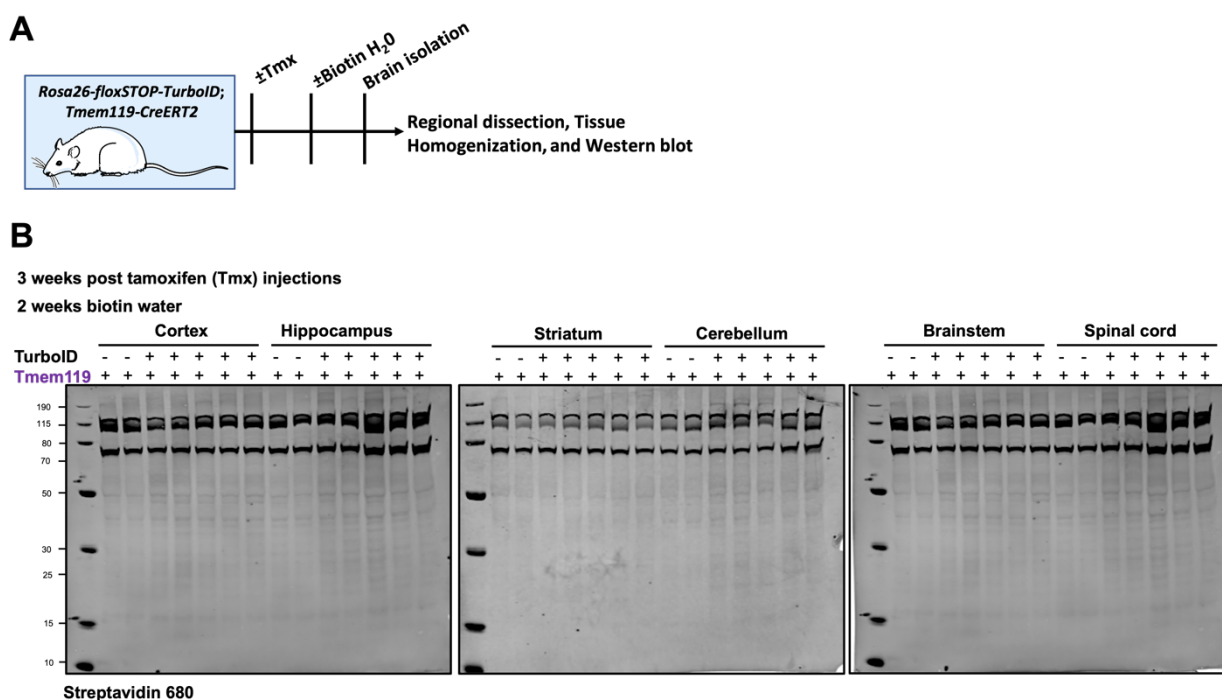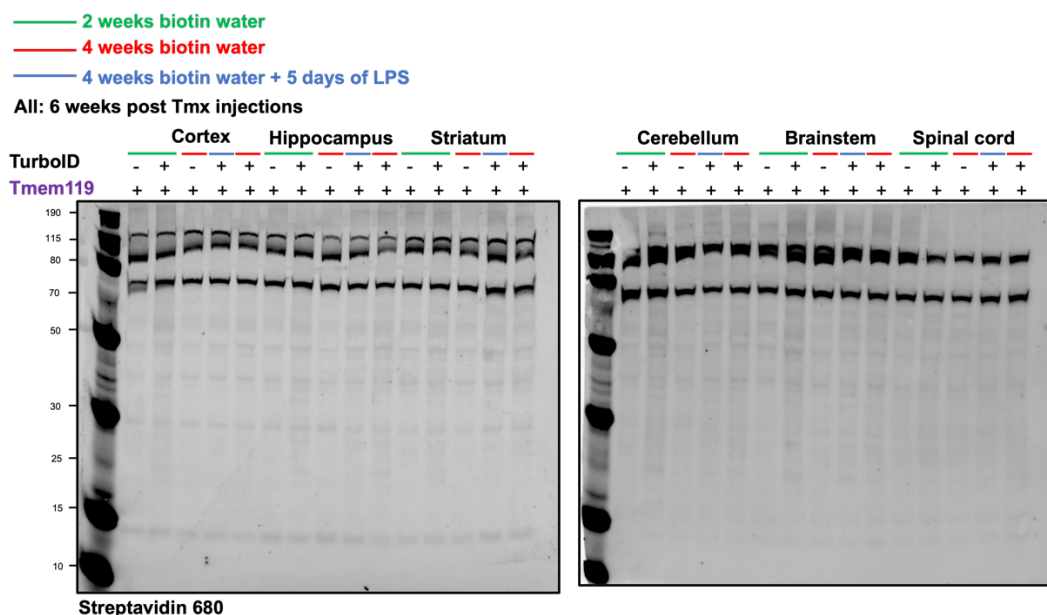
D
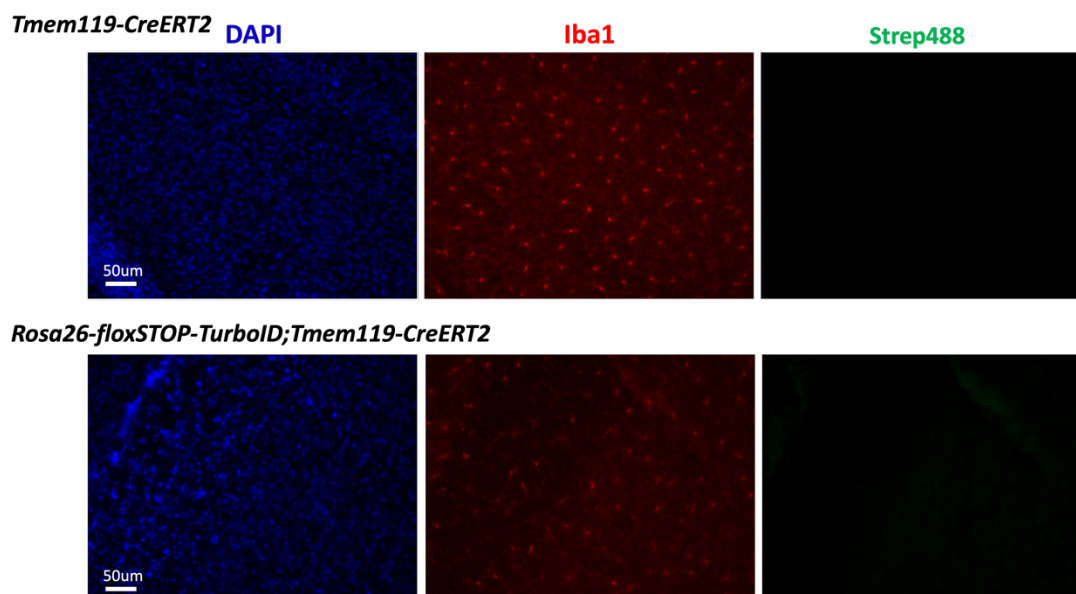
Figure 3.4. CIBOP approach for labeling microglia-specific proteomes. A: *Rosa26-floxSTOP-TurboID;Tmem119-CreERT2* and *Tmem119-CreERT2* mice received tamoxifen intraperitoneally for 5 days. After 3 weeks (standard protocol) or 6 weeks, mice received biotin water for 2 weeks (standard protocol) or 4 weeks. **B:** Representative Western blots from brain region lysates of mice that had a 3 week period following tamoxifen injections which was followed by 2 week biotin water (n=5 Turbo positive, n=2 Turbo negative), probed for biotin (Streptavidin Alexa680). **C:** Representative Western blots from brain region lysates from mice that had a 6 week period following tamoxifen injections which was followed by either 2 weeks of biotin water (n=2), 4 weeks of biotin water (n=2), or 4 weeks of biotin water + 5 days of

LPS (n=1), probed with Streptavidin Alexa680. **D:** Representative immunofluorescence images (n = 2 mice/group) DAPI (nuclear maker) and Iba1 (microglia marker) labeling and no biotinylation (streptavidin Alexa488) from *Rosa26-floxSTOP-TurboID;Tmem119-CreERT2* and *Tmem119-CreERT2* mice that had a had a 6 week period following tamoxifen injections which was followed by 2 weeks of biotin water.
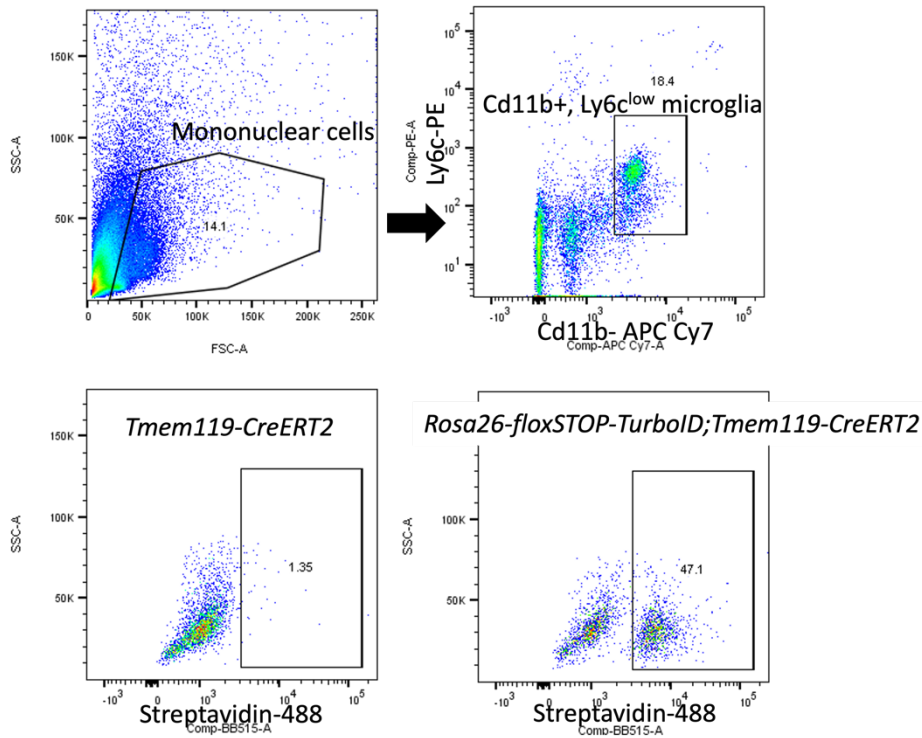
Figure 3.5. Flow cytometric analysis of *Rosa26-floxSTOP-TurboID;Tmem119-CreERT2* and *Tmem119-CreERT2* mice. Flow cytometric gating strategy of acutely isolated brain mononuclear cells from fresh, unfrozen mouse brain. Within live mononuclear cells, there were 18.4% Cd11b^{positve}Ly6c^{Low} microglia. Further gating of this group was conducted with Streptavidin 488 to compare the percentage of biotinylation between of *Rosa26-floxSTOP-TurboID;Tmem119-CreERT2* and *Tmem119-CreERT2* mouse microglia. Forty-seven percent of microglia cells are biotinylated in *Rosa26-floxSTOP-TurboID;Tmem119-CreERT2* mice compared to 1.35% in *Tmem119-CreERT2* control mice.
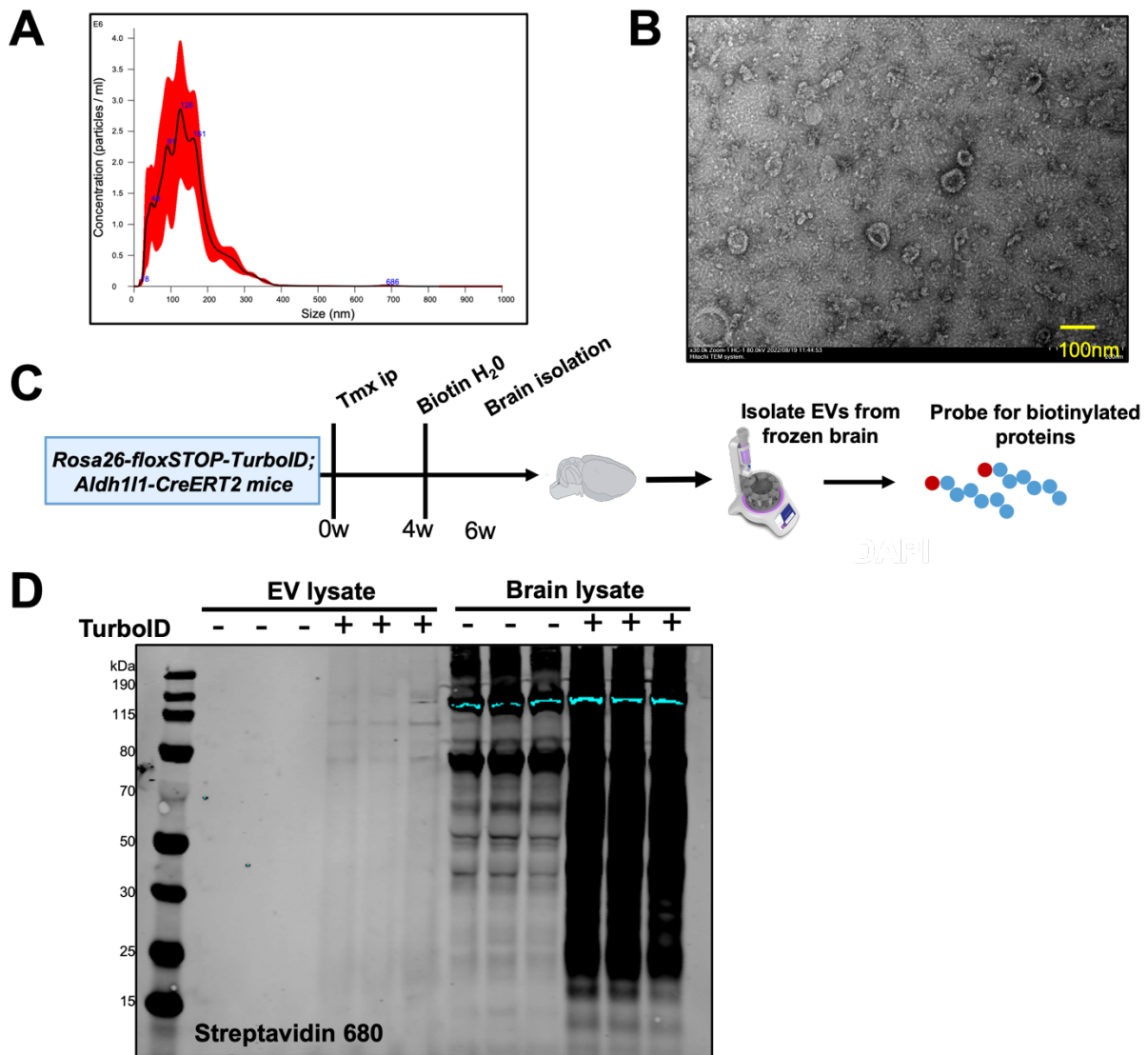
Figure 3.6. CIBOP approach to label *Rosa26-floxSTOP-TurboID;Aldh1l1-CreERT2* derived extracellular vesicles. A: Nanoparticle tracking analysis shows size and concentration of isolated EVs from mouse brain. **B:** Transmission electron microscopy image of isolated EVs from mouse brain. Scale bar is 100nm. **C:** Experimental outline for biotin labeling astrocyte-derived EVs using *Rosa26-floxSTOP-TurboID;Aldh1l1-CreERT2* mice. **D:** Western blot (left) of EV lysates from *Rosa26-floxSTOP-TurboID;Aldh1l1-CreERT2* brain probed with streptavidin 680 (to detect biotin) confirms increased biotinylation in TurboID EV lysates compared to control. Western blot (right) confirming robust biotinylation of proteins (streptavidin 680) in TurboID expressing brain lysates as compared to endogenous biotinylation in controls.

IV.   Discussion

i.   Integrated summary of findings

Microglia, the resident immune cell type of the brain, play an essential role in mediating inflammatory responses in the CNS. Microglia can alter their morphology, molecular profile, and function in response to immune activators, thus exerting different functions in disease states[123]. Microglia-mediated neuroinflammation is a key pathological component of several neurodegenerative diseases[96]. Compelling evidence has suggested that EVs can have an indirect role in regulation of inflammatory signals and propagation of pathogenic cargo[186, 240]. However, the characterization of microglia-derived EVs at the proteomic and transcriptomic level, and how these are impacted by microglial state, have not been well studied. This thesis includes foundational in vitro studies identifying unique molecular profiles of microglia-derived EVs that are determined by microglial activation state. By combining proteomic and transcriptomic methods, we obtained comprehensive molecular profiles of BV2 microglia-derived EVs under homeostatic and stimulated conditions. Our analyses revealed novel state-specific proteomic and transcriptomic signatures of microglia-derived EVs. Particularly, lipopolysaccharide (LPS) activation had the most profound impact on proteomic and transcriptomic compositions of microglia-derived EVs. Additionally, we found that EVs derived from LPS-activated microglia were able to induce pro-inflammatory transcriptomic changes in recipient microglia, confirming the ability of microglia-derived EVs to relay functionally-relevant inflammatory signals. These in vitro experiments were fundamental for developing a novel method to characterize the proteome of microglia and their EVs in vivo using TurboID-based proximity labeling. Our findings reveal that the microglial proteome cannot be labeled in vivo using TurboID-based proximity labeling with the *Rosa26-floxSTOP-TurboID;Tmem119-CreERT2* mice, despite successful labeling of the cell proteome and EV proteome in BV2 microglia and the astrocytic *Rosa26-floxSTOP-TurboID;Aldh1l1-CreERT2* mice. This thesis includes foundational experiments along with newly developed techniques to interrogate the possibility of characterizing cell-type specific EVs in vivo.

Proteomic signatures of BV2 microglia-derived EVs

For our in vitro studies, we applied size exclusion chromatography (Izon qEV) based methods to isolate EVs from BV2 microglia culture supernatants. Our transmission electron microscopy, nanoparticle tracking, and western blot analyses demonstrate successful EV isolation based on morphology, size, concentration, and presence of classical EV markers. We characterized the proteome of BV2 microglia and their EVs using LFQ-MS. BV2 microglia were treated with either LPS to polarize to a pro-inflammatory state, IL-10 to polarize to a protective state, TGF-β to polarize to a homeostatic state, or untreated. LFQ-MS identified 533 proteins in the EV proteome and 1,882 proteins in BV2 cell proteome, across all conditions. Our results revealed that canonical exosome/EV related proteins expected to be present in all EVs independent of cell type of origin were significantly enriched in the EV proteome compared to the whole cell proteome. In contrast, endoplasmic reticulum proteins expected to be present in cell lysates but not in EV lysates were enriched in the whole cell proteome. When comparing our BV2-derived EV proteome to the ExoCarta protein list of EV proteins detected across all mouse cell types we observed modest overlap but also discovered proteins novel to BV2 microglia derived EVs. Proteins unique to BV2 microglia-derived EVs were enriched in ontologies related to positive regulation of transporter activity, regulation of RNA splicing, cytosolic large ribosomal subunit, and aminoacyl-tRNA synthetase complex. On the other hand, the proteins not captured in our BV2-derived EV proteome showed enrichment of proteins related to protein heterodimerization activity, chromosome organization, and protein kinase activity. This suggests that proteins contained within microglia-derived EVs could play a role in mRNA processing as well as protein synthesis in the recipient cell. Taken together, these analyses verify the validity of our EV proteomes by confirming enrichment abundances of canonical EV markers, highlight the increased depth of our EV proteome as compared to prior studies, and identify novel proteomic characteristics of microglia-derived EVs that are distinct from non-microglial EVs which may have functional implications.

Microglia activation state impacts proteomic and transcriptomic characteristics of BV2 microglia-derived EVs

After establishing the validity of our EV preparations, we interrogated the impact of microglia activation state (LPS, IL-10, or TGF-β treated) on the proteome and transcriptome of microglia-derived EVs. We observed 334 differentially enriched proteins with unique enrichment patterns across polarization states, as compared to control, in the BV2 cell proteome. This confirmed that our in vitro conditions induced distinct microglial activation states. Upon examining the BV2-dervied EV proteome, our results revealed that EVs derived from BV2 cells treated with LPS demonstrated an enrichment in proteins related to proteasome activity and reduction in proteins related to chromosomal organization and clathrin/receptor mediated endocytosis. Prior work has shown that proteasome systems are involved in regulating pro-inflammatory pathways[244]. Thus, EVs derived from LPS-activated microglia can potentially enhance inflammation through enrichment of proteasomes. Conversely, EVs derived from BV2 cells treated with IL-10 and TGFβ demonstrated a reduction in cytosolic chaperonin Cct ring complex proteins. Previous studies have shown that chaperonin Cct subunits show increased quantities in disease states and participate in the regulation of protein folding as pathological protein aggregation, therefore it is also possible that CCT changes in microglia-derived EVs could impact pathogenic mechanisms of neurodegeneration[243]. The results of these studies align well with the reduction in Cct ring complex proteins following treatment with IL-10 and TGF-β. These proteomic analyses of EVs confirm that microglial activation states can determine the proteomic compositions of EVs.

Beyond proteins, we also characterized the mRNA composition of BV2 microglia-derived EVs using mRNA sequencing. Our results revealed that LPS activation elicited the strongest effect on EV transcriptomic composition. We found that LPS treated BV2 cells showed enrichment in immune response, RNA binding, and metabolism. In contrast, EV transcriptomes from LPS treated BV2 cells, showed enrichment in signaling and ion channel activity. Furthermore, we found that the majority of EV transcriptomic changes induced by LPS are not observed in the whole cell transcriptomes. This suggests that pro-inflammatory activation of microglia not only induces whole cell gene expression changes, but

also likely impacts mechanisms that govern mRNA export into EVs, consistent with our observation of LPS-induced altered expression of genes involved in mRNA transport at the whole cell level. Our studies also revealed distinct effects of pro-inflammatory activation on EV transcriptomic signatures, confirming microglial state-dependent effects on EV composition at the mRNA level, many of which do not occur at the whole-cell level.

Potential role of BV2 microglia-derived EVs in RNA binding and translation

When comparing our BV2-derived EV proteomics dataset to our BV2-derived EV mRNA transcriptomic dataset, we found that the major overlapping molecular pathways between the EV proteome and transcriptome are RNA binding, ribosomal large and small subunit binding and biogenesis, extracellular region part, and translation. These results suggest that BV2-derived EV cargo contains ribosomal proteins and mRNAs that can encode ribosomal proteins. This correlation further highlights the point EV cargo may regulate translation in a recipient cell, a hypothesis that needs future investigation. It also suggests that there is an inter-relationship between the RNA and protein cargo in EVs that may work together to achieve a regulatory function in a recipient cell.

BV2 microglia-derived EVs exhibit unique microRNA signatures under pro-inflammatory conditions

Next we sought to characterize the miRNA cargo of BV2-derived EVs using small RNA sequencing. Similarly to our mRNA studies, LPS activation demonstrated the strongest effect with group-based clustering primarily based on LPS treatment. When comparing the whole cell and EV miRNA transcriptomes, we were able to identify very high levels of miRNAs (ex. mmu-mir-6240) that were distinct to EVs and not cells. Furthermore, we found that miRNAs in EVs from LPS treated BV2 cells have been previously implicated in modulating inflammatory responses[236, 237]. Focusing on the miRNAs that are differentially expressed in EVs from the LPS treated group versus control, we found that miRNAs in the EVs from LPS treated group target unique mRNAs compared to control, which are involved in androgen and corticosteroid receptor signaling pathway and the cytoplasmic mRNA processing pathway. By targeting

distinct mRNAs, the miRNA cargo in these EVs could impact gene expression and modulate inflammation in a recipient cell.

EVs derived from LPS activated BV2 microglia can elicit pro-inflammatory changes in responder microglia

Our complementary multi-omics characterization of microglia-derived EVs suggest that EVs from distinct microglia states have unique protein and RNA cargo, which may be able to impact other cells. To test this hypothesis we dosed resting responder BV2 microglia with equal amounts of EVs from untreated and LPS-treated BV2 microglia and then assessed the transcriptomic alterations induced by EVs using bulk RNA sequencing. Our results revealed that responder BV2 microglia exposed to LPS-treated BV2-derived EVs display upregulation of genes related to GTPase activity and downregulation of genes related to G-protein coupled receptor protein signaling and regulation of synaptic plasticity. Interestingly, previous work has shown that increased Rho-GTPase activity levels in microglia is observed following LPS stimulation[247]. In addition, we found that the overall effect of LPS-microglia-derived EVs on responder microglia was consistent with a pro-inflammatory profile previously reported in mouse microglia[109]. These results demonstrate the ability of EVs to relay the inflammatory state of microglia of origin to responder microglia.

TurboID proximity labeling as a promising approach to label the proteome of EVs in vivo with cell-type specificity

Given our in vitro results with BV2-dervied EVs, we sought to explore ways to investigate these same questions in vivo. We used *Rosa26-floxSTOP-TurboID;Tmem119-CreERT2* mice to characterize the molecular composition of microglia by using a Cre/flox approach to express a biotin ligase, TurboID, in an inducible manner. We found that *Rosa26-floxSTOP-TurboID;Tmem119-CreERT2* mice and control *Tmem119-CreERT2* mice showed no difference in biotin labeling by western blot analysis and immunofluorescence studies. This was observed regardless of LPS stimulation, increased duration for Cre-recombination to occur, or increased duration of biotin water. Furthermore, flow cytometry experiments revealed that 47% of microglia from *Rosa26-floxSTOP-TurboID;Tmem119-CreERT2* are biotinylated compared to 1.5% in *Tmem119-CreERT2* control mice; however, this level of biotinylation is still not robust

enough to be detected by immunofluorescence, western blot analyses, or mass spectrometry. Overall, these results contrast greatly from previous studies in the lab utilizing *Rosa26-floxSTOP-TurboID;Camk2a-CreERT2* mice and *Rosa26-floxSTOP-TurboID;Aldh1l1-CreERT2* mice.

Since *Rosa26-floxSTOP-TurboID;Tmem119-CreERT2* mice reveal insufficient biotin labeling of microglia, we decided to assess biotin labeling of brain-derived EVs with the validated *Rosa26-floxSTOP-TurboID;Aldh1l1-CreERT2* mice. We validated our approach to isolate EVs from frozen mouse brain using transmission electron microscopy and nano tracking analyses. we found that the brain lysates and brain-derived EV lysates from *Rosa26-floxSTOP-TurboID;Aldh1l1-CreERT2* mice demonstrated robust biotin labeling compared to control *Aldh1l1-CreERT2* mice, based on western blot analyses probing with streptavidin-680. These results demonstrate a promising approach to labeling the EV proteome of labeling specific cell types in vivo.

Conclusion

Our in vitro studies described in *Chapter 2*, suggest that EVs from distinct microglia states have unique proteomic and transcriptomic profiles. Furthermore, our comprehensive omics data sets have identified novel EV proteins in microglia not seen in other EVs, thereby increasing the depth of the microglia-derived EV proteome that has not been previously reported on. Through our transcriptomic analysis, we discovered that LPS activation of BV2 cells had the strongest impact on EV composition, possibly increasing the amount of mRNAs transported and packaged into the EVs. Lastly, our data suggests that EVs from LPS-activated microglia can elicit a transcriptomic change in resting recipient microglia that mimics that of a pro-inflammatory response. Our study highlights the value of characterizing the cargo of EVs from distinct cell types. Since microglia are highly dynamic cells and can transform to different phenotypes in response to their environment, it is to be inquired if their EVs might have distinct functions and contents. Therefore, the uptake of microglia-derived EVs by other cells could indirectly mediate downstream signaling events and disease processes. More research is needed to understand the mechanisms of microglia-derived EVs in neurodegenerative disease, specifically whether the presence or absence of certain cargo can impact disease progression.

Given our in vitro results, we sought to explore ways to investigate these same questions in vivo. *Chapter 3* of this thesis describes our approach at characterizing the proteome of specific cell types and their EVs in vivo using TurboID proximity labeling. This study represents the first effort to label the proteome of microglia by applying the CIBOP approach to *Rosa26-floxSTOP-TurboID;Tmem119-CreERT2* mice. Using western blot analysis, immunofluorescence, and flow cytometry to detect biotinylation levels, we determined that *Rosa26-floxSTOP-TurboID;Tmem119-CreERT2* mouse microglia, regardless of experimental parameters, are not robustly labeled compared to previous CIBOP models (*Rosa26-floxSTOP-TurboID;Aldh1l1-CreERT2* and *Rosa26-floxSTOP-TurboID;Camk2a-CreERT2*) and control mice. Although there was modest biotinylation of *Rosa26-floxSTOP-TurboID;Tmem119-CreERT2* mouse microglia compared to control, this difference was not sufficient for detection via western blot analysis, immunofluorescence, and LFQ-mass spectrometry. On the other hand, BV2 microglia transduced with TurboID-NES demonstrate robust labeling compared to control cells. However, this mechanism of biotin labeling by TurboID is somehow ineffective in vivo compared to in vitro approaches with BV2 cells. This may be due to low levels or suppressed activity of biotin transporter molecules in vivo, however further studies need to be performed to understand the biology behind this inability to be biotin labeled. On the other hand, EVs isolated from the brains of *Rosa26-floxSTOP-TurboID;Aldh1l1-CreERT2* mice demonstrated successful biotin labeling via western blot analyses. These developed protocols and experimental data provide can be valuable resource for work seeking to define the proteome of microglia and their EVs in vivo. Overall the work presented in this thesis, highlight the importance of using -omics approaches to characterize the molecular composition of specific cell types and their EVs to further understand their role in disease processes.

ii.   Future Applications

Investigating the potential of BV2 microglia-derived EVs from pro-inflammatory microglia to initiate translation of mRNAs in recipient cells

Data from our in vitro omics studies suggest that the cargo of EVs from pro-inflammatory (LPS treated) BV2 cells may be involved in transporting mRNA and ribosomal proteins to recipient cells for translation. However, for this hypotheses to be proven, future studies would have to demonstrate delivery of functional mRNAs to recipient cells and subsequent translation. A proposed idea to determine if the mRNA delivered by BV2-dervied EVs could be expressed in recipient cells is to transduce BV2 cells with a with a lentivirus vector encoding the secreted luciferase Gaussia[145, 268]. Gaussia luciferase or Gluc is a reporter that is naturally secreted from mammalian cells in an active form and can be used as a marker to monitor different in vivo biological events[269]. By using RT-PCR analysis, we can confirm that the mRNA for Gluc (555 bp product) is present in the EVs purified from cell culture media. Purified EVs containing Gluc mRNA can then be added to recipient resting microglia. Gluc activity released into the cell culture medium by the recipient microglia can then be monitored overtime to see if there is an observed increase, supporting the idea of ongoing translation of the Gluc mRNA. This method could show that the mRNA incorporated into the BV2-derived EVs can be delivered into recipient resting cells and generate a functional protein. If successful, this method could be used to compare the level of translation in recipient cells treated with EVs from pro-inflammatory BV2 cells to that of EVs from untreated BV2 cells and further highlight the role of EVs inflammatory processes.

Possible ways to resolve the inability to label microglia in vivo using TurboID proximity labeling

Our results using the *Rosa26-floxSTOP-TurboID;Tmem119-CreERT2* floxed mice revealed the inability to label microglia in vivo using TurboID-NES proximity labeling, despite success with labeling the proteome of microglia in vitro using BV2 cells. However, the biological reason behind this remains unknown. One idea is that small molecule transporters that are responsible for the transport of vitamins including biotin (ex. Slc5a6/SMVT) may be less abundant or active in microglia in vivo. Previous studies have shown that the expression of Na(+)-dependent multivitamin transporter (SLC5A6/SMVT) is critical to transport of biotin, pantothenate, and lipoic acid into the brain via the blood-brain barrier[264]. However, Slc5a6/SMVT levels in microglia compared to other cell types has not previously been reported. Experiments that can be performed to investigate this hypothesis would be to delete Slc5a6 globally in the

microglia of *Rosa26-floxSTOP-TurboID;Tmem119-CreERT2* floxed mice to see if biotinylation decreased or to modify the dose of biotin to see if that improves transporter activity. Limitations to these approaches are that deletion of Slc5a6 may induce a metabolic disorder and increased biotin dose may cause toxicity. If the inability of microglia to take up biotin is associated with less active or abundant Slc5a6 in microglia, future experiments can attempt to over express Slc5a6 in our *Rosa26-floxSTOP-TurboID;Tmem119-CreERT2* floxed mice to see if microglia biotinylation can be achieved. These experiments could help understand the biological or mechanistic reason behind microglia resistant to TurboID labeling in vivo.

Future applications of TurboID proximity labeling to investigate the proteome of EVs from specific cell types

Despite success with labeling EVs isolated from the brains of *Rosa26-floxSTOP-TurboID;Aldh1l1-CreERT2* mice as determined by western blot, it is essential to further validate this labeling using mass spectrometry based approaches. However, a difficult aspect of affinity purification of biotinylated proteins using the streptavidin beads pulldown method is the requirement for a large amount of protein (~1mg), as demonstrated in previous studies in our lab[201, 219]. Future experiments should ensure that the ratio of magnetic streptavidin coated beats to protein is scaled appropriately to reflect the smaller amount of protein in EVs. Furthermore, samples should be run on highly sensitive mass spectrometry instruments such as the Thermal Ionization Mass Spectrometry (TIMS), to allow for maximum detection of peptides in EV samples. Additional labeling methods such as the newly discovered "TurboID-EV" method which involves TurboID being tethered to the EV membrane instead of targeting the cytosol, should also be considered[266]. This TurboID-EV system applied with cell-type specificity, could potentially elucidate various EV subtypes and recipient cell types, providing a tool to further dissect the role of EVs in cellular communication and disease processes and offer novel insights for biomarker development.

V.   Bibliography

1.   Ghosh SK. Camillo Golgi (1843-1926): scientist extraordinaire and pioneer figure of modern neurology. Anat Cell Biol. 2020;53(4):385-92. doi: 10.5115/acb.20.196. PubMed PMID: 33012727; PMCID: PMC7769101.

2.   Jones EG. Golgi, Cajal and the Neuron Doctrine. J Hist Neurosci. 1999;8(2):170-8. doi: 10.1076/jhin.8.2.170.1838. PubMed PMID: 11624298.

3.   Garcia-Marin V, Garcia-Lopez P, Freire M. Cajal's contributions to glia research. Trends Neurosci. 2007;30(9):479-87. Epub 20070831. doi: 10.1016/j.tins.2007.06.008. PubMed PMID: 17765327.

4.   Ginhoux F, Lim S, Hoeffel G, Low D, Huber T. Origin and differentiation of microglia. Front Cell Neurosci. 2013;7:45. Epub 20130417. doi: 10.3389/fncel.2013.00045. PubMed PMID: 23616747; PMCID: PMC3627983.

5.   Rezaie P, Male D. Mesoglia & microglia--a historical review of the concept of mononuclear phagocytes within the central nervous system. J Hist Neurosci. 2002;11(4):325-74. doi: 10.1076/jhin.11.4.325.8531. PubMed PMID: 12557654.

6.   Del Rio-Hortega P. Studies on neuroglia: Glia with very few processes (oligodendroglia) by PA-o del RA-o-Hortega. 1921. Clin Neuropathol. 2012;31(6):440-59. PubMed PMID: 23083463.

7.   Penfield W. A Method of Staining Oligodendroglia and Microglia (Combined Method). Am J Pathol. 1928;4(2):153-7. PubMed PMID: 19969784; PMCID: PMC2006725.

8.   Perry VH, Hume DA, Gordon S. Immunohistochemical localization of macrophages and microglia in the adult and developing mouse brain. Neuroscience. 1985;15(2):313-26. doi: 10.1016/0306-4522(85)90215-5. PubMed PMID: 3895031.

9.   Takahashi K, Naito M. Development, differentiation, and proliferation of macrophages in the rat yolk sac. Tissue Cell. 1993;25(3):351-62. doi: 10.1016/0040-8166(93)90077-x. PubMed PMID: 8332987.

10.   Hutchins KD, Dickson DW, Rashbaum WK, Lyman WD. Localization of morphologically distinct microglial populations in the developing human fetal brain: implications for ontogeny. Brain Res Dev Brain Res. 1990;55(1):95-102. doi: 10.1016/0165-3806(90)90109-c. PubMed PMID: 2208643.

11.   Rezaie P, Dean A, Male D, Ulfig N. Microglia in the cerebral wall of the human telencephalon at second trimester. Cereb Cortex. 2005;15(7):938-49. Epub 20041013. doi: 10.1093/cercor/bhh194. PubMed PMID: 15483047.

12.   Wang CC, Wu CH, Shieh JY, Wen CY, Ling EA. Immunohistochemical study of amoeboid microglial cells in fetal rat brain. J Anat. 1996;189 (Pt 3)(Pt 3):567-74. PubMed PMID: 8982832; PMCID: PMC1167699.

13.   Morris L, Graham CF, Gordon S. Macrophages in haemopoietic and other tissues of the developing mouse detected by the monoclonal antibody F4/80. Development. 1991;112(2):517-26. doi: 10.1242/dev.112.2.517. PubMed PMID: 1794320.

14.   Nayak D, Roth TL, McGavern DB. Microglia development and function. Annu Rev Immunol. 2014;32:367-402. Epub 20140122. doi: 10.1146/annurev-immunol-032713-120240. PubMed PMID: 24471431; PMCID: PMC5001846.

15.   Butovsky O, Jedrychowski MP, Moore CS, Cialic R, Lanser AJ, Gabriely G, Koeglsperger T, Dake B, Wu PM, Doykan CE, Fanek Z, Liu L, Chen Z, Rothstein JD, Ransohoff RM, Gygi SP, Antel JP, Weiner HL. Identification of a unique TGF-beta-dependent molecular and functional signature in microglia. Nat Neurosci. 2014;17(1):131-43. Epub 20131208. doi: 10.1038/nn.3599. PubMed PMID: 24316888; PMCID: PMC4066672.

16.   Lawson LJ, Perry VH, Dri P, Gordon S. Heterogeneity in the distribution and morphology of microglia in the normal adult mouse brain. Neuroscience. 1990;39(1):151-70. doi: 10.1016/0306-4522(90)90229-w. PubMed PMID: 2089275.

17.   Nimmerjahn A, Kirchhoff F, Helmchen F. Resting microglial cells are highly dynamic surveillants of brain parenchyma in vivo. Science. 2005;308(5726):1314-8. Epub 20050414. doi: 10.1126/science.1110647. PubMed PMID: 15831717.

18.   Lull ME, Block ML. Microglial activation and chronic neurodegeneration. Neurotherapeutics. 2010;7(4):354-65. doi: 10.1016/j.nurt.2010.05.014. PubMed PMID: 20880500; PMCID: PMC2951017.

19.   Aloisi F. Immune function of microglia. Glia. 2001;36(2):165-79. doi: 10.1002/glia.1106. PubMed PMID: 11596125.

20.   Stevens B, Allen NJ, Vazquez LE, Howell GR, Christopherson KS, Nouri N, Micheva KD, Mehalow AK, Huberman AD, Stafford B, Sher A, Litke AM, Lambris JD, Smith SJ, John SW, Barres BA. The classical complement cascade mediates CNS synapse elimination. Cell. 2007;131(6):1164-78. doi: 10.1016/j.cell.2007.10.036. PubMed PMID: 18083105.

21.   Crapser JD, Arreola MA, Tsourmas KI, Green KN. Microglia as hackers of the matrix: sculpting synapses and the extracellular space. Cell Mol Immunol. 2021;18(11):2472-88. Epub 20210819. doi: 10.1038/s41423-021-00751-3. PubMed PMID: 34413489; PMCID: PMC8546068.

22.   Yang I, Han SJ, Kaur G, Crane C, Parsa AT. The role of microglia in central nervous system immunity and glioma immunology. J Clin Neurosci. 2010;17(1):6-10. Epub 20091118. doi: 10.1016/j.jocn.2009.05.006. PubMed PMID: 19926287; PMCID: PMC3786731.

23.   Kawai T, Akira S. Signaling to NF-kappaB by Toll-like receptors. Trends Mol Med. 2007;13(11):460-9. Epub 20071029. doi: 10.1016/j.molmed.2007.09.002. PubMed PMID: 18029230.

24.   Hartlage-Rubsamen M, Lemke R, Schliebs R. Interleukin-1beta, inducible nitric oxide synthase, and nuclear factor-kappaB are induced in morphologically distinct microglia after rat hippocampal lipopolysaccharide/interferon-gamma injection. J Neurosci Res. 1999;57(3):388-98. PubMed PMID: 10412030.

25.   Suzumura A, Sawada M, Marunouchi T. Selective induction of interleukin-6 in mouse microglia by granulocyte-macrophage colony-stimulating factor. Brain Res. 1996;713(1-2):192-8. doi: 10.1016/0006-8993(95)01535-3. PubMed PMID: 8724991; PMCID: PMC7111018.

26.   Floden AM, Li S, Combs CK. Beta-amyloid-stimulated microglia induce neuron death via synergistic stimulation of tumor necrosis factor alpha and NMDA receptors. J Neurosci. 2005;25(10):2566-75. doi: 10.1523/JNEUROSCI.4998-04.2005. PubMed PMID: 15758166; PMCID: PMC6725188.

27.   Schartz ND, Tenner AJ. The good, the bad, and the opportunities of the complement system in neurodegenerative disease. J Neuroinflammation. 2020;17(1):354. Epub 20201125. doi: 10.1186/s12974-020-02024-8. PubMed PMID: 33239010; PMCID: PMC7690210.

28.   Raetz CR, Whitfield C. Lipopolysaccharide endotoxins. Annu Rev Biochem. 2002;71:635-700. Epub 20011109. doi: 10.1146/annurev.biochem.71.110601.135414. PubMed PMID: 12045108; PMCID: PMC2569852.

29.   Skrzypczak-Wiercioch A, Salat K. Lipopolysaccharide-Induced Model of Neuroinflammation: Mechanisms of Action, Research Application and Future Directions for Its Use. Molecules. 2022;27(17). Epub 20220826. doi: 10.3390/molecules27175481. PubMed PMID: 36080253; PMCID: PMC9457753.

30.   Tang D, Kang R, Coyne CB, Zeh HJ, Lotze MT. PAMPs and DAMPs: signal 0s that spur autophagy and immunity. Immunol Rev. 2012;249(1):158-75. doi: 10.1111/j.1600-065X.2012.01146.x. PubMed PMID: 22889221; PMCID: PMC3662247.

31.   De Nardo D. Toll-like receptors: Activation, signalling and transcriptional modulation. Cytokine. 2015;74(2):181-9. Epub 20150403. doi: 10.1016/j.cyto.2015.02.025. PubMed PMID: 25846205.

32.   Leitner GR, Wenzel TJ, Marshall N, Gates EJ, Klegeris A. Targeting toll-like receptor 4 to modulate neuroinflammation in central nervous system disorders. Expert Opin Ther Targets. 2019;23(10):865-82. Epub 20191020. doi: 10.1080/14728222.2019.1676416. PubMed PMID: 31580163.

33.   Owen AM, Fults JB, Patil NK, Hernandez A, Bohannon JK. TLR Agonists as Mediators of Trained Immunity: Mechanistic Insight and Immunotherapeutic Potential to Combat Infection. Front Immunol. 2020;11:622614. Epub 20210218. doi: 10.3389/fimmu.2020.622614. PubMed PMID: 33679711; PMCID: PMC7930332.

34.   Mazgaeen L, Gurung P. Recent Advances in Lipopolysaccharide Recognition Systems. Int J Mol Sci. 2020;21(2). Epub 20200107. doi: 10.3390/ijms21020379. PubMed PMID: 31936182; PMCID: PMC7013859.

35.   Boonen B, Alpizar YA, Sanchez A, Lopez-Requena A, Voets T, Talavera K. Differential effects of lipopolysaccharide on mouse sensory TRP channels. Cell Calcium. 2018;73:72-81. Epub 20180414. doi: 10.1016/j.ceca.2018.04.004. PubMed PMID: 29689522.

36.   Serra MP, Boi M, Carta A, Murru E, Carta G, Banni S, Quartu M. Anti-Inflammatory Effect of Beta-Caryophyllene Mediated by the Involvement of TRPV1, BDNF and trkB in the Rat Cerebral Cortex after Hypoperfusion/Reperfusion. Int J Mol Sci. 2022;23(7). Epub 20220326. doi: 10.3390/ijms23073633. PubMed PMID: 35408995; PMCID: PMC8998979.

37.   Lu J, Zhou W, Dou F, Wang C, Yu Z. TRPV1 sustains microglial metabolic reprogramming in Alzheimer's disease. EMBO Rep. 2021;22(6):e52013. Epub 20210517. doi: 10.15252/embr.202052013. PubMed PMID: 33998138; PMCID: PMC8183394.

38.   Meseguer V, Alpizar YA, Luis E, Tajada S, Denlinger B, Fajardo O, Manenschijn JA, Fernandez-Pena C, Talavera A, Kichko T, Navia B, Sanchez A, Senaris R, Reeh P, Perez-Garcia MT, Lopez-Lopez JR, Voets T, Belmonte C, Talavera K, Viana F. TRPA1 channels mediate acute neurogenic inflammation and pain produced by bacterial endotoxins. Nat Commun. 2014;5:3125. doi: 10.1038/ncomms4125. PubMed PMID: 24445575; PMCID: PMC3905718.

39.   Zeng ML, Cheng JJ, Kong S, Yang XL, Jia XL, Cheng XL, Chen L, He FG, Liu YM, Fan YT, Gongga L, Chen TX, Liu WH, He XH, Peng BW. Inhibition of Transient Receptor Potential Vanilloid 4 (TRPV4) Mitigates Seizures. Neurotherapeutics. 2022;19(2):660-81. Epub 20220218. doi: 10.1007/s13311-022-01198-8. PubMed PMID: 35182379; PMCID: PMC9226259.

40.   Shi J, Zhao Y, Wang Y, Gao W, Ding J, Li P, Hu L, Shao F. Inflammatory caspases are innate immune receptors for intracellular LPS. Nature. 2014;514(7521):187-92. Epub 20140806. doi: 10.1038/nature13683. PubMed PMID: 25119034.

41.   Rathinam VAK, Zhao Y, Shao F. Innate immunity to intracellular LPS. Nat Immunol. 2019;20(5):527-33. Epub 20190408. doi: 10.1038/s41590-019-0368-3. PubMed PMID: 30962589; PMCID: PMC7668400.

42.   Hagar JA, Powell DA, Aachoui Y, Ernst RK, Miao EA. Cytoplasmic LPS activates caspase-11: implications in TLR4-independent endotoxic shock. Science. 2013;341(6151):1250-3. doi: 10.1126/science.1240988. PubMed PMID: 24031018; PMCID: PMC3931427.

43.   Kwon HS, Koh SH. Neuroinflammation in neurodegenerative disorders: the roles of microglia and astrocytes. Transl Neurodegener. 2020;9(1):42. Epub 20201126. doi: 10.1186/s40035-020-00221-2. PubMed PMID: 33239064; PMCID: PMC7689983.

44.   Wee Yong V. Inflammation in neurological disorders: a help or a hindrance? Neuroscientist. 2010;16(4):408-20. doi: 10.1177/1073858410371379. PubMed PMID: 20817918.

45.   Lehnardt S. Innate immunity and neuroinflammation in the CNS: the role of microglia in Toll-like receptor-mediated neuronal injury. Glia. 2010;58(3):253-63. doi: 10.1002/glia.20928. PubMed PMID: 19705460.

46.   Huffman WJ, Subramaniyan S, Rodriguiz RM, Wetsel WC, Grill WM, Terrando N. Modulation of neuroinflammation and memory dysfunction using percutaneous vagus nerve stimulation in mice. Brain Stimul. 2019;12(1):19-29. Epub 20181009. doi: 10.1016/j.brs.2018.10.005. PubMed PMID: 30337243; PMCID: PMC6301148.

47.   Qin L, Wu X, Block ML, Liu Y, Breese GR, Hong JS, Knapp DJ, Crews FT. Systemic LPS causes chronic neuroinflammation and progressive neurodegeneration. Glia. 2007;55(5):453-62. doi: 10.1002/glia.20467. PubMed PMID: 17203472; PMCID: PMC2871685.

48.   Kim HS, Kim S, Shin SJ, Park YH, Nam Y, Kim CW, Lee KW, Kim SM, Jung ID, Yang HD, Park YM, Moon M. Gram-negative bacteria and their lipopolysaccharides in Alzheimer's disease: pathologic roles and therapeutic implications. Transl Neurodegener. 2021;10(1):49. Epub 20211207. doi: 10.1186/s40035-021-00273-y. PubMed PMID: 34876226; PMCID: PMC8650380.

49.   Zhao Y, Cong L, Jaber V, Lukiw WJ. Microbiome-Derived Lipopolysaccharide Enriched in the Perinuclear Region of Alzheimer's Disease Brain. Front Immunol. 2017;8:1064. Epub 20170904. doi: 10.3389/fimmu.2017.01064. PubMed PMID: 28928740; PMCID: PMC5591429.
50.   Bachstetter AD, Xing B, de Almeida L, Dimayuga ER, Watterson DM, Van Eldik LJ. Microglial p38alpha MAPK is a key regulator of proinflammatory cytokine up-regulation induced by toll-like receptor (TLR) ligands or beta-amyloid (Abeta). J Neuroinflammation. 2011;8:79. Epub 20110706. doi: 10.1186/1742-2094-8-79. PubMed PMID: 21733175; PMCID: PMC3142505.
51.   McMillian M, Kong LY, Sawin SM, Wilson B, Das K, Hudson P, Hong JS, Bing G. Selective killing of cholinergic neurons by microglial activation in basal forebrain mixed neuronal/glial cultures. Biochem Biophys Res Commun. 1995;215(2):572-7. doi: 10.1006/bbrc.1995.2503. PubMed PMID: 7487994.
52.   Wu D, Zhang X, Zhao M, Zhou AL. The role of the TLR4/NF-kappaB signaling pathway in Abeta accumulation in primary hippocampal neurons. Sheng Li Xue Bao. 2015;67(3):319-28. PubMed PMID: 26109305.
53.   Go M, Kou J, Lim JE, Yang J, Fukuchi KI. Microglial response to LPS increases in wild-type mice during aging but diminishes in an Alzheimer's mouse model: Implication of TLR4 signaling in disease progression. Biochem Biophys Res Commun. 2016;479(2):331-7. Epub 20160915. doi: 10.1016/j.bbrc.2016.09.073. PubMed PMID: 27641666; PMCID: PMC5048480.
54.   Turner RC, Naser ZJ, Lucke-Wold BP, Logsdon AF, Vangilder RL, Matsumoto RR, Huber JD, Rosen CL. Single low-dose lipopolysaccharide preconditioning: neuroprotective against axonal injury and modulates glial cells. Neuroimmunol Neuroinflamm. 2017;4:6-15. Epub 20170120. doi: 10.20517/2347-8659.2016.40. PubMed PMID: 28164149; PMCID: PMC5289820.
55.   Wang D, Liu Y, Zhao YR, Zhou JL. Low dose of lipopolysaccharide pretreatment can alleviate the in?ammatory response in wound infection mouse model. Chin J Traumatol. 2016;19(4):193-8. doi: 10.1016/j.cjtee.2016.06.001. PubMed PMID: 27578373; PMCID: PMC4992131.
56.   Knopman DS, Amieva H, Petersen RC, Chetelat G, Holtzman DM, Hyman BT, Nixon RA, Jones DT. Alzheimer disease. Nat Rev Dis Primers. 2021;7(1):33. Epub 20210513. doi: 10.1038/s41572-021-00269-y. PubMed PMID: 33986301; PMCID: PMC8574196.
57.   National Institute on Aging. Alzheimer's Disease Fact Sheet 2019, May 22. Available from: https://www.nia.nih.gov/health/alzheimers-disease-fact-sheet.
58.   Guerreiro R, Bras J. The age factor in Alzheimer's disease. Genome Med. 2015;7:106. Epub 20151020. doi: 10.1186/s13073-015-0232-5. PubMed PMID: 26482651; PMCID: PMC4617238.
59.   Thambisetty M, An Y, Tanaka T. Alzheimer's disease risk genes and the age-at-onset phenotype. Neurobiol Aging. 2013;34(11):2696 e1-5. Epub 20130717. doi: 10.1016/j.neurobiolaging.2013.05.028. PubMed PMID: 23870418; PMCID: PMC4038407.
60.   Campion D, Dumanchin C, Hannequin D, Dubois B, Belliard S, Puel M, Thomas-Anterion C, Michon A, Martin C, Charbonnier F, Raux G, Camuzat A, Penet C, Mesnage V, Martinez M, Clerget-Darpoux F, Brice A, Frebourg T. Early-onset autosomal dominant Alzheimer disease: prevalence, genetic heterogeneity, and mutation spectrum. Am J Hum Genet. 1999;65(3):664-70. doi: 10.1086/302553. PubMed PMID: 10441572; PMCID: PMC1377972.
61.   Lanoiselee HM, Nicolas G, Wallon D, Rovelet-Lecrux A, Lacour M, Rousseau S, Richard AC, Pasquier F, Rollin-Sillaire A, Martinaud O, Quillard-Muraine M, de la Sayette V, Boutoleau-Bretonniere C, Etcharry-Bouyx F, Chauvire V, Sarazin M, le Ber I, Epelbaum S, Jonveaux T, Rouaud O, Ceccaldi M, Felician O, Godefroy O, Formaglio M, Croisile B, Auriacombe S, Chamard L, Vincent JL, Sauvee M, Marelli-Tosi C, Gabelle A, Ozsancak C, Pariente J, Paquet C, Hannequin D, Campion D, collaborators of the CNRMAJp. APP, PSEN1, and PSEN2 mutations in early-onset Alzheimer disease: A genetic screening study of familial and sporadic cases. PLoS Med. 2017;14(3):e1002270. Epub 20170328. doi: 10.1371/journal.pmed.1002270. PubMed PMID: 28350801; PMCID: PMC5370101.
62.   Perez FP, Bose D, Maloney B, Nho K, Shah K, Lahiri DK. Late-onset Alzheimer's disease, heating up and foxed by several proteins: pathomolecular effects of the aging process. J Alzheimers Dis. 2014;40(1):1-17. doi: 10.3233/JAD-131544. PubMed PMID: 24326519; PMCID: PMC4126605.

63.	van der Lee SJ, Wolters FJ, Ikram MK, Hofman A, Ikram MA, Amin N, van Duijn CM. The effect of APOE and other common genetic variants on the onset of Alzheimer's disease and dementia: a community-based cohort study. Lancet Neurol. 2018;17(5):434-44. Epub 20180316. doi: 10.1016/S1474-4422(18)30053-X. PubMed PMID: 29555425.

64.	Bellenguez C, Charbonnier C, Grenier-Boley B, Quenez O, Le Guennec K, Nicolas G, Chauhan G, Wallon D, Rousseau S, Richard AC, Boland A, Bourque G, Munter HM, Olaso R, Meyer V, Rollin-Sillaire A, Pasquier F, Letenneur L, Redon R, Dartigues JF, Tzourio C, Frebourg T, Lathrop M, Deleuze JF, Hannequin D, Genin E, Amouyel P, Debette S, Lambert JC, Campion D, collaborators CM. Contribution to Alzheimer's disease risk of rare variants in TREM2, SORL1, and ABCA7 in 1779 cases and 1273 controls. Neurobiol Aging. 2017;59:220 e1- e9. Epub 20170714. doi: 10.1016/j.neurobiolaging.2017.07.001. PubMed PMID: 28789839.

65.	Dong HK, Gim JA, Yeo SH, Kim HS. Integrated late onset Alzheimer's disease (LOAD) susceptibility genes: Cholesterol metabolism and trafficking perspectives. Gene. 2017;597:10-6. Epub 20161020. doi: 10.1016/j.gene.2016.10.022. PubMed PMID: 27773727.

66.	Litke R, Garcharna LC, Jiwani S, Neugroschl J. Modifiable Risk Factors in Alzheimer Disease and Related Dementias: A Review. Clin Ther. 2021;43(6):953-65. Epub 20210606. doi: 10.1016/j.clinthera.2021.05.006. PubMed PMID: 34108080; PMCID: PMC8440362.

67.	Breijyeh Z, Karaman R. Comprehensive Review on Alzheimer's Disease: Causes and Treatment. Molecules. 2020;25(24). Epub 20201208. doi: 10.3390/molecules25245789. PubMed PMID: 33302541; PMCID: PMC7764106.

68.	Michel JP, Gold G. Behavioural symptoms in Alzheimer's disease: validity of targets and present treatments. Age Ageing. 2001;30(2):105-6. doi: 10.1093/ageing/30.2.105. PubMed PMID: 11395335.

69.	Mangialasche F, Solomon A, Winblad B, Mecocci P, Kivipelto M. Alzheimer's disease: clinical trials and drug development. Lancet Neurol. 2010;9(7):702-16. doi: 10.1016/S1474-4422(10)70119-8. PubMed PMID: 20610346.

70.	Swanson CJ, Zhang Y, Dhadda S, Wang J, Kaplow J, Lai RYK, Lannfelt L, Bradley H, Rabe M, Koyama A, Reyderman L, Berry DA, Berry S, Gordon R, Kramer LD, Cummings JL. A randomized, double-blind, phase 2b proof-of-concept clinical trial in early Alzheimer's disease with lecanemab, an anti-Abeta protofibril antibody. Alzheimers Res Ther. 2021;13(1):80. Epub 20210417. doi: 10.1186/s13195-021-00813-8. PubMed PMID: 33865446; PMCID: PMC8053280.

71.	Arndt JW, Qian F, Smith BA, Quan C, Kilambi KP, Bush MW, Walz T, Pepinsky RB, Bussiere T, Hamann S, Cameron TO, Weinreb PH. Structural and kinetic basis for the selectivity of aducanumab for aggregated forms of amyloid-beta. Sci Rep. 2018;8(1):6412. Epub 20180423. doi: 10.1038/s41598-018-24501-0. PubMed PMID: 29686315; PMCID: PMC5913127.

72.	Cummings J, Aisen P, Apostolova LG, Atri A, Salloway S, Weiner M. Aducanumab: Appropriate Use Recommendations. J Prev Alzheimers Dis. 2021;8(4):398-410. doi: 10.14283/jpad.2021.41. PubMed PMID: 34585212; PMCID: PMC8835345.

73.	Alzheimer A, Stelzmann RA, Schnitzlein HN, Murtagh FR. An English translation of Alzheimer's 1907 paper, "Uber eine eigenartige Erkankung der Hirnrinde". Clin Anat. 1995;8(6):429-31. doi: 10.1002/ca.980080612. PubMed PMID: 8713166.

74.	Murray ME, Graff-Radford NR, Ross OA, Petersen RC, Duara R, Dickson DW. Neuropathologically defined subtypes of Alzheimer's disease with distinct clinical characteristics: a retrospective study. Lancet Neurol. 2011;10(9):785-96. Epub 20110727. doi: 10.1016/S1474-4422(11)70156-9. PubMed PMID: 21802369; PMCID: PMC3175379.

75.	Aisen PS, Cummings J, Jack CR, Jr., Morris JC, Sperling R, Frolich L, Jones RW, Dowsett SA, Matthews BR, Raskin J, Scheltens P, Dubois B. On the path to 2025: understanding the Alzheimer's disease continuum. Alzheimers Res Ther. 2017;9(1):60. Epub 20170809. doi: 10.1186/s13195-017-0283-5. PubMed PMID: 28793924; PMCID: PMC5549378.

76.	Jack CR, Jr., Knopman DS, Jagust WJ, Petersen RC, Weiner MW, Aisen PS, Shaw LM, Vemuri P, Wiste HJ, Weigand SD, Lesnick TG, Pankratz VS, Donohue MC, Trojanowski JQ. Tracking pathophysiological processes in Alzheimer's disease: an updated hypothetical model of dynamic

biomarkers. Lancet Neurol. 2013;12(2):207-16. doi: 10.1016/S1474-4422(12)70291-0. PubMed PMID: 23332364; PMCID: PMC3622225.

77.   Bateman RJ, Xiong C, Benzinger TL, Fagan AM, Goate A, Fox NC, Marcus DS, Cairns NJ, Xie X, Blazey TM, Holtzman DM, Santacruz A, Buckles V, Oliver A, Moulder K, Aisen PS, Ghetti B, Klunk WE, McDade E, Martins RN, Masters CL, Mayeux R, Ringman JM, Rossor MN, Schofield PR, Sperling RA, Salloway S, Morris JC, Dominantly Inherited Alzheimer N. Clinical and biomarker changes in dominantly inherited Alzheimer's disease. N Engl J Med. 2012;367(9):795-804. Epub 20120711. doi: 10.1056/NEJMoa1202753. PubMed PMID: 22784036; PMCID: PMC3474597.

78.   DeTure MA, Dickson DW. The neuropathological diagnosis of Alzheimer's disease. Mol Neurodegener. 2019;14(1):32. Epub 20190802. doi: 10.1186/s13024-019-0333-5. PubMed PMID: 31375134; PMCID: PMC6679484.

79.   Kumar A, Singh A, Ekavali. A review on Alzheimer's disease pathophysiology and its management: an update. Pharmacol Rep. 2015;67(2):195-203. Epub 20140922. doi: 10.1016/j.pharep.2014.09.004. PubMed PMID: 25712639.

80.   Goedert M. Oskar Fischer and the study of dementia. Brain. 2009;132(Pt 4):1102-11. Epub 20081024. doi: 10.1093/brain/awn256. PubMed PMID: 18952676; PMCID: PMC2668940.

81.   Metaxas A, Kempf SJ. Neurofibrillary tangles in Alzheimer's disease: elucidation of the molecular mechanism by immunohistochemistry and tau protein phospho-proteomics. Neural Regen Res. 2016;11(10):1579-81. doi: 10.4103/1673-5374.193234. PubMed PMID: 27904486; PMCID: PMC5116834.

82.   Braak H, Braak E. Frequency of stages of Alzheimer-related lesions in different age categories. Neurobiol Aging. 1997;18(4):351-7. doi: 10.1016/s0197-4580(97)00056-0. PubMed PMID: 9330961.

83.   Braak H, Braak E. Neuropathological stageing of Alzheimer-related changes. Acta Neuropathol. 1991;82(4):239-59. doi: 10.1007/BF00308809. PubMed PMID: 1759558.

84.   Franceschi C, Bonafe M, Valensin S, Olivieri F, De Luca M, Ottaviani E, De Benedictis G. Inflamm-aging. An evolutionary perspective on immunosenescence. Ann N Y Acad Sci. 2000;908:244-54. doi: 10.1111/j.1749-6632.2000.tb06651.x. PubMed PMID: 10911963.

85.   Bruunsgaard H, Skinhoj P, Qvist J, Pedersen BK. Elderly humans show prolonged in vivo inflammatory activity during pneumococcal infections. J Infect Dis. 1999;180(2):551-4. doi: 10.1086/314873. PubMed PMID: 10395881.

86.   Zanni F, Vescovini R, Biasini C, Fagnoni F, Zanlari L, Telera A, Di Pede P, Passeri G, Pedrazzoni M, Passeri M, Franceschi C, Sansoni P. Marked increase with age of type 1 cytokines within memory and effector/cytotoxic CD8+ T cells in humans: a contribution to understand the relationship between inflammation and immunosenescence. Exp Gerontol. 2003;38(9):981-7. doi: 10.1016/s0531-5565(03)00160-8. PubMed PMID: 12954485.

87.   Pawelec G. When T cells get old. Sci Aging Knowledge Environ. 2005;2005(50):pe39. Epub 20051214. doi: 10.1126/sageke.2005.50.pe39. PubMed PMID: 16354906.

88.   Solana R, Pawelec G, Tarazona R. Aging and innate immunity. Immunity. 2006;24(5):491-4. doi: 10.1016/j.immuni.2006.05.003. PubMed PMID: 16713963.

89.   McGeer PL, McGeer EG. The inflammatory response system of brain: implications for therapy of Alzheimer and other neurodegenerative diseases. Brain Res Brain Res Rev. 1995;21(2):195-218. doi: 10.1016/0165-0173(95)00011-9. PubMed PMID: 8866675.

90.   Wang WY, Tan MS, Yu JT, Tan L. Role of pro-inflammatory cytokines released from microglia in Alzheimer's disease. Ann Transl Med. 2015;3(10):136. doi: 10.3978/j.issn.2305-5839.2015.03.49. PubMed PMID: 26207229; PMCID: PMC4486922.

91.   Giunta B, Fernandez F, Nikolic WV, Obregon D, Rrapo E, Town T, Tan J. Inflammaging as a prodrome to Alzheimer's disease. J Neuroinflammation. 2008;5:51. Epub 20081111. doi: 10.1186/1742-2094-5-51. PubMed PMID: 19014446; PMCID: PMC2615427.

92.   McGeer PL, McGeer EG. Anti-inflammatory drugs in the fight against Alzheimer's disease. Ann N Y Acad Sci. 1996;777:213-20. doi: 10.1111/j.1749-6632.1996.tb34421.x. PubMed PMID: 8624086.

93.   Weggen S, Eriksen JL, Das P, Sagi SA, Wang R, Pietrzik CU, Findlay KA, Smith TE, Murphy MP, Bulter T, Kang DE, Marquez-Sterling N, Golde TE, Koo EH. A subset of NSAIDs lower amyloidogenic Abeta42 independently of cyclooxygenase activity. Nature. 2001;414(6860):212-6. doi: 10.1038/35102591. PubMed PMID: 11700559.

94.   Aisen PS, Schafer KA, Grundman M, Pfeiffer E, Sano M, Davis KL, Farlow MR, Jin S, Thomas RG, Thal LJ, Alzheimer's Disease Cooperative S. Effects of rofecoxib or naproxen vs placebo on Alzheimer disease progression: a randomized controlled trial. JAMA. 2003;289(21):2819-26. doi: 10.1001/jama.289.21.2819. PubMed PMID: 12783912.

95.   Efthymiou AG, Goate AM. Late onset Alzheimer's disease genetics implicates microglial pathways in disease risk. Mol Neurodegener. 2017;12(1):43. Epub 20170526. doi: 10.1186/s13024-017-0184-x. PubMed PMID: 28549481; PMCID: PMC5446752.

96.   Hansen DV, Hanson JE, Sheng M. Microglia in Alzheimer's disease. J Cell Biol. 2018;217(2):459-72. Epub 2017/12/03. doi: 10.1083/jcb.201709069. PubMed PMID: 29196460; PMCID: PMC5800817.

97.   Lambert JC, Heath S, Even G, Campion D, Sleegers K, Hiltunen M, Combarros O, Zelenika D, Bullido MJ, Tavernier B, Letenneur L, Bettens K, Berr C, Pasquier F, Fievet N, Barberger-Gateau P, Engelborghs S, De Deyn P, Mateo I, Franck A, Helisalmi S, Porcellini E, Hanon O, European Alzheimer's Disease Initiative I, de Pancorbo MM, Lendon C, Dufouil C, Jaillard C, Leveillard T, Alvarez V, Bosco P, Mancuso M, Panza F, Nacmias B, Bossu P, Piccardi P, Annoni G, Seripa D, Galimberti D, Hannequin D, Licastro F, Soininen H, Ritchie K, Blanche H, Dartigues JF, Tzourio C, Gut I, Van Broeckhoven C, Alperovitch A, Lathrop M, Amouyel P. Genome-wide association study identifies variants at CLU and CR1 associated with Alzheimer's disease. Nat Genet. 2009;41(10):1094-9. Epub 20090906. doi: 10.1038/ng.439. PubMed PMID: 19734903.

98.   Naj AC, Jun G, Beecham GW, Wang LS, Vardarajan BN, Buros J, Gallins PJ, Buxbaum JD, Jarvik GP, Crane PK, Larson EB, Bird TD, Boeve BF, Graff-Radford NR, De Jager PL, Evans D, Schneider JA, Carrasquillo MM, Ertekin-Taner N, Younkin SG, Cruchaga C, Kauwe JS, Nowotny P, Kramer P, Hardy J, Huentelman MJ, Myers AJ, Barmada MM, Demirci FY, Baldwin CT, Green RC, Rogaeva E, St George-Hyslop P, Arnold SE, Barber R, Beach T, Bigio EH, Bowen JD, Boxer A, Burke JR, Cairns NJ, Carlson CS, Carney RM, Carroll SL, Chui HC, Clark DG, Corneveaux J, Cotman CW, Cummings JL, DeCarli C, DeKosky ST, Diaz-Arrastia R, Dick M, Dickson DW, Ellis WG, Faber KM, Fallon KB, Farlow MR, Ferris S, Frosch MP, Galasko DR, Ganguli M, Gearing M, Geschwind DH, Ghetti B, Gilbert JR, Gilman S, Giordani B, Glass JD, Growdon JH, Hamilton RL, Harrell LE, Head E, Honig LS, Hulette CM, Hyman BT, Jicha GA, Jin LW, Johnson N, Karlawish J, Karydas A, Kaye JA, Kim R, Koo EH, Kowall NW, Lah JJ, Levey AI, Lieberman AP, Lopez OL, Mack WJ, Marson DC, Martiniuk F, Mash DC, Masliah E, McCormick WC, McCurry SM, McDavid AN, McKee AC, Mesulam M, Miller BL, Miller CA, Miller JW, Parisi JE, Perl DP, Peskind E, Petersen RC, Poon WW, Quinn JF, Rajbhandary RA, Raskind M, Reisberg B, Ringman JM, Roberson ED, Rosenberg RN, Sano M, Schneider LS, Seeley W, Shelanski ML, Slifer MA, Smith CD, Sonnen JA, Spina S, Stern RA, Tanzi RE, Trojanowski JQ, Troncoso JC, Van Deerlin VM, Vinters HV, Vonsattel JP, Weintraub S, Welsh-Bohmer KA, Williamson J, Woltjer RL, Cantwell LB, Dombroski BA, Beekly D, Lunetta KL, Martin ER, Kamboh MI, Saykin AJ, Reiman EM, Bennett DA, Morris JC, Montine TJ, Goate AM, Blacker D, Tsuang DW, Hakonarson H, Kukull WA, Foroud TM, Haines JL, Mayeux R, Pericak-Vance MA, Farrer LA, Schellenberg GD. Common variants at MS4A4/MS4A6E, CD2AP, CD33 and EPHA1 are associated with late-onset Alzheimer's disease. Nat Genet. 2011;43(5):436-41. Epub 20110403. doi: 10.1038/ng.801. PubMed PMID: 21460841; PMCID: PMC3090745.

99.   Karch CM, Jeng AT, Nowotny P, Cady J, Cruchaga C, Goate AM. Expression of novel Alzheimer's disease risk genes in control and Alzheimer's disease brains. PLoS One. 2012;7(11):e50976. Epub 20121130. doi: 10.1371/journal.pone.0050976. PubMed PMID: 23226438; PMCID: PMC3511432.

100.   Karch CM, Goate AM. Alzheimer's disease risk genes and mechanisms of disease pathogenesis. Biol Psychiatry. 2015;77(1):43-51. Epub 20140517. doi: 10.1016/j.biopsych.2014.05.006. PubMed PMID: 24951455; PMCID: PMC4234692.

101. Reitz C, Jun G, Naj A, Rajbhandary R, Vardarajan BN, Wang LS, Valladares O, Lin CF, Larson EB, Graff-Radford NR, Evans D, De Jager PL, Crane PK, Buxbaum JD, Murrell JR, Raj T, Ertekin-Taner N, Logue M, Baldwin CT, Green RC, Barnes LL, Cantwell LB, Fallin MD, Go RC, Griffith P, Obisesan TO, Manly JJ, Lunetta KL, Kamboh MI, Lopez OL, Bennett DA, Hendrie H, Hall KS, Goate AM, Byrd GS, Kukull WA, Foroud TM, Haines JL, Farrer LA, Pericak-Vance MA, Schellenberg GD, Mayeux R, Alzheimer Disease Genetics C. Variants in the ATP-binding cassette transporter (ABCA7), apolipoprotein E ε4,and the risk of late-onset Alzheimer disease in African Americans. JAMA. 2013;309(14):1483-92. doi: 10.1001/jama.2013.2973. PubMed PMID: 23571587; PMCID: PMC3667653.

102. Guerreiro R, Wojtas A, Bras J, Carrasquillo M, Rogaeva E, Majounie E, Cruchaga C, Sassi C, Kauwe JS, Younkin S, Hazrati L, Collinge J, Pocock J, Lashley T, Williams J, Lambert JC, Amouyel P, Goate A, Rademakers R, Morgan K, Powell J, St George-Hyslop P, Singleton A, Hardy J, Alzheimer Genetic Analysis G. TREM2 variants in Alzheimer's disease. N Engl J Med. 2013;368(2):117-27. Epub 20121114. doi: 10.1056/NEJMoa1211851. PubMed PMID: 23150934; PMCID: PMC3631573.

103. Wang Y, Cella M, Mallinson K, Ulrich JD, Young KL, Robinette ML, Gilfillan S, Krishnan GM, Sudhakar S, Zinselmeyer BH, Holtzman DM, Cirrito JR, Colonna M. TREM2 lipid sensing sustains the microglial response in an Alzheimer's disease model. Cell. 2015;160(6):1061-71. Epub 20150226. doi: 10.1016/j.cell.2015.01.049. PubMed PMID: 25728668; PMCID: PMC4477963.

104. Wang Y, Ulland TK, Ulrich JD, Song W, Tzaferis JA, Hole JT, Yuan P, Mahan TE, Shi Y, Gilfillan S, Cella M, Grutzendler J, DeMattos RB, Cirrito JR, Holtzman DM, Colonna M. TREM2-mediated early microglial response limits diffusion and toxicity of amyloid plaques. J Exp Med. 2016;213(5):667-75. Epub 20160418. doi: 10.1084/jem.20151948. PubMed PMID: 27091843; PMCID: PMC4854736.

105. Griciuc A, Serrano-Pozo A, Parrado AR, Lesinski AN, Asselin CN, Mullin K, Hooli B, Choi SH, Hyman BT, Tanzi RE. Alzheimer's disease risk gene CD33 inhibits microglial uptake of amyloid beta. Neuron. 2013;78(4):631-43. Epub 20130425. doi: 10.1016/j.neuron.2013.04.014. PubMed PMID: 23623698; PMCID: PMC3706457.

106. Keren-Shaul H, Spinrad A, Weiner A, Matcovitch-Natan O, Dvir-Szternfeld R, Ulland TK, David E, Baruch K, Lara-Astaiso D, Toth B, Itzkovitz S, Colonna M, Schwartz M, Amit I. A Unique Microglia Type Associated with Restricting Development of Alzheimer's Disease. Cell. 2017;169(7):1276-90 e17. Epub 20170608. doi: 10.1016/j.cell.2017.05.018. PubMed PMID: 28602351.

107. Lambert JC, Ibrahim-Verbaas CA, Harold D, Naj AC, Sims R, Bellenguez C, DeStafano AL, Bis JC, Beecham GW, Grenier-Boley B, Russo G, Thorton-Wells TA, Jones N, Smith AV, Chouraki V, Thomas C, Ikram MA, Zelenika D, Vardarajan BN, Kamatani Y, Lin CF, Gerrish A, Schmidt H, Kunkle B, Dunstan ML, Ruiz A, Bihoreau MT, Choi SH, Reitz C, Pasquier F, Cruchaga C, Craig D, Amin N, Berr C, Lopez OL, De Jager PL, Deramecourt V, Johnston JA, Evans D, Lovestone S, Letenneur L, Moron FJ, Rubinsztein DC, Eiriksdottir G, Sleegers K, Goate AM, Fievet N, Huentelman MW, Gill M, Brown K, Kamboh MI, Keller L, Barberger-Gateau P, McGuiness B, Larson EB, Green R, Myers AJ, Dufouil C, Todd S, Wallon D, Love S, Rogaeva E, Gallacher J, St George-Hyslop P, Clarimon J, Lleo A, Bayer A, Tsuang DW, Yu L, Tsolaki M, Bossu P, Spalletta G, Proitsi P, Collinge J, Sorbi S, Sanchez-Garcia F, Fox NC, Hardy J, Deniz Naranjo MC, Bosco P, Clarke R, Brayne C, Galimberti D, Mancuso M, Matthews F, European Alzheimer's Disease I, Genetic, Environmental Risk in Alzheimer's D, Alzheimer's Disease Genetic C, Cohorts for H, Aging Research in Genomic E, Moebus S, Mecocci P, Del Zompo M, Maier W, Hampel H, Pilotto A, Bullido M, Panza F, Caffarra P, Nacmias B, Gilbert JR, Mayhaus M, Lannefelt L, Hakonarson H, Pichler S, Carrasquillo MM, Ingelsson M, Beekly D, Alvarez V, Zou F, Valladares O, Younkin SG, Coto E, Hamilton-Nelson KL, Gu W, Razquin C, Pastor P, Mateo I, Owen MJ, Faber KM, Jonsson PV, Combarros O, O'Donovan MC, Cantwell LB, Soininen H, Blacker D, Mead S, Mosley TH, Jr., Bennett DA, Harris TB, Fratiglioni L, Holmes C, de Bruijn RF, Passmore P, Montine TJ, Bettens K, Rotter JI, Brice A, Morgan K, Foroud TM, Kukull WA, Hannequin D, Powell JF, Nalls MA, Ritchie K, Lunetta KL, Kauwe JS, Boerwinkle E, Riemenschneider M, Boada M, Hiltuenen M,

Martin ER, Schmidt R, Rujescu D, Wang LS, Dartigues JF, Mayeux R, Tzourio C, Hofman A, Nothen MM, Graff C, Psaty BM, Jones L, Haines JL, Holmans PA, Lathrop M, Pericak-Vance MA, Launer LJ, Farrer LA, van Duijn CM, Van Broeckhoven C, Moskvina V, Seshadri S, Williams J, Schellenberg GD, Amouyel P. Meta-analysis of 74,046 individuals identifies 11 new susceptibility loci for Alzheimer's disease. Nat Genet. 2013;45(12):1452-8. Epub 20131027. doi: 10.1038/ng.2802. PubMed PMID: 24162737; PMCID: PMC3896259.

108.   Deczkowska A, Keren-Shaul H, Weiner A, Colonna M, Schwartz M, Amit I. Disease-Associated Microglia: A Universal Immune Sensor of Neurodegeneration. Cell. 2018;173(5):1073-81. doi: 10.1016/j.cell.2018.05.003. PubMed PMID: 29775591.

109.   Rangaraju S, Dammer EB, Raza SA, Rathakrishnan P, Xiao H, Gao T, Duong DM, Pennington MW, Lah JJ, Seyfried NT, Levey AI. Identification and therapeutic modulation of a pro-inflammatory subset of disease-associated-microglia in Alzheimer's disease. Mol Neurodegener. 2018;13(1):24. Epub 2018/05/23. doi: 10.1186/s13024-018-0254-8. PubMed PMID: 29784049; PMCID: PMC5963076.

110.   Yuan P, Condello C, Keene CD, Wang Y, Bird TD, Paul SM, Luo W, Colonna M, Baddeley D, Grutzendler J. TREM2 Haplodeficiency in Mice and Humans Impairs the Microglia Barrier Function Leading to Decreased Amyloid Compaction and Severe Axonal Dystrophy. Neuron. 2016;90(4):724-39. doi: 10.1016/j.neuron.2016.05.003. PubMed PMID: 27196974; PMCID: PMC4898967.

111.   Olah M, Menon V, Habib N, Taga MF, Ma Y, Yung CJ, Cimpean M, Khairallah A, Coronas-Samano G, Sankowski R, Grun D, Kroshilina AA, Dionne D, Sarkis RA, Cosgrove GR, Helgager J, Golden JA, Pennell PB, Prinz M, Vonsattel JPG, Teich AF, Schneider JA, Bennett DA, Regev A, Elyaman W, Bradshaw EM, De Jager PL. Single cell RNA sequencing of human microglia uncovers a subset associated with Alzheimer's disease. Nat Commun. 2020;11(1):6129. Epub 20201130. doi: 10.1038/s41467-020-19737-2. PubMed PMID: 33257666; PMCID: PMC7704703.

112.   Gratuze M, Leyns CEG, Holtzman DM. New insights into the role of TREM2 in Alzheimer's disease. Mol Neurodegener. 2018;13(1):66. Epub 20181220. doi: 10.1186/s13024-018-0298-9. PubMed PMID: 30572908; PMCID: PMC6302500.

113.   Humphrey MB, Daws MR, Spusta SC, Niemi EC, Torchia JA, Lanier LL, Seaman WE, Nakamura MC. TREM2, a DAP12-associated receptor, regulates osteoclast differentiation and function. J Bone Miner Res. 2006;21(2):237-45. Epub 20051020. doi: 10.1359/JBMR.051016. PubMed PMID: 16418779.

114.   Lanier LL, Corliss BC, Wu J, Leong C, Phillips JH. Immunoreceptor DAP12 bearing a tyrosine-based activation motif is involved in activating NK cells. Nature. 1998;391(6668):703-7. doi: 10.1038/35642. PubMed PMID: 9490415.

115.   Mocsai A, Ruland J, Tybulewicz VL. The SYK tyrosine kinase: a crucial player in diverse biological functions. Nat Rev Immunol. 2010;10(6):387-402. doi: 10.1038/nri2765. PubMed PMID: 20467426; PMCID: PMC4782221.

116.   Ennerfelt H, Frost EL, Shapiro DA, Holliday C, Zengeler KE, Voithofer G, Bolte AC, Lammert CR, Kulas JA, Ulland TK, Lukens JR. SYK coordinates neuroprotective microglial responses in neurodegenerative disease. Cell. 2022;185(22):4135-52 e22. Epub 20221017. doi: 10.1016/j.cell.2022.09.030. PubMed PMID: 36257314; PMCID: PMC9617784.

117.   Peng Q, Malhotra S, Torchia JA, Kerr WG, Coggeshall KM, Humphrey MB. TREM2- and DAP12-dependent activation of PI3K requires DAP10 and is inhibited by SHIP1. Sci Signal. 2010;3(122):ra38. Epub 20100518. doi: 10.1126/scisignal.2000500. PubMed PMID: 20484116; PMCID: PMC2900152.

118.   Kawabori M, Kacimi R, Kauppinen T, Calosing C, Kim JY, Hsieh CL, Nakamura MC, Yenari MA. Triggering receptor expressed on myeloid cells 2 (TREM2) deficiency attenuates phagocytic activities of microglia and exacerbates ischemic damage in experimental stroke. J Neurosci. 2015;35(8):3384-96. doi: 10.1523/JNEUROSCI.2620-14.2015. PubMed PMID: 25716838; PMCID: PMC4339351.

119.   Sunna S, Bowen CA, Ramelow CC, Santiago JV, Kumar P, Rangaraju S. Advances in proteomic phenotyping of microglia in neurodegeneration. Proteomics. 2023;23(13-14):e2200183. Epub 20230502. doi: 10.1002/pmic.202200183. PubMed PMID: 37060300; PMCID: PMC10528430.

120.   Chen MJ, Ramesha S, Weinstock LD, Gao T, Ping L, Xiao H, Dammer EB, Duong DD, Levey AI, Lah JJ, Seyfried NT, Wood LB, Rangaraju S. Extracellular signal-regulated kinase regulates microglial immune responses in Alzheimer's disease. J Neurosci Res. 2021;99(6):1704-21. Epub 20210317. doi: 10.1002/jnr.24829. PubMed PMID: 33729626; PMCID: PMC8919593.

121.   Bemiller SM, McCray TJ, Allan K, Formica SV, Xu G, Wilson G, Kokiko-Cochran ON, Crish SD, Lasagna-Reeves CA, Ransohoff RM, Landreth GE, Lamb BT. TREM2 deficiency exacerbates tau pathology through dysregulated kinase signaling in a mouse model of tauopathy. Mol Neurodegener. 2017;12(1):74. Epub 20171016. doi: 10.1186/s13024-017-0216-6. PubMed PMID: 29037207; PMCID: PMC5644120.

122.   Dejanovic B, Huntley MA, De Maziere A, Meilandt WJ, Wu T, Srinivasan K, Jiang Z, Gandham V, Friedman BA, Ngu H, Foreman O, Carano RAD, Chih B, Klumperman J, Bakalarski C, Hanson JE, Sheng M. Changes in the Synaptic Proteome in Tauopathy and Rescue of Tau-Induced Synapse Loss by C1q Antibodies. Neuron. 2018;100(6):1322-36 e7. Epub 20181101. doi: 10.1016/j.neuron.2018.10.014. PubMed PMID: 30392797.

123.   Heneka MT, Kummer MP, Latz E. Innate immune activation in neurodegenerative disease. Nat Rev Immunol. 2014;14(7):463-77. doi: 10.1038/nri3705. PubMed PMID: 24962261.

124.   Kawai T, Akira S. The role of pattern-recognition receptors in innate immunity: update on Toll-like receptors. Nat Immunol. 2010;11(5):373-84. Epub 20100420. doi: 10.1038/ni.1863. PubMed PMID: 20404851.

125.   Chargaff E. The isolation of preparations of thromboplastic protein from human organs. J Biol Chem. 1945;161:389-94. PubMed PMID: 21005746.

126.   Chargaff E, West R. The biological significance of the thromboplastic protein of blood. J Biol Chem. 1946;166(1):189-97. PubMed PMID: 20273687.

127.   Hougie C. The activation of platelets by plasma. Br J Haematol. 1955;1(2):213-22. doi: 10.1111/j.1365-2141.1955.tb05502.x. PubMed PMID: 13240009.

128.   O'Brien JR. The platelet-like activity of serum. Br J Haematol. 1955;1(2):223-8. PubMed PMID: 13240010.

129.   Wolf P. The nature and significance of platelet products in human plasma. Br J Haematol. 1967;13(3):269-88. doi: 10.1111/j.1365-2141.1967.tb08741.x. PubMed PMID: 6025241.

130.   Crawford N. The presence of contractile proteins in platelet microparticles isolated from human and animal platelet-free plasma. Br J Haematol. 1971;21(1):53-69. doi: 10.1111/j.1365-2141.1971.tb03416.x. PubMed PMID: 4254312.

131.   Anderson HC. Vesicles associated with calcification in the matrix of epiphyseal cartilage. J Cell Biol. 1969;41(1):59-72. doi: 10.1083/jcb.41.1.59. PubMed PMID: 5775794; PMCID: PMC2107736.

132.   Bonucci E. Fine structure of early cartilage calcification. J Ultrastruct Res. 1967;20(1):33-50. doi: 10.1016/s0022-5320(67)80034-0. PubMed PMID: 4195919.

133.   Nunez EA, Wallis J, Gershon MD. Secretory processes in follicular cells of the bat thyroid. 3. The occurrence of extracellular vesicles and colloid droplets during arousal from hibernation. Am J Anat. 1974;141(2):179-201. doi: 10.1002/aja.1001410203. PubMed PMID: 4415703.

134.   Fawcett DW. Electron microscope observations on intracellular virus-like particles associated with the cells of the Lucke renal adenocarcinoma. J Biophys Biochem Cytol. 1956;2(6):725-41. doi: 10.1083/jcb.2.6.725. PubMed PMID: 13398440; PMCID: PMC2224004.

135.   Lunger PD, Lucas JC, Jr., Shipkey FH. The Ultramorphology of Milk Fractions for Normal and Breast Cancer Patients. A Preliminary Report. Cancer. 1964;17:549-57. doi: 10.1002/1097-0142(196405)17:5<549::aid-cncr2820170502>3.0.co;2-f. PubMed PMID: 14159804.

136.   Levine PH, Horoszewicz JS, Grace JT, Jr., Chai LS, Ellison RR, Holland JF. Relationship between clinical status of leukemic patients and virus-like particles in their plasma. Cancer.

1967;20(10):1563-77. doi: 10.1002/1097-0142(196710)20:10<1563::aid-cncr2820201002>3.0.co;2-n. PubMed PMID: 5234301.

137.   Dmochowski L, Langford PL, Williams WC, Liebelt AG, Liebelt RA. Electron microscopic and bioassay studies of milk from mice of high and low mammary-cancer and high and low leukemia strains. J Natl Cancer Inst. 1968;40(6):1339-58. PubMed PMID: 4298257.

138.   Johnstone RM, Adam M, Hammond JR, Orr L, Turbide C. Vesicle formation during reticulocyte maturation. Association of plasma membrane activities with released vesicles (exosomes). J Biol Chem. 1987;262(19):9412-20. PubMed PMID: 3597417.

139.   Harding C, Heuser J, Stahl P. Receptor-mediated endocytosis of transferrin and recycling of the transferrin receptor in rat reticulocytes. J Cell Biol. 1983;97(2):329-39. doi: 10.1083/jcb.97.2.329. PubMed PMID: 6309857; PMCID: PMC2112509.

140.   Thery C, Boussac M, Veron P, Ricciardi-Castagnoli P, Raposo G, Garin J, Amigorena S. Proteomic analysis of dendritic cell-derived exosomes: a secreted subcellular compartment distinct from apoptotic vesicles. J Immunol. 2001;166(12):7309-18. doi: 10.4049/jimmunol.166.12.7309. PubMed PMID: 11390481.

141.   Wubbolts R, Leckie RS, Veenhuizen PT, Schwarzmann G, Mobius W, Hoernschemeyer J, Slot JW, Geuze HJ, Stoorvogel W. Proteomic and biochemical analyses of human B cell-derived exosomes. Potential implications for their function and multivesicular body formation. J Biol Chem. 2003;278(13):10963-72. Epub 20030107. doi: 10.1074/jbc.M207550200. PubMed PMID: 12519789.

142.   Fourcade O, Simon MF, Viode C, Rugani N, Leballe F, Ragab A, Fournie B, Sarda L, Chap H. Secretory phospholipase A2 generates the novel lipid mediator lysophosphatidic acid in membrane microvesicles shed from activated cells. Cell. 1995;80(6):919-27. doi: 10.1016/0092-8674(95)90295-3. PubMed PMID: 7697722.

143.   Zitvogel L, Regnault A, Lozier A, Wolfers J, Flament C, Tenza D, Ricciardi-Castagnoli P, Raposo G, Amigorena S. Eradication of established murine tumors using a novel cell-free vaccine: dendritic cell-derived exosomes. Nat Med. 1998;4(5):594-600. doi: 10.1038/nm0598-594. PubMed PMID: 9585234.

144.   Ratajczak J, Miekus K, Kucia M, Zhang J, Reca R, Dvorak P, Ratajczak MZ. Embryonic stem cell-derived microvesicles reprogram hematopoietic progenitors: evidence for horizontal transfer of mRNA and protein delivery. Leukemia. 2006;20(5):847-56. doi: 10.1038/sj.leu.2404132. PubMed PMID: 16453000.

145.   Skog J, Wurdinger T, van Rijn S, Meijer DH, Gainche L, Sena-Esteves M, Curry WT, Jr., Carter BS, Krichevsky AM, Breakefield XO. Glioblastoma microvesicles transport RNA and proteins that promote tumour growth and provide diagnostic biomarkers. Nat Cell Biol. 2008;10(12):1470-6. Epub 20081116. doi: 10.1038/ncb1800. PubMed PMID: 19011622; PMCID: PMC3423894.

146.   Valadi H, Ekstrom K, Bossios A, Sjostrand M, Lee JJ, Lotvall JO. Exosome-mediated transfer of mRNAs and microRNAs is a novel mechanism of genetic exchange between cells. Nat Cell Biol. 2007;9(6):654-9. Epub 20070507. doi: 10.1038/ncb1596. PubMed PMID: 17486113.

147.   Araldi E, Kramer-Albers EM, Hoen EN, Peinado H, Psonka-Antonczyk KM, Rao P, van Niel G, Yanez-Mo M, Nazarenko I. International Society for Extracellular Vesicles: first annual meeting, April 17-21, 2012: ISEV-2012. J Extracell Vesicles. 2012;1:19995. Epub 20121228. doi: 10.3402/jev.v1i0.19995. PubMed PMID: 26082071; PMCID: PMC3760652.

148.   Thery C, Zitvogel L, Amigorena S. Exosomes: composition, biogenesis and function. Nat Rev Immunol. 2002;2(8):569-79. Epub 2002/08/03. doi: 10.1038/nri855. PubMed PMID: 12154376.

149.   Zaborowski MP, Balaj L, Breakefield XO, Lai CP. Extracellular Vesicles: Composition, Biological Relevance, and Methods of Study. Bioscience. 2015;65(8):783-97. Epub 20150626. doi: 10.1093/biosci/biv084. PubMed PMID: 26955082; PMCID: PMC4776721.

150.   Heijnen HF, Schiel AE, Fijnheer R, Geuze HJ, Sixma JJ. Activated platelets release two types of membrane vesicles: microvesicles by surface shedding and exosomes derived from exocytosis of multivesicular bodies and alpha-granules. Blood. 1999;94(11):3791-9. PubMed PMID: 10572093.

151.   Thery C, Witwer KW, Aikawa E, Alcaraz MJ, Anderson JD, Andriantsitohaina R, Antoniou A, Arab T, Archer F, Atkin-Smith GK, Ayre DC, Bach JM, Bachurski D, Baharvand H, Balaj L, Baldacchino S, Bauer NN, Baxter AA, Bebawy M, Beckham C, Bedina Zavec A, Benmoussa A, Berardi AC, Bergese P, Bielska E, Blenkiron C, Bobis-Wozowicz S, Boilard E, Boireau W, Bongiovanni A, Borras FE, Bosch S, Boulanger CM, Breakefield X, Breglio AM, Brennan MA, Brigstock DR, Brisson A, Broekman ML, Bromberg JF, Bryl-Gorecka P, Buch S, Buck AH, Burger D, Busatto S, Buschmann D, Bussolati B, Buzas EI, Byrd JB, Camussi G, Carter DR, Caruso S, Chamley LW, Chang YT, Chen C, Chen S, Cheng L, Chin AR, Clayton A, Clerici SP, Cocks A, Cocucci E, Coffey RJ, Cordeiro-da-Silva A, Couch Y, Coumans FA, Coyle B, Crescitelli R, Criado MF, D'Souza-Schorey C, Das S, Datta Chaudhuri A, de Candia P, De Santana EF, De Wever O, Del Portillo HA, Demaret T, Deville S, Devitt A, Dhondt B, Di Vizio D, Dieterich LC, Dolo V, Dominguez Rubio AP, Dominici M, Dourado MR, Driedonks TA, Duarte FV, Duncan HM, Eichenberger RM, Ekstrom K, El Andaloussi S, Elie-Caille C, Erdbrugger U, Falcon-Perez JM, Fatima F, Fish JE, Flores-Bellver M, Forsonits A, Frelet-Barrand A, Fricke F, Fuhrmann G, Gabrielsson S, Gamez-Valero A, Gardiner C, Gartner K, Gaudin R, Gho YS, Giebel B, Gilbert C, Gimona M, Giusti I, Goberdhan DC, Gorgens A, Gorski SM, Greening DW, Gross JC, Gualerzi A, Gupta GN, Gustafson D, Handberg A, Haraszti RA, Harrison P, Hegyesi H, Hendrix A, Hill AF, Hochberg FH, Hoffmann KF, Holder B, Holthofer H, Hosseinkhani B, Hu G, Huang Y, Huber V, Hunt S, Ibrahim AG, Ikezu T, Inal JM, Isin M, Ivanova A, Jackson HK, Jacobsen S, Jay SM, Jayachandran M, Jenster G, Jiang L, Johnson SM, Jones JC, Jong A, Jovanovic-Talisman T, Jung S, Kalluri R, Kano SI, Kaur S, Kawamura Y, Keller ET, Khamari D, Khomyakova E, Khvorova A, Kierulf P, Kim KP, Kislinger T, Klingeborn M, Klinke DJ, 2nd, Kornek M, Kosanovic MM, Kovacs AF, Kramer-Albers EM, Krasemann S, Krause M, Kurochkin IV, Kusuma GD, Kuypers S, Laitinen S, Langevin SM, Languino LR, Lannigan J, Lasser C, Laurent LC, Lavieu G, Lazaro-Ibanez E, Le Lay S, Lee MS, Lee YXF, Lemos DS, Lenassi M, Leszczynska A, Li IT, Liao K, Libregts SF, Ligeti E, Lim R, Lim SK, Line A, Linnemannstons K, Llorente A, Lombard CA, Lorenowicz MJ, Lorincz AM, Lotvall J, Lovett J, Lowry MC, Loyer X, Lu Q, Lukomska B, Lunavat TR, Maas SL, Malhi H, Marcilla A, Mariani J, Mariscal J, Martens-Uzunova ES, Martin-Jaular L, Martinez MC, Martins VR, Mathieu M, Mathivanan S, Maugeri M, McGinnis LK, McVey MJ, Meckes DG, Jr., Meehan KL, Mertens I, Minciacchi VR, Moller A, Moller Jorgensen M, Morales-Kastresana A, Morhayim J, Mullier F, Muraca M, Musante L, Mussack V, Muth DC, Myburgh KH, Najrana T, Nawaz M, Nazarenko I, Nejsum P, Neri C, Neri T, Nieuwland R, Nimrichter L, Nolan JP, Nolte-'t Hoen EN, Noren Hooten N, O'Driscoll L, O'Grady T, O'Loghlen A, Ochiya T, Olivier M, Ortiz A, Ortiz LA, Osteikoetxea X, Ostergaard O, Ostrowski M, Park J, Pegtel DM, Peinado H, Perut F, Pfaffl MW, Phinney DG, Pieters BC, Pink RC, Pisetsky DS, Pogge von Strandmann E, Polakovicova I, Poon IK, Powell BH, Prada I, Pulliam L, Quesenberry P, Radeghieri A, Raffai RL, Raimondo S, Rak J, Ramirez MI, Raposo G, Rayyan MS, Regev-Rudzki N, Ricklefs FL, Robbins PD, Roberts DD, Rodrigues SC, Rohde E, Rome S, Rouschop KM, Rughetti A, Russell AE, Saa P, Sahoo S, Salas-Huenuleo E, Sanchez C, Saugstad JA, Saul MJ, Schiffelers RM, Schneider R, Schoyen TH, Scott A, Shahaj E, Sharma S, Shatnyeva O, Shekari F, Shelke GV, Shetty AK, Shiba K, Siljander PR, Silva AM, Skowronek A, Snyder OL, 2nd, Soares RP, Sodar BW, Soekmadji C, Sotillo J, Stahl PD, Stoorvogel W, Stott SL, Strasser EF, Swift S, Tahara H, Tewari M, Timms K, Tiwari S, Tixeira R, Tkach M, Toh WS, Tomasini R, Torrecilhas AC, Tosar JP, Toxavidis V, Urbanelli L, Vader P, van Balkom BW, van der Grein SG, Van Deun J, van Herwijnen MJ, Van Keuren-Jensen K, van Niel G, van Royen ME, van Wijnen AJ, Vasconcelos MH, Vechetti IJ, Jr., Veit TD, Vella LJ, Velot E, Verweij FJ, Vestad B, Vinas JL, Visnovitz T, Vukman KV, Wahlgren J, Watson DC, Wauben MH, Weaver A, Webber JP, Weber V, Wehman AM, Weiss DJ, Welsh JA, Wendt S, Wheelock AM, Wiener Z, Witte L, Wolfram J, Xagorari A, Xander P, Xu J, Yan X, Yanez-Mo M, Yin H, Yuana Y, Zappulli V, Zarubova J, Zekas V, Zhang JY, Zhao Z, Zheng L, Zheutlin AR, Zickler AM, Zimmermann P, Zivkovic AM, Zocco D, Zuba-Surma EK. Minimal information for studies of extracellular vesicles 2018 (MISEV2018): a position statement of the International Society for Extracellular Vesicles and update of the MISEV2014 guidelines. J Extracell Vesicles. 2018;7(1):1535750. Epub 20181123. doi: 10.1080/20013078.2018.1535750. PubMed PMID: 30637094; PMCID: PMC6322352.

152.   Liangsupree T, Multia E, Riekkola ML. Modern isolation and separation techniques for extracellular vesicles. J Chromatogr A. 2021;1636:461773. Epub 20201203. doi: 10.1016/j.chroma.2020.461773. PubMed PMID: 33316564.

153.   Laulagnier K, Motta C, Hamdi S, Roy S, Fauvelle F, Pageaux JF, Kobayashi T, Salles JP, Perret B, Bonnerot C, Record M. Mast cell- and dendritic cell-derived exosomes display a specific lipid composition and an unusual membrane organization. Biochem J. 2004;380(Pt 1):161-71. doi: 10.1042/BJ20031594. PubMed PMID: 14965343; PMCID: PMC1224152.

154.   Gurung S, Perocheau D, Touramanidou L, Baruteau J. The exosome journey: from biogenesis to uptake and intracellular signalling. Cell Commun Signal. 2021;19(1):47. Epub 20210423. doi: 10.1186/s12964-021-00730-1. PubMed PMID: 33892745; PMCID: PMC8063428.

155.   Schmidt O, Teis D. The ESCRT machinery. Curr Biol. 2012;22(4):R116-20. doi: 10.1016/j.cub.2012.01.028. PubMed PMID: 22361144; PMCID: PMC3314914.

156.   Buschow SI, Liefhebber JM, Wubbolts R, Stoorvogel W. Exosomes contain ubiquitinated proteins. Blood Cells Mol Dis. 2005;35(3):398-403. Epub 20051003. doi: 10.1016/j.bcmd.2005.08.005. PubMed PMID: 16203162.

157.   Colombo M, Moita C, van Niel G, Kowal J, Vigneron J, Benaroch P, Manel N, Moita LF, Thery C, Raposo G. Analysis of ESCRT functions in exosome biogenesis, composition and secretion highlights the heterogeneity of extracellular vesicles. J Cell Sci. 2013;126(Pt 24):5553-65. Epub 20131008. doi: 10.1242/jcs.128868. PubMed PMID: 24105262.

158.   Trajkovic K, Hsu C, Chiantia S, Rajendran L, Wenzel D, Wieland F, Schwille P, Brugger B, Simons M. Ceramide triggers budding of exosome vesicles into multivesicular endosomes. Science. 2008;319(5867):1244-7. doi: 10.1126/science.1153124. PubMed PMID: 18309083.

159.   Catalano M, O'Driscoll L. Inhibiting extracellular vesicles formation and release: a review of EV inhibitors. J Extracell Vesicles. 2020;9(1):1703244. Epub 20191219. doi: 10.1080/20013078.2019.1703244. PubMed PMID: 32002167; PMCID: PMC6968539.

160.   Doyle LM, Wang MZ. Overview of Extracellular Vesicles, Their Origin, Composition, Purpose, and Methods for Exosome Isolation and Analysis. Cells. 2019;8(7). Epub 20190715. doi: 10.3390/cells8070727. PubMed PMID: 31311206; PMCID: PMC6678302.

161.   Xu D, Di K, Fan B, Wu J, Gu X, Sun Y, Khan A, Li P, Li Z. MicroRNAs in extracellular vesicles: Sorting mechanisms, diagnostic value, isolation, and detection technology. Front Bioeng Biotechnol. 2022;10:948959. Epub 20221017. doi: 10.3389/fbioe.2022.948959. PubMed PMID: 36324901; PMCID: PMC9618890.

162.   Prieto-Vila M, Yoshioka Y, Ochiya T. Biological Functions Driven by mRNAs Carried by Extracellular Vesicles in Cancer. Front Cell Dev Biol. 2021;9:620498. Epub 20210830. doi: 10.3389/fcell.2021.620498. PubMed PMID: 34527665; PMCID: PMC8435577.

163.   Zomer A, Steenbeek SC, Maynard C, van Rheenen J. Studying extracellular vesicle transfer by a Cre-loxP method. Nat Protoc. 2016;11(1):87-101. Epub 20151210. doi: 10.1038/nprot.2015.138. PubMed PMID: 26658469.

164.   Redzic JS, Balaj L, van der Vos KE, Breakefield XO. Extracellular RNA mediates and marks cancer progression. Semin Cancer Biol. 2014;28:14-23. Epub 20140428. doi: 10.1016/j.semcancer.2014.04.010. PubMed PMID: 24783980; PMCID: PMC4162815.

165.   Rana S, Yue S, Stadel D, Zoller M. Toward tailored exosomes: the exosomal tetraspanin web contributes to target cell selection. Int J Biochem Cell Biol. 2012;44(9):1574-84. Epub 20120619. doi: 10.1016/j.biocel.2012.06.018. PubMed PMID: 22728313.

166.   Zech D, Rana S, Buchler MW, Zoller M. Tumor-exosomes and leukocyte activation: an ambivalent crosstalk. Cell Commun Signal. 2012;10(1):37. Epub 20121128. doi: 10.1186/1478-811X-10-37. PubMed PMID: 23190502; PMCID: PMC3519567.

167.   Sancho-Albero M, Navascues N, Mendoza G, Sebastian V, Arruebo M, Martin-Duque P, Santamaria J. Exosome origin determines cell targeting and the transfer of therapeutic nanoparticles towards target cells. J Nanobiotechnology. 2019;17(1):16. Epub 20190125. doi: 10.1186/s12951-018-0437-z. PubMed PMID: 30683120; PMCID: PMC6346572.

168.	Escrevente C, Keller S, Altevogt P, Costa J. Interaction and uptake of exosomes by ovarian cancer cells. BMC Cancer. 2011;11:108. Epub 20110327. doi: 10.1186/1471-2407-11-108. PubMed PMID: 21439085; PMCID: PMC3072949.

169.	Belhadj Z, He B, Deng H, Song S, Zhang H, Wang X, Dai W, Zhang Q. A combined "eat me/don't eat me" strategy based on extracellular vesicles for anticancer nanomedicine. J Extracell Vesicles. 2020;9(1):1806444. Epub 20200819. doi: 10.1080/20013078.2020.1806444. PubMed PMID: 32944191; PMCID: PMC7480498.

170.	Tkach M, Kowal J, Zucchetti AE, Enserink L, Jouve M, Lankar D, Saitakis M, Martin-Jaular L, Thery C. Qualitative differences in T-cell activation by dendritic cell-derived extracellular vesicle subtypes. EMBO J. 2017;36(20):3012-28. Epub 20170918. doi: 10.15252/embj.201696003. PubMed PMID: 28923825; PMCID: PMC5641679.

171.	Guan S, Li Q, Liu P, Xuan X, Du Y. Umbilical cord blood-derived dendritic cells loaded with BGC823 tumor antigens and DC-derived exosomes stimulate efficient cytotoxic T-lymphocyte responses and antitumor immunity in vitro and in vivo. Cent Eur J Immunol. 2014;39(2):142-51. Epub 20140627. doi: 10.5114/ceji.2014.43713. PubMed PMID: 26155115; PMCID: PMC4440031.

172.	Prada I, Meldolesi J. Binding and Fusion of Extracellular Vesicles to the Plasma Membrane of Their Cell Targets. Int J Mol Sci. 2016;17(8). Epub 20160809. doi: 10.3390/ijms17081296. PubMed PMID: 27517914; PMCID: PMC5000693.

173.	Parolini I, Federici C, Raggi C, Lugini L, Palleschi S, De Milito A, Coscia C, Iessi E, Logozzi M, Molinari A, Colone M, Tatti M, Sargiacomo M, Fais S. Microenvironmental pH is a key factor for exosome traffic in tumor cells. J Biol Chem. 2009;284(49):34211-22. Epub 20090930. doi: 10.1074/jbc.M109.041152. PubMed PMID: 19801663; PMCID: PMC2797191.

174.	Mettlen M, Chen PH, Srinivasan S, Danuser G, Schmid SL. Regulation of Clathrin-Mediated Endocytosis. Annu Rev Biochem. 2018;87:871-96. Epub 20180416. doi: 10.1146/annurev-biochem-062917-012644. PubMed PMID: 29661000; PMCID: PMC6383209.

175.	Mulcahy LA, Pink RC, Carter DR. Routes and mechanisms of extracellular vesicle uptake. J Extracell Vesicles. 2014;3. Epub 20140804. doi: 10.3402/jev.v3.24641. PubMed PMID: 25143819; PMCID: PMC4122821.

176.	Kiss AL, Botos E. Endocytosis via caveolae: alternative pathway with distinct cellular compartments to avoid lysosomal degradation? J Cell Mol Med. 2009;13(7):1228-37. Epub 20090327. doi: 10.1111/j.1582-4934.2009.00754.x. PubMed PMID: 19382909; PMCID: PMC4496137.

177.	Feng D, Zhao WL, Ye YY, Bai XC, Liu RQ, Chang LF, Zhou Q, Sui SF. Cellular internalization of exosomes occurs through phagocytosis. Traffic. 2010;11(5):675-87. doi: 10.1111/j.1600-0854.2010.01041.x. PubMed PMID: 20136776.

178.	Kerr MC, Teasdale RD. Defining macropinocytosis. Traffic. 2009;10(4):364-71. Epub 20090124. doi: 10.1111/j.1600-0854.2009.00878.x. PubMed PMID: 19192253.

179.	Livshits MA, Khomyakova E, Evtushenko EG, Lazarev VN, Kulemin NA, Semina SE, Generozov EV, Govorun VM. Isolation of exosomes by differential centrifugation: Theoretical analysis of a commonly used protocol. Sci Rep. 2015;5:17319. Epub 20151130. doi: 10.1038/srep17319. PubMed PMID: 26616523; PMCID: PMC4663484.

180.	Tauro BJ, Greening DW, Mathias RA, Ji H, Mathivanan S, Scott AM, Simpson RJ. Comparison of ultracentrifugation, density gradient separation, and immunoaffinity capture methods for isolating human colon cancer cell line LIM1863-derived exosomes. Methods. 2012;56(2):293-304. Epub 20120121. doi: 10.1016/j.ymeth.2012.01.002. PubMed PMID: 22285593.

181.	Gamez-Valero A, Monguio-Tortajada M, Carreras-Planella L, Franquesa M, Beyer K, Borras FE. Size-Exclusion Chromatography-based isolation minimally alters Extracellular Vesicles' characteristics compared to precipitating agents. Sci Rep. 2016;6:33641. Epub 20160919. doi: 10.1038/srep33641. PubMed PMID: 27640641; PMCID: PMC5027519.

182.	Patel GK, Khan MA, Zubair H, Srivastava SK, Khushman M, Singh S, Singh AP. Comparative analysis of exosome isolation methods using culture supernatant for optimum yield, purity and

downstream applications. Sci Rep. 2019;9(1):5335. Epub 20190329. doi: 10.1038/s41598-019-41800-2. PubMed PMID: 30926864; PMCID: PMC6441044.

183.   Li P, Kaslan M, Lee SH, Yao J, Gao Z. Progress in Exosome Isolation Techniques. Theranostics. 2017;7(3):789-804. Epub 20170126. doi: 10.7150/thno.18133. PubMed PMID: 28255367; PMCID: PMC5327650.

184.   Hill AF. Extracellular Vesicles and Neurodegenerative Diseases. J Neurosci. 2019;39(47):9269-73. Epub 2019/11/22. doi: 10.1523/JNEUROSCI.0147-18.2019. PubMed PMID: 31748282; PMCID: PMC6867808.

185.   Braak H, Rub U, Gai WP, Del Tredici K. Idiopathic Parkinson's disease: possible routes by which vulnerable neuronal types may be subject to neuroinvasion by an unknown pathogen. J Neural Transm (Vienna). 2003;110(5):517-36. doi: 10.1007/s00702-002-0808-2. PubMed PMID: 12721813.

186.   Asai H, Ikezu S, Tsunoda S, Medalla M, Luebke J, Haydar T, Wolozin B, Butovsky O, Kugler S, Ikezu T. Depletion of microglia and inhibition of exosome synthesis halt tau propagation. Nat Neurosci. 2015;18(11):1584-93. Epub 2015/10/06. doi: 10.1038/nn.4132. PubMed PMID: 26436904; PMCID: PMC4694577.

187.   Wang P, Lan G, Xu B, Yu Z, Tian C, Lei X, Meissner WG, Feng T, Yang Y, Zhang J. alpha-Synuclein-carrying astrocytic extracellular vesicles in Parkinson pathogenesis and diagnosis. Transl Neurodegener. 2023;12(1):40. Epub 20230825. doi: 10.1186/s40035-023-00372-y. PubMed PMID: 37620916; PMCID: PMC10463943.

188.   Sardar Sinha M, Ansell-Schultz A, Civitelli L, Hildesjo C, Larsson M, Lannfelt L, Ingelsson M, Hallbeck M. Alzheimer's disease pathology propagation by exosomes containing toxic amyloid-beta oligomers. Acta Neuropathol. 2018;136(1):41-56. Epub 20180613. doi: 10.1007/s00401-018-1868-1. PubMed PMID: 29934873; PMCID: PMC6015111.

189.   Dinkins MB, Dasgupta S, Wang G, Zhu G, Bieberich E. Exosome reduction in vivo is associated with lower amyloid plaque load in the 5XFAD mouse model of Alzheimer's disease. Neurobiol Aging. 2014;35(8):1792-800. Epub 20140215. doi: 10.1016/j.neurobiolaging.2014.02.012. PubMed PMID: 24650793; PMCID: PMC4035236.

190.   Yuyama K, Sun H, Usuki S, Sakai S, Hanamatsu H, Mioka T, Kimura N, Okada M, Tahara H, Furukawa J, Fujitani N, Shinohara Y, Igarashi Y. A potential function for neuronal exosomes: sequestering intracerebral amyloid-beta peptide. FEBS Lett. 2015;589(1):84-8. Epub 20141129. doi: 10.1016/j.febslet.2014.11.027. PubMed PMID: 25436414.

191.   Fiandaca MS, Kapogiannis D, Mapstone M, Boxer A, Eitan E, Schwartz JB, Abner EL, Petersen RC, Federoff HJ, Miller BL, Goetzl EJ. Identification of preclinical Alzheimer's disease by a profile of pathogenic proteins in neurally derived blood exosomes: A case-control study. Alzheimers Dement. 2015;11(6):600-7 e1. Epub 20140815. doi: 10.1016/j.jalz.2014.06.008. PubMed PMID: 25130657; PMCID: PMC4329112.

192.   Yin Q, Ji X, Lv R, Pei JJ, Du Y, Shen C, Hou X. Targetting Exosomes as a New Biomarker and Therapeutic Approach for Alzheimer's Disease. Clin Interv Aging. 2020;15:195-205. Epub 20200213. doi: 10.2147/CIA.S240400. PubMed PMID: 32103922; PMCID: PMC7025655.

193.   Gupta A, Pulliam L. Exosomes as mediators of neuroinflammation. J Neuroinflammation. 2014;11:68. Epub 20140403. doi: 10.1186/1742-2094-11-68. PubMed PMID: 24694258; PMCID: PMC3994210.

194.   Alexander M, Hu R, Runtsch MC, Kagele DA, Mosbruger TL, Tolmachova T, Seabra MC, Round JL, Ward DM, O'Connell RM. Exosome-delivered microRNAs modulate the inflammatory response to endotoxin. Nat Commun. 2015;6:7321. Epub 20150618. doi: 10.1038/ncomms8321. PubMed PMID: 26084661; PMCID: PMC4557301.

195.   Potolicchio I, Carven GJ, Xu X, Stipp C, Riese RJ, Stern LJ, Santambrogio L. Proteomic analysis of microglia-derived exosomes: metabolic role of the aminopeptidase CD13 in neuropeptide catabolism. J Immunol. 2005;175(4):2237-43. doi: 10.4049/jimmunol.175.4.2237. PubMed PMID: 16081791.

196.   Yang Y, Boza-Serrano A, Dunning CJR, Clausen BH, Lambertsen KL, Deierborg T. Inflammation leads to distinct populations of extracellular vesicles from microglia. J Neuroinflammation.

2018;15(1):168. Epub 20180528. doi: 10.1186/s12974-018-1204-7. PubMed PMID: 29807527; PMCID: PMC5972400.

197.   Verderio C, Muzio L, Turola E, Bergami A, Novellino L, Ruffini F, Riganti L, Corradini I, Francolini M, Garzetti L, Maiorino C, Servida F, Vercelli A, Rocca M, Dalla Libera D, Martinelli V, Comi G, Martino G, Matteoli M, Furlan R. Myeloid microvesicles are a marker and therapeutic target for neuroinflammation. Ann Neurol. 2012;72(4):610-24. doi: 10.1002/ana.23627. PubMed PMID: 23109155.

198.   Lee S, Mankhong S, Kang JH. Extracellular Vesicle as a Source of Alzheimer's Biomarkers: Opportunities and Challenges. Int J Mol Sci. 2019;20(7). Epub 20190408. doi: 10.3390/ijms20071728. PubMed PMID: 30965555; PMCID: PMC6479979.

199.   Vogel C, Marcotte EM. Insights into the regulation of protein abundance from proteomic and transcriptomic analyses. Nat Rev Genet. 2012;13(4):227-32. Epub 20120313. doi: 10.1038/nrg3185. PubMed PMID: 22411467; PMCID: PMC3654667.

200.   Manzoni C, Kia DA, Vandrovcova J, Hardy J, Wood NW, Lewis PA, Ferrari R. Genome, transcriptome and proteome: the rise of omics data and their integration in biomedical sciences. Brief Bioinform. 2018;19(2):286-302. Epub 2016/11/25. doi: 10.1093/bib/bbw114. PubMed PMID: 27881428; PMCID: PMC6018996.

201.   Rayaprolu S, Bitarafan S, Santiago JV, Betarbet R, Sunna S, Cheng L, Xiao H, Nelson RS, Kumar P, Bagchi P, Duong DM, Goettemoeller AM, Olah VJ, Rowan M, Levey AI, Wood LB, Seyfried NT, Rangaraju S. Cell type-specific biotin labeling in vivo resolves regional neuronal and astrocyte proteomic differences in mouse brain. Nat Commun. 2022;13(1):2927. Epub 20220525. doi: 10.1038/s41467-022-30623-x. PubMed PMID: 35614064; PMCID: PMC9132937.

202.   Liang JW, Fang ZY, Huang Y, Liuyang ZY, Zhang XL, Wang JL, Wei H, Wang JZ, Wang XC, Zeng J, Liu R. Application of Weighted Gene Co-Expression Network Analysis to Explore the Key Genes in Alzheimer's Disease. J Alzheimers Dis. 2018;65(4):1353-64. doi: 10.3233/JAD-180400. PubMed PMID: 30124448; PMCID: PMC6218130.

203.   Seyfried NT, Dammer EB, Swarup V, Nandakumar D, Duong DM, Yin L, Deng Q, Nguyen T, Hales CM, Wingo T, Glass J, Gearing M, Thambisetty M, Troncoso JC, Geschwind DH, Lah JJ, Levey AI. A Multi-network Approach Identifies Protein-Specific Co-expression in Asymptomatic and Symptomatic Alzheimer's Disease. Cell Syst. 2017;4(1):60-72 e4. Epub 2016/12/19. doi: 10.1016/j.cels.2016.11.006. PubMed PMID: 27989508; PMCID: PMC5269514.

204.   Johnson ECB, Dammer EB, Duong DM, Ping L, Zhou M, Yin L, Higginbotham LA, Guajardo A, White B, Troncoso JC, Thambisetty M, Montine TJ, Lee EB, Trojanowski JQ, Beach TG, Reiman EM, Haroutunian V, Wang M, Schadt E, Zhang B, Dickson DW, Ertekin-Taner N, Golde TE, Petyuk VA, De Jager PL, Bennett DA, Wingo TS, Rangaraju S, Hajjar I, Shulman JM, Lah JJ, Levey AI, Seyfried NT. Large-scale proteomic analysis of Alzheimer's disease brain and cerebrospinal fluid reveals early changes in energy metabolism associated with microglia and astrocyte activation. Nat Med. 2020;26(5):769-80. Epub 20200413. doi: 10.1038/s41591-020-0815-6. PubMed PMID: 32284590; PMCID: PMC7405761.

205.   Vander Heiden MG, Cantley LC, Thompson CB. Understanding the Warburg effect: the metabolic requirements of cell proliferation. Science. 2009;324(5930):1029-33. doi: 10.1126/science.1160809. PubMed PMID: 19460998; PMCID: PMC2849637.

206.   Rayaprolu S, Higginbotham L, Bagchi P, Watson CM, Zhang T, Levey AI, Rangaraju S, Seyfried NT. Systems-based proteomics to resolve the biology of Alzheimer's disease beyond amyloid and tau. Neuropsychopharmacology. 2021;46(1):98-115. Epub 20200908. doi: 10.1038/s41386-020-00840-3. PubMed PMID: 32898852; PMCID: PMC7689445.

207.   Hodes RJ, Buckholtz N. Accelerating Medicines Partnership: Alzheimer's Disease (AMP-AD) Knowledge Portal Aids Alzheimer's Drug Discovery through Open Data Sharing. Expert Opin Ther Targets. 2016;20(4):389-91. Epub 20160207. doi: 10.1517/14728222.2016.1135132. PubMed PMID: 26853544.

208.   Ramesha S, Rayaprolu S, Rangaraju S. Flow Cytometry Approach to Characterize Phagocytic Properties of Acutely-Isolated Adult Microglia and Brain Macrophages In Vitro. J Vis Exp. 2020(160). Epub 20200623. doi: 10.3791/61467. PubMed PMID: 32658196.

209.   Bennett ML, Bennett FC, Liddelow SA, Ajami B, Zamanian JL, Fernhoff NB, Mulinyawe SB, Bohlen CJ, Adil A, Tucker A, Weissman IL, Chang EF, Li G, Grant GA, Hayden Gephart MG, Barres BA. New tools for studying microglia in the mouse and human CNS. Proc Natl Acad Sci U S A. 2016;113(12):E1738-46. Epub 20160216. doi: 10.1073/pnas.1525528113. PubMed PMID: 26884166; PMCID: PMC4812770.

210.   Hickman SE, Kingery ND, Ohsumi TK, Borowsky ML, Wang LC, Means TK, El Khoury J. The microglial sensome revealed by direct RNA sequencing. Nat Neurosci. 2013;16(12):1896-905. Epub 20131027. doi: 10.1038/nn.3554. PubMed PMID: 24162652; PMCID: PMC3840123.

211.   Crotti A, Ransohoff RM. Microglial Physiology and Pathophysiology: Insights from Genome-wide Transcriptional Profiling. Immunity. 2016;44(3):505-15. doi: 10.1016/j.immuni.2016.02.013. PubMed PMID: 26982357.

212.   Rangaraju S, Dammer EB, Raza SA, Gao T, Xiao H, Betarbet R, Duong DM, Webster JA, Hales CM, Lah JJ, Levey AI, Seyfried NT. Quantitative proteomics of acutely-isolated mouse microglia identifies novel immune Alzheimer's disease-related proteins. Mol Neurodegener. 2018;13(1):34. Epub 2018/06/30. doi: 10.1186/s13024-018-0266-4. PubMed PMID: 29954413; PMCID: PMC6025801.

213.   Boza-Serrano A, Yang Y, Paulus A, Deierborg T. Innate immune alterations are elicited in microglial cells before plaque deposition in the Alzheimer's disease mouse model 5xFAD. Sci Rep. 2018;8(1):1550. Epub 20180124. doi: 10.1038/s41598-018-19699-y. PubMed PMID: 29367720; PMCID: PMC5784016.

214.   Dieterich DC, Link AJ, Graumann J, Tirrell DA, Schuman EM. Selective identification of newly synthesized proteins in mammalian cells using bioorthogonal noncanonical amino acid tagging (BONCAT). Proc Natl Acad Sci U S A. 2006;103(25):9482-7. Epub 20060612. doi: 10.1073/pnas.0601637103. PubMed PMID: 16769897; PMCID: PMC1480433.

215.   Alvarez-Castelao B, Schanzenbacher CT, Hanus C, Glock C, Tom Dieck S, Dorrbaum AR, Bartnik I, Nassim-Assir B, Ciirdaeva E, Mueller A, Dieterich DC, Tirrell DA, Langer JD, Schuman EM. Cell-type-specific metabolic labeling of nascent proteomes in vivo. Nat Biotechnol. 2017;35(12):1196-201. Epub 20171106. doi: 10.1038/nbt.4016. PubMed PMID: 29106408.

216.   Prabhakar P, Pielot R, Landgraf P, Wissing J, Bayrhammer A, van Ham M, Gundelfinger ED, Jansch L, Dieterich DC, Muller A. Monitoring regional astrocyte diversity by cell type-specific proteomic labeling in vivo. Glia. 2023;71(3):682-703. Epub 20221119. doi: 10.1002/glia.24304. PubMed PMID: 36401581.

217.   Roux KJ, Kim DI, Raida M, Burke B. A promiscuous biotin ligase fusion protein identifies proximal and interacting proteins in mammalian cells. J Cell Biol. 2012;196(6):801-10. Epub 20120312. doi: 10.1083/jcb.201112098. PubMed PMID: 22412018; PMCID: PMC3308701.

218.   Cho KF, Branon TC, Udeshi ND, Myers SA, Carr SA, Ting AY. Proximity labeling in mammalian cells with TurboID and split-TurboID. Nat Protoc. 2020;15(12):3971-99. Epub 20201102. doi: 10.1038/s41596-020-0399-0. PubMed PMID: 33139955.

219.   Sunna S, Bowen C, Zeng H, Rayaprolu S, Kumar P, Bagchi P, Dammer EB, Guo Q, Duong DM, Bitarafan S, Natu A, Wood L, Seyfried NT, Rangaraju S. Cellular Proteomic Profiling Using Proximity Labeling by TurboID-NES in Microglial and Neuronal Cell Lines. Mol Cell Proteomics. 2023;22(6):100546. Epub 20230414. doi: 10.1016/j.mcpro.2023.100546. PubMed PMID: 37061046; PMCID: PMC10205547.

220.   Cai ZY, Xiao M, Quazi SH, Ke ZY. Exosomes: a novel therapeutic target for Alzheimer's disease? Neural Regen Res. 2018;13(5):930-5. Epub 2018/06/05. doi: 10.4103/1673-5374.232490. PubMed PMID: 29863025; PMCID: PMC5998631.

221.   Kowal J, Arras G, Colombo M, Jouve M, Morath JP, Primdal-Bengtson B, Dingli F, Loew D, Tkach M, Thery C. Proteomic comparison defines novel markers to characterize heterogeneous populations of extracellular vesicle subtypes. Proc Natl Acad Sci U S A. 2016;113(8):E968-77. Epub 2016/02/10. doi: 10.1073/pnas.1521230113. PubMed PMID: 26858453; PMCID: PMC4776515.

222.   Kowal J, Tkach M, Thery C. Biogenesis and secretion of exosomes. Curr Opin Cell Biol. 2014;29:116-25. Epub 20140622. doi: 10.1016/j.ceb.2014.05.004. PubMed PMID: 24959705.

223.   Ratajczak J, Wysoczynski M, Hayek F, Janowska-Wieczorek A, Ratajczak MZ. Membrane-derived microvesicles: important and underappreciated mediators of cell-to-cell communication. Leukemia. 2006;20(9):1487-95. Epub 20060720. doi: 10.1038/sj.leu.2404296. PubMed PMID: 16791265.

224.   Spires-Jones TL, Hyman BT. The intersection of amyloid beta and tau at synapses in Alzheimer's disease. Neuron. 2014;82(4):756-71. Epub 2014/05/24. doi: 10.1016/j.neuron.2014.05.004. PubMed PMID: 24853936; PMCID: PMC4135182.

225.   Buckley NJ, Johnson R, Zuccato C, Bithell A, Cattaneo E. The role of REST in transcriptional and epigenetic dysregulation in Huntington's disease. Neurobiol Dis. 2010;39(1):28-39. Epub 20100217. doi: 10.1016/j.nbd.2010.02.003. PubMed PMID: 20170730.

226.   Hu G, Drescher KM, Chen XM. Exosomal miRNAs: Biological Properties and Therapeutic Potential. Front Genet. 2012;3:56. Epub 20120420. doi: 10.3389/fgene.2012.00056. PubMed PMID: 22529849; PMCID: PMC3330238.

227.   Huang S, Ge X, Yu J, Han Z, Yin Z, Li Y, Chen F, Wang H, Zhang J, Lei P. Increased miR-124-3p in microglial exosomes following traumatic brain injury inhibits neuronal inflammation and contributes to neurite outgrowth via their transfer into neurons. FASEB J. 2018;32(1):512-28. Epub 20170921. doi: 10.1096/fj.201700673R. PubMed PMID: 28935818.

228.   Dong L, Lin W, Qi P, Xu MD, Wu X, Ni S, Huang D, Weng WW, Tan C, Sheng W, Zhou X, Du X. Circulating Long RNAs in Serum Extracellular Vesicles: Their Characterization and Potential Application as Biomarkers for Diagnosis of Colorectal Cancer. Cancer Epidemiol Biomarkers Prev. 2016;25(7):1158-66. Epub 20160518. doi: 10.1158/1055-9965.EPI-16-0006. PubMed PMID: 27197301.

229.   Durafourt BA, Moore CS, Zammit DA, Johnson TA, Zaguia F, Guiot MC, Bar-Or A, Antel JP. Comparison of polarization properties of human adult microglia and blood-derived macrophages. Glia. 2012;60(5):717-27. Epub 20120130. doi: 10.1002/glia.22298. PubMed PMID: 22290798.

230.   Jha MK, Lee WH, Suk K. Functional polarization of neuroglia: Implications in neuroinflammation and neurological disorders. Biochem Pharmacol. 2016;103:1-16. Epub 2015/11/12. doi: 10.1016/j.bcp.2015.11.003. PubMed PMID: 26556658.

231.   Lively S, Schlichter LC. Microglia Responses to Pro-inflammatory Stimuli (LPS, IFNgamma+TNFalpha) and Reprogramming by Resolving Cytokines (IL-4, IL-10). Front Cell Neurosci. 2018;12:215. Epub 20180724. doi: 10.3389/fncel.2018.00215. PubMed PMID: 30087595; PMCID: PMC6066613.

232.   Rangaraju S, Raza SA, Pennati A, Deng Q, Dammer EB, Duong D, Pennington MW, Tansey MG, Lah JJ, Betarbet R, Seyfried NT, Levey AI. A systems pharmacology-based approach to identify novel Kv1.3 channel-dependent mechanisms in microglial activation. J Neuroinflammation. 2017;14(1):128. Epub 20170626. doi: 10.1186/s12974-017-0906-6. PubMed PMID: 28651603; PMCID: PMC5485721.

233.   Gao T, Jernigan J, Raza SA, Dammer EB, Xiao H, Seyfried NT, Levey AI, Rangaraju S. Transcriptional regulation of homeostatic and disease-associated-microglial genes by IRF1, LXRbeta, and CEBPalpha. Glia. 2019;67(10):1958-75. Epub 20190713. doi: 10.1002/glia.23678. PubMed PMID: 31301160; PMCID: PMC7190149.

234.   Chen TY, Gonzalez-Kozlova E, Soleymani T, La Salvia S, Kyprianou N, Sahoo S, Tewari AK, Cordon-Cardo C, Stolovitzky G, Dogra N. Extracellular vesicles carry distinct proteo-transcriptomic signatures that are different from their cancer cell of origin. iScience. 2022;25(6):104414. Epub 20220518. doi: 10.1016/j.isci.2022.104414. PubMed PMID: 35663013; PMCID: PMC9157216.

235.   Sork H, Corso G, Krjutskov K, Johansson HJ, Nordin JZ, Wiklander OPB, Lee YXF, Westholm JO, Lehtio J, Wood MJA, Mager I, El Andaloussi S. Heterogeneity and interplay of the extracellular vesicle small RNA transcriptome and proteome. Sci Rep. 2018;8(1):10813. Epub 20180717. doi: 10.1038/s41598-018-28485-9. PubMed PMID: 30018314; PMCID: PMC6050237.

236.   Pontis F, Roz L, Mensah M, Segale M, Moro M, Bertolini G, Petraroia I, Centonze G, Ferretti AM, Suatoni P, Pastorino U, Fortunato O, Sozzi G. Circulating extracellular vesicles from individuals at high-risk of lung cancer induce pro-tumorigenic conversion of stromal cells through transfer of miR-126

and miR-320. J Exp Clin Cancer Res. 2021;40(1):237. Epub 20210721. doi: 10.1186/s13046-021-02040-3. PubMed PMID: 34289890; PMCID: PMC8293562.

237.	Giunti D, Marini C, Parodi B, Usai C, Milanese M, Bonanno G, Kerlero de Rosbo N, Uccelli A. Role of miRNAs shuttled by mesenchymal stem cell-derived small extracellular vesicles in modulating neuroinflammation. Sci Rep. 2021;11(1):1740. Epub 20210118. doi: 10.1038/s41598-021-81039-4. PubMed PMID: 33462263; PMCID: PMC7814007.

238.	Macfarlane LA, Murphy PR. MicroRNA: Biogenesis, Function and Role in Cancer. Curr Genomics. 2010;11(7):537-61. doi: 10.2174/138920210793175895. PubMed PMID: 21532838; PMCID: PMC3048316.

239.	Chen Y, Wang X. miRDB: an online database for prediction of functional microRNA targets. Nucleic Acids Res. 2020;48(D1):D127-D31. doi: 10.1093/nar/gkz757. PubMed PMID: 31504780; PMCID: PMC6943051.

240.	Szabo GT, Tarr B, Paloczi K, Eder K, Lajko E, Kittel A, Toth S, Gyorgy B, Pasztoi M, Nemeth A, Osteikoetxea X, Pallinger E, Falus A, Szabo-Taylor K, Buzas EI. Critical role of extracellular vesicles in modulating the cellular effects of cytokines. Cell Mol Life Sci. 2014;71(20):4055-67. Epub 20140406. doi: 10.1007/s00018-014-1618-z. PubMed PMID: 24705984.

241.	Oh Y, Jung HJ, Hong S, Cho Y, Park J, Cho D, Kim TS. Aminoacyl transfer ribonucleic acid synthetase complex-interacting multifunctional protein 1 induces microglial activation and M1 polarization via the mitogen-activated protein kinase/nuclear factor-kappa B signaling pathway. Front Cell Neurosci. 2022;16:977205. Epub 20220907. doi: 10.3389/fncel.2022.977205. PubMed PMID: 36159396; PMCID: PMC9491728.

242.	Macario AJL, Conway de Macario E. Chaperonins in cancer: Expression, function, and migration in extracellular vesicles. Semin Cancer Biol. 2022;86(Pt 1):26-35. Epub 20210601. doi: 10.1016/j.semcancer.2021.05.029. PubMed PMID: 34087417.

243.	Grantham J. The Molecular Chaperone CCT/TRiC: An Essential Component of Proteostasis and a Potential Modulator of Protein Aggregation. Front Genet. 2020;11:172. Epub 20200319. doi: 10.3389/fgene.2020.00172. PubMed PMID: 32265978; PMCID: PMC7096549.

244.	Goetzke CC, Ebstein F, Kallinich T. Role of Proteasomes in Inflammation. J Clin Med. 2021;10(8). Epub 20210420. doi: 10.3390/jcm10081783. PubMed PMID: 33923887; PMCID: PMC8072576.

245.	O'Brien K, Breyne K, Ughetto S, Laurent LC, Breakefield XO. RNA delivery by extracellular vesicles in mammalian cells and its applications. Nat Rev Mol Cell Biol. 2020;21(10):585-606. Epub 20200526. doi: 10.1038/s41580-020-0251-y. PubMed PMID: 32457507; PMCID: PMC7249041.

246.	Hebert SS, Horre K, Nicolai L, Papadopoulou AS, Mandemakers W, Silahtaroglu AN, Kauppinen S, Delacourte A, De Strooper B. Loss of microRNA cluster miR-29a/b-1 in sporadic Alzheimer's disease correlates with increased BACE1/beta-secretase expression. Proc Natl Acad Sci U S A. 2008;105(17):6415-20. Epub 20080423. doi: 10.1073/pnas.0710263105. PubMed PMID: 18434550; PMCID: PMC2359789.

247.	Mukai T, Di Martino E, Tsuji S, Blomgren K, Nagamura-Inoue T, Aden U. Umbilical cord-derived mesenchymal stromal cells immunomodulate and restore actin dynamics and phagocytosis of LPS-activated microglia via PI3K/Akt/Rho GTPase pathway. Cell Death Discov. 2021;7(1):46. Epub 20210315. doi: 10.1038/s41420-021-00436-w. PubMed PMID: 33723246; PMCID: PMC7961004.

248.	Blasi E, Barluzzi R, Bocchini V, Mazzolla R, Bistoni F. Immortalization of murine microglial cells by a v-raf/v-myc carrying retrovirus. J Neuroimmunol. 1990;27(2-3):229-37. Epub 1990/05/01. doi: 10.1016/0165-5728(90)90073-v. PubMed PMID: 2110186.

249.	Henn A, Lund S, Hedtjarn M, Schrattenholz A, Porzgen P, Leist M. The suitability of BV2 cells as alternative model system for primary microglia cultures or for animal experiments examining brain inflammation. ALTEX. 2009;26(2):83-94. doi: 10.14573/altex.2009.2.83. PubMed PMID: 19565166.

250.	Timmerman R, Burm SM, Bajramovic JJ. An Overview of in vitro Methods to Study Microglia. Front Cell Neurosci. 2018;12:242. Epub 20180806. doi: 10.3389/fncel.2018.00242. PubMed PMID: 30127723; PMCID: PMC6087748.

251.   Lobb RJ, Becker M, Wen SW, Wong CS, Wiegmans AP, Leimgruber A, Moller A. Optimized exosome isolation protocol for cell culture supernatant and human plasma. J Extracell Vesicles. 2015;4:27031. Epub 2015/07/22. doi: 10.3402/jev.v4.27031. PubMed PMID: 26194179; PMCID: PMC4507751.

252.   Reales-Calderon JA, Vaz C, Monteoliva L, Molero G, Gil C. Candida albicans Modifies the Protein Composition and Size Distribution of THP-1 Macrophage-Derived Extracellular Vesicles. J Proteome Res. 2017;16(1):87-105. Epub 20161102. doi: 10.1021/acs.jproteome.6b00605. PubMed PMID: 27740763.

253.   Ping L, Duong DM, Yin L, Gearing M, Lah JJ, Levey AI, Seyfried NT. Global quantitative analysis of the human brain proteome in Alzheimer's and Parkinson's Disease. Sci Data. 2018;5:180036. Epub 2018/03/14. doi: 10.1038/sdata.2018.36. PubMed PMID: 29533394; PMCID: PMC5848788.

254.   Hebert AS, Prasad S, Belford MW, Bailey DJ, McAlister GC, Abbatiello SE, Huguet R, Wouters ER, Dunyach JJ, Brademan DR, Westphall MS, Coon JJ. Comprehensive Single-Shot Proteomics with FAIMS on a Hybrid Orbitrap Mass Spectrometer. Anal Chem. 2018;90(15):9529-37. Epub 20180718. doi: 10.1021/acs.analchem.8b02233. PubMed PMID: 29969236; PMCID: PMC6145172.

255.   Liu W, Wang X. Prediction of functional microRNA targets by integrative modeling of microRNA binding and target expression data. Genome Biol. 2019;20(1):18. Epub 20190122. doi: 10.1186/s13059-019-1629-z. PubMed PMID: 30670076; PMCID: PMC6341724.

256.   Keerthikumar S, Chisanga D, Ariyaratne D, Al Saffar H, Anand S, Zhao K, Samuel M, Pathan M, Jois M, Chilamkurti N, Gangoda L, Mathivanan S. ExoCarta: A Web-Based Compendium of Exosomal Cargo. J Mol Biol. 2016;428(4):688-92. Epub 20151003. doi: 10.1016/j.jmb.2015.09.019. PubMed PMID: 26434508; PMCID: PMC4783248.

257.   Sarlus H, Heneka MT. Microglia in Alzheimer's disease. J Clin Invest. 2017;127(9):3240-9. Epub 2017/09/02. doi: 10.1172/JCI90606. PubMed PMID: 28862638; PMCID: PMC5669553.

258.   Zhao R, Hu W, Tsai J, Li W, Gan WB. Microglia limit the expansion of beta-amyloid plaques in a mouse model of Alzheimer's disease. Mol Neurodegener. 2017;12(1):47. Epub 2017/06/14. doi: 10.1186/s13024-017-0188-6. PubMed PMID: 28606182; PMCID: PMC5468952.

259.   Rayaprolu S, Gao T, Xiao H, Ramesha S, Weinstock LD, Shah J, Duong DM, Dammer EB, Webster JA, Jr., Lah JJ, Wood LB, Betarbet R, Levey AI, Seyfried NT, Rangaraju S. Flow-cytometric microglial sorting coupled with quantitative proteomics identifies moesin as a highly-abundant microglial protein with relevance to Alzheimer's disease. Mol Neurodegener. 2020;15(1):28. Epub 20200507. doi: 10.1186/s13024-020-00377-5. PubMed PMID: 32381088; PMCID: PMC7206797.

260.   Branon TC, Bosch JA, Sanchez AD, Udeshi ND, Svinkina T, Carr SA, Feldman JL, Perrimon N, Ting AY. Efficient proximity labeling in living cells and organisms with TurboID. Nat Biotechnol. 2018;36(9):880-7. Epub 2018/08/21. doi: 10.1038/nbt.4201. PubMed PMID: 30125270; PMCID: PMC6126969.

261.   Erdmann G, Schutz G, Berger S. Inducible gene inactivation in neurons of the adult mouse forebrain. BMC Neurosci. 2007;8:63. Epub 20070802. doi: 10.1186/1471-2202-8-63. PubMed PMID: 17683525; PMCID: PMC1955451.

262.   Winchenbach J, Duking T, Berghoff SA, Stumpf SK, Hulsmann S, Nave KA, Saher G. Inducible targeting of CNS astrocytes in Aldh1l1-CreERT2 BAC transgenic mice. F1000Res. 2016;5:2934. Epub 20161230. doi: 10.12688/f1000research.10509.1. PubMed PMID: 28149504; PMCID: PMC5265728.

263.   Sharma K, Schmitt S, Bergner CG, Tyanova S, Kannaiyan N, Manrique-Hoyos N, Kongi K, Cantuti L, Hanisch UK, Philips MA, Rossner MJ, Mann M, Simons M. Cell type- and brain region-resolved mouse brain proteome. Nat Neurosci. 2015;18(12):1819-31. Epub 20151102. doi: 10.1038/nn.4160. PubMed PMID: 26523646; PMCID: PMC7116867.

264.   Uchida Y, Ito K, Ohtsuki S, Kubo Y, Suzuki T, Terasaki T. Major involvement of Na(+) - dependent multivitamin transporter (SLC5A6/SMVT) in uptake of biotin and pantothenic acid by human brain capillary endothelial cells. J Neurochem. 2015;134(1):97-112. Epub 20150408. doi: 10.1111/jnc.13092. PubMed PMID: 25809983.

265.   Lesur A, Schmit PO, Bernardin F, Letellier E, Brehmer S, Decker J, Dittmar G. Highly Multiplexed Targeted Proteomics Acquisition on a TIMS-QTOF. Anal Chem. 2021;93(3):1383-92. Epub 20201217. doi: 10.1021/acs.analchem.0c03180. PubMed PMID: 33331761.

266.   Li Y, Kanao E, Yamano T, Ishihama Y, Imami K. TurboID-EV: Proteomic Mapping of Recipient Cellular Proteins Proximal to Small Extracellular Vesicles. Anal Chem. 2023;95(38):14159-64. Epub 20230914. doi: 10.1021/acs.analchem.3c01015. PubMed PMID: 37709279; PMCID: PMC10534987.

267.   Ramesha S, Rayaprolu S, Bowen CA, Giver CR, Bitarafan S, Nguyen HM, Gao T, Chen MJ, Nwabueze N, Dammer EB, Engstrom AK, Xiao H, Pennati A, Seyfried NT, Katz DJ, Galipeau J, Wulff H, Waller EK, Wood LB, Levey AI, Rangaraju S. Unique molecular characteristics and microglial origin of Kv1.3 channel-positive brain myeloid cells in Alzheimer's disease. Proc Natl Acad Sci U S A. 2021;118(11). doi: 10.1073/pnas.2013545118. PubMed PMID: 33649184; PMCID: PMC7980378.

268.   Tannous BA, Kim DE, Fernandez JL, Weissleder R, Breakefield XO. Codon-optimized Gaussia luciferase cDNA for mammalian gene expression in culture and in vivo. Mol Ther. 2005;11(3):435-43. doi: 10.1016/j.ymthe.2004.10.016. PubMed PMID: 15727940.

269.   Tannous BA. Gaussia luciferase reporter assay for monitoring biological processes in culture and in vivo. Nat Protoc. 2009;4(4):582-91. doi: 10.1038/nprot.2009.28. PubMed PMID: 19373229; PMCID: PMC2692611.